PRODUCTION AND EVALUATION OF HIGH SPECIFIC ACTIVITY ^{186}RE: AN ISOTOPE FOR RADIOIMMUNOTHERAPY IN CANCER TREATMENT

By

Suzanne Lapi

M. Sc., Simon Fraser University, 2003

B. Sc., Simon Fraser University, 2001

Thesis submitted in partial fulfillment of the
requirements for the degree of

Doctor of Philosophy

in the

Department of Chemistry

SIMON FRASER UNIVERSITY

2007

APPROVAL

Name: Suzanne Lapi

Degree: Doctor of Philosophy

Title of Thesis: Production and Evaluation of High Specific Activity Re-186: An Isotope for Radioimmunotherapy in Cancer Treatment

Examining Committee:

Dr. Michael H. Eikerling
Chairperson
Assistant Professor, Department of Chemistry

Dr. Paul W. Percival
Co-Senior Supervisor
Professor, Department of Chemistry

Dr. Thomas J. Ruth
Co-Senior Supervisor
Adjunct Professor, Department of Chemistry
Senior Research Scientist, TRIUMF

Dr. John M. D'Auria
Supervisor
Professor Emeritus, Department of Chemistry

Dr. Dipankar Sen
Internal Examiner
Professor, Department of Chemistry

Dr. Michael E. Cox
Internal Examiner
Assistant Professor, Faculty of Medicine - UBC

Dr. Jeanne M. Link
External Examiner
Associate Professor, Radiology
University of Washington

Date Defended/Approved: August 8, 2007

Abstract

The goal of this research project was to investigate the feasibility of Rhenium-186 (^{186}Re) as an isotope for radioimmunotherapy. ^{186}Re is commonly produced via neutron capture in a reactor. This leads to a product with low specific activity (LSA), which is not optimal for site specific targeting. As such, the possibility of producing high specific activity (HSA) ^{186}Re from a charged particle reaction was investigated. The HSA ^{186}Re was produced via the ^{186}W(p,n) reaction at TRIUMF using the TR13 cyclotron. A dry distillation chemistry method was developed for the separation of trace rhenium from tungsten targets. Antibodies were labeled with both HSA ^{186}Re and reactor produced LSA ^{186}Re using a mercaptoacetyltriglycine chelate, which was synthesized as previously described in the literature.

Cell lines that do (R+) and do not (R-) express the IGF receptor were examined for radiosensitivity to external beam irradiation and exposure to free ^{186}Re using traditional methods including vital dye exclusion, clonogenicity and fluorescence activated cell sorting. An antibody known to be specific for the IGF receptor (1H7) was labeled with HSA and LSA ^{186}Re and incubated with both R+ and R- cell lines. Specific antibody binding was assessed.

In addition, experiments were conducted at both Oak Ridge National Laboratory using an electron beam plasma ion source and at a TRIUMF with a proof-of-principle cusp ion source test stand to determine the feasibility of producing carrier-free ^{186}Re from a neutron irradiated target.

This work demonstrates that ^{186}Re can be produced in high specific activity from the ^{186}W(p,n) reaction. Although yields from the cyclotron reaction

were determined to be too low to produce HSA ^{186}Re in patient quantities in an economically feasible manner using current technology, significant quantities could be produced for subsequent experiments. Antibodies were successfully labeled with both HSA and LSA ^{186}Re. No increased binding was observed with the HSA ^{186}Re. A cusp ion source test stand was successfully constructed at TRIUMF and beams of 10^{12} Re ions per second have been accelerated, illustrating the possibility of producing HSA ^{186}Re from reactor targets.

Keywords: Rhenium-186, radioimmunotherapy, IGF-1R

To my friends and family,
who have always supported me in whatever crazy thing I wanted to do

"There is a theory which states that if ever anyone discovers exactly what the Universe is for and why it is here, it will instantly disappear and be replaced by something even more bizarre and inexplicable.

There is another theory which states that this has already happened."

-- Douglas Adams

Acknowledgements

Thanks to my supervisors: Tom Ruth and Paul Percival. Tom, for treating my like a colleague while I was still a student and always taking my ideas seriously, whatever they were, and Paul, for his continued support throughout the entire process and for stepping in a during few stumbling blocks.

Thanks to John D'Auria, for getting me into this incredibly diverse and wonderful field.

Thanks to Michael Cox, for being completely unafraid to jump into a totally different area of science.

Thanks to the TRIUMF PET group past, present and associated, Ken Buckley (the cyclotron magician), James Inkster (synthesist extraordinaire), Prateek Katri, Mike Adam, Wade English, Kelly Worth, Hayes Dougan, Jain-ming Lu, Dirk Becker, Jennifer Greene, Salma Jivan, Wayne Sievers, Andrei Studenov, Milan Vukovic and Yulia Rozen.

Thanks to everyone from Oak Ridge National Laboratory, Ken Carter, Dan Stracener, Andreas Kronenberg and John Wenzel, who treated me like one of the gang during my visit.

Thanks to John Wilson and Steve McQuarrie at EPC and Dave Schlyer and Mike Schueller from BNL for assistance with the cross-section work.

Thanks to Susan MacPhail and Peggy Olive at the BC Cancer Agency for invaluable help with the external beam irradiations.

Thanks to Mike MacDonald and Keerthi Jayamanna for their extensive ion sourcery knowledge.

Thanks to Darrell Fisher for alerting me to the use of Varskin3 for dose calculations.

Special thanks to Katie Gagnon and Peter Machule, who could always be relied upon for assistance far beyond the call of duty.

Table of Contents:

List Of Tables

List of Figures

Glossary

Antagonist	A binding partner (ligand) of a receptor that inhibits the function of the receptor by blocking it's active site
Antigen	A substance that causes an immune system to produce antibodies against it.
Apoptosis	Programmed cell death. A cascade of biochemical events resulting in cell suicide and decomposition of the cell components.
Apoptotic bodies	Formed when a cell undergoes apoptosis, causing degradation of its organelles.
Auger electron	A relatively low energy electron emitted during electron capture decay as an alternative to x-ray emission.
Bombesin	A 14-amino acid peptide that shows high affinity towards the Gastrin Releasing Peptide receptor that is commonly over-expressed in prostate cancer.
CD20 antigen	A non-glycosylated phophoprotein expressed on the surface of all mature B-cells.
1-ethyl-3-(3-dimethlyaminopropyl) carbodiimide (EDC)	A common coupling agent used in peptide synthesis. It is a carboxyl-activating agent for the coupling of amines to yield amide bonds.
Fibroblasts	Cells that provide structural framework for many tissues. A common cell type found in connective tissue.
Flow cytometry	Technique for sorting microscopic particles suspended in a stream of liquid.

Follicular histology	Predominantly small, cleaved cells. Normal follicular B-cells reside in the lymph nodes, hence the name.
G_0 phase	State of withdrawal from the cell cycle.
G_1 phase	Gap-1 phase between the end of cytokinesis and the start of DNA synthesis.
G_2 phase	Gap-2 phase between the end of DNA synthesis and the beginning of mitosis.
Gray	Used to denote energy deposited per unit mass from radiation. Equal to 1 Joule/kg.
Hematologic	Pertaining to the blood
Humanized antibodies	Produced to circumvent the human body's immune system, typically resulting in half-human/half- mouse antibodies.
Immortalized cell line	A cell line capable of an unlimited number of cell divisions.
Immunoprecipitation	Technique in which a receptor can be precipitated out of solution using an antibody specific for that receptor.
J-value	Coupling constant in Nuclear Magnetic Resonance Spectroscopy (NMR). The frequency difference in Hz between the component peaks of a doublet.
M phase	Mitotic phase. The period of cell cycle in which the nucleus and cytoplasm divide.
Metastable state	Denoted A^m, where A is the element. An excited state of an isotope.

Monoclonal	Cloned from a single parent cell.
Phosphate Buffered Saline (PBS)	Saline containing a phosphate buffer to help maintain a constant pH and isotonic conditions.
R- cell line	Mouse embryonic fibroblast cell line that has had the IGF-1R knocked out.
R+ cell line	R- cell line that has had the IGF-1R reintroduced.
Recoil Energy	Energy imparted to the daughter species of a radioactive decay due to conservation of momentum.
S phase	Period of the cell cycle in which DNA is synthesized.
SDS-PAGE (Sodium Dodecyl Sulfate PolyAcrylamide Gel Electrophoresis)	Technique used to separate proteins via their rate of migration in an electric field. This is dependent on the size, charge and shape or the molecule.
Specific Activity	Radioactivity per mass of product.
Szilard-Chalmers	Effect in which the recoil of an atom produced by a neutron capture nuclear reaction breaks free of its chemical bonds.
Tyrosine kinase	Enzyme that phosphorylates a specific tyrosine residue on a protein.
Western Blot	Analytical technique in which proteins separated via gel electrophoresis are transferred to a sheet of paper for further analysis, usually by means of a labeled antibody.

Chapter 1

Introduction and Thesis Overview

1.1 Radiotherapy and the Interaction of Radiation in Tissue

Studies on the effect of radiation on the human body have been ongoing since Roentgen discovered X-rays in 1895 [1]. Now, over one half of cancer patients will have radiotherapy at some point during their course of treatment [2]. This radiation therapy can be in the form of X-rays from a medical linear accelerator, gamma rays from a ^{60}Co source, heavy ions from a particle accelerator (mainly protons or α particles), or from radioactive α or β emitters, which are injected into the patient.

Biological effects from ionizing radiation damage are mainly due to damage to DNA. These DNA lesions can be produced by direct ionization of the DNA or indirectly, mainly via chemical interaction of free radicals [3]. The

degree of ionization along a radiation track by various types of radiation varies greatly. Heavy ions, such as α particles produce dense tracks of ionization in their path, while X-rays and high energy β particles have much sparser ionization tracks [3]. Thus the distribution of ionizations and the types of lesion (single strand breaks, double strand breaks and multiple damaged sites) will depend on the nature of the incident particle. As little as 1-4 α-particle traversals through a cell nucleus can kill a mammalian cell, while up to 20,000 β-particle traversals may be necessary to invoke cell death [3].

Although radiation delivered from linear accelerators or ^{60}Co sources is still the most common form of radiotherapy, much progress has been made into conjugating radioisotopes to molecules for targeted delivery of radiation.

1.2 Radioisotopes for Cancer Treatments and Radioimmunotherapy

Therapeutic radiopharmaceuticals are radiolabeled molecules which are designed to deliver therapeutic doses of ionizing radiation to specific disease sites (most often cancerous tumors) with high specificity in the body [4]. Often this type of therapy is palliative, and not intended to be curative, but recently there has been much progress into development of site-specific radiopharmaceuticals where complete remission of the disease is possible [5] . These so-called "magic bullet" radiopharmaceuticals hold hope for patients who

have relapsed following traditional chemo- or radiation therapy or whose disease has been refractory to conventional treatment. Treatment with compounds of this type based on radiolabeled antibodies is known as radioimmunotherapy (RIT). This subject will be covered in detail in Chapter 2. With the approval of two compounds, ^{131}I-tositumab (Bexxar®; Corixa/GlaxoSmithKline) and ^{90}Y-ibritumomab tiuxetan (Zevalin®, Biogen Idec, Inc.), based on this technology by Health Canada in 2005 for Non-Hodgkins Lymphoma (NHL), this type of therapy is gaining importance [6].

1.3 Radiolabeling of Antibodies and the Importance of Specific Activity

Recently much work had been conducted into the radiolabeling of monoclonal antibodies to test the efficacy of radioimmunotherapy [7-9]. Many different radionuclides have been used for this purpose including α, β and Auger electron emitters [10, 11]. There are two general methods for radiolabeling of antibodies: direct labeling and labeling via a chelator molecule. Typically the former is used for radiohalogen labeling and the latter is used for radiometal labeling.

For site-specific therapy, high specific activity or a large number of radiolabeled (hot) molecules per number of unlabeled (cold) molecules is

desirable. If an excess of "cold" (non-radioactive) labeled antibodies are present, they may saturate the binding sites on the target (cancer) cells and hence the radiation dose delivered to the cells will not be sufficient to induce apoptosis (programmed cell death). This is illustrated in Figure 1.1

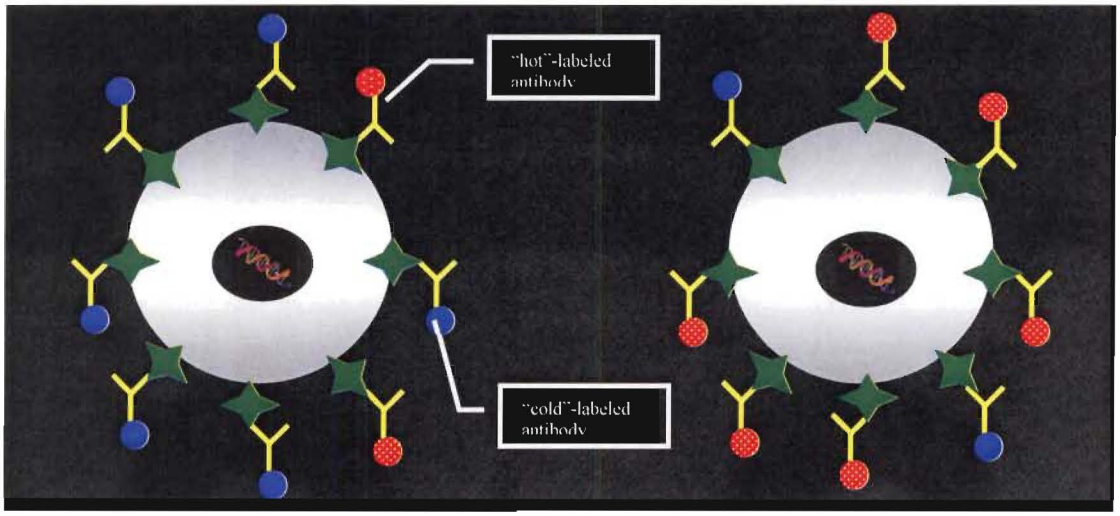

Figure 1.1
Illustration of low (left) vs. high (right)
specific activity radioisotopes in radioimmunotherapy

While this fact is mentioned repeatedly in the literature, no in-depth studies into the effect of specific activity on *in vitro* cell kill have been conducted. In addition, *in vivo* studies with ^{186}Re-labeled antibodies have shown that larger numbers of chelate groups per antibody can alter the biodistribution of the antibody [12], and thus the specific activity problem cannot be solved by conjugating more groups to each antibody.

1.4 Current Methods of Production of ^{186}Re

^{186}Re has been considered a good candidate for radiotherapy because it decays by β^- emission and it has a half-life of 3.7 days, which matches the biological half-life of many antibodies in humans [13]. In addition, it also emits a γ-ray at 137 keV (branching ratio of 9.5 %), which can be imaged by Single Photon Emission Computed Tomography (SPECT) to determine the distribution of the radioactivity in the body. A decay scheme of ^{186}Re is shown below.

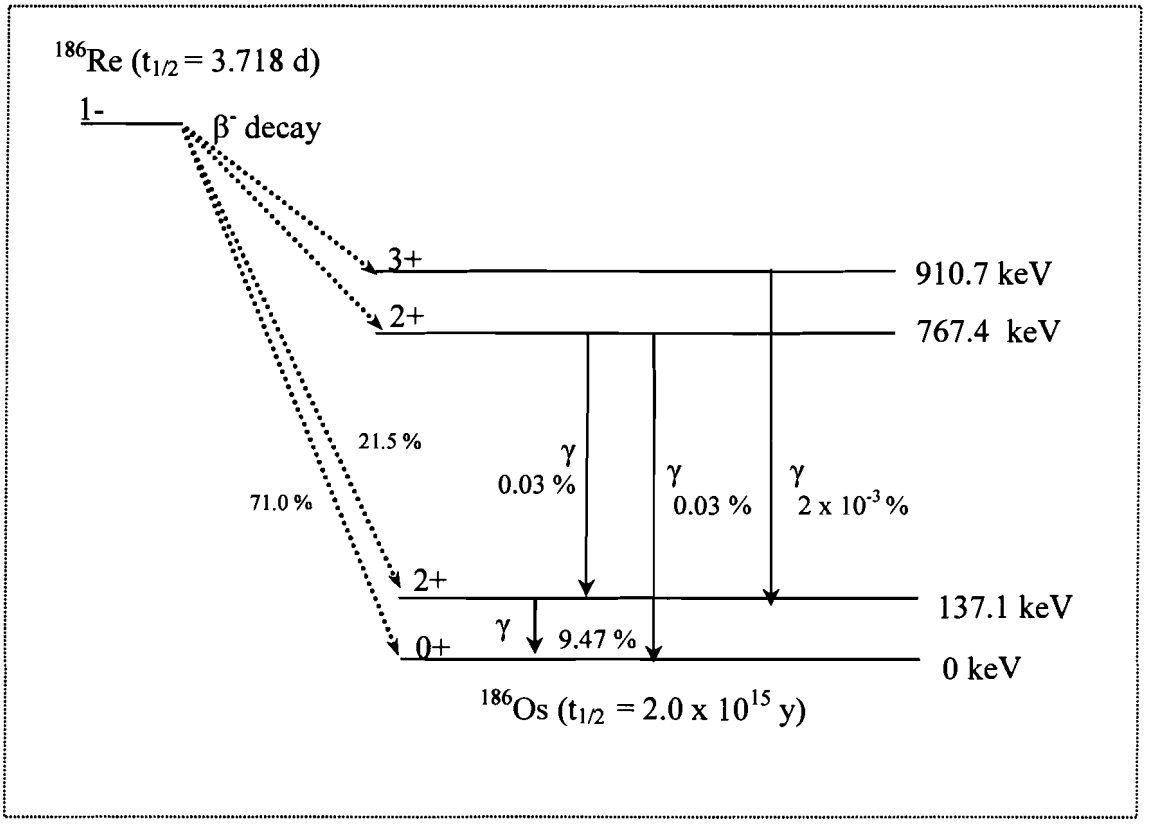

Figure 1.2
^{186}Re decay scheme (adapted from [14])

This isotope is also a good choice because it is chemically similar to the commonly used gamma emitter ^{99m}Tc, which has already been extensively studied. 85% of all nuclear medicine imaging studies involve some form of ^{99m}Tc. Both ^{186}Re and ^{99m}Tc are group 7 transition metals and are commonly found in high oxidation states (+5 to +7).

^{186}Re is commonly produced by neutron capture in reactors via the ^{185}Re(n, γ) reaction. This results in a product with low specific activity (LSA) as the target atom is the same element as the product and thus cannot be separated chemically. Progress has been made using the recoil energy of this reaction to separate ^{185}Re from ^{186}Re via the Szilard-Chalmers effect with some success, but this method is not commonly used [15]. Despite the lack of availability of high specific activity, several groups have reported success with radioimmunotherapy with ^{186}Re [16-18]. ^{186}Re has also been produced via the ^{186}W(p,n)reaction in high specific activity [19, 20]. Unfortunately, the yield for this reaction is low and this route for therapeutic doses of ^{186}Re is not presently economically feasible [21].

Although one *in vivo* study indicated similar localization pattern for bombesin (a 14 amino acid peptide) labeled with high versus low specific activity ^{186}Re, more in depth studies are required to understand the impact of high specific activity ^{186}Re in therapeutic applications [22].

1.5 Thesis Overview

The goal of this research project was to investigate the feasibility of ^{186}Re as a radionuclide for radioimmunotherapy. ^{186}Re is commonly produced via neutron capture in a reactor. This leads to a product with low specific activity, which is not optimal for site specific targeting. As such, the possibility of producing high specific activity (HSA) ^{186}Re from a charged particle reaction was investigated. High specific activity ^{186}Re was produced via the ^{186}W(p,n) reaction at TRIUMF using the TR13 cyclotron. A chemistry method for the separation of trace rhenium from tungsten targets was developed. Antibodies specific for the Insulin-like Growth Factor Receptor–1 (IGF-1R) were labeled with HSA and LSA ^{186}Re and incubated with mouse embryonic fibroblasts that do and do not express IGF-1R to determine specific receptor binding. The role of the IGF-1R in radiation therapy was also investigated.

In addition, studies with an ion source and a mass separator were conducted at Oak Ridge National Lab and at TRIUMF with radioactive rhenium isotopes to determine the feasibility of producing no carrier added ^{186}Re from a neutron-irradiated target.

1.6 References:

1. Rockwell, S., *Experimental radiotherapy: a brief history.* Radiat Res, 1998. **150**(5 Suppl): p. S157-69.

2. *RadiologyInfo.* [cited 2007 July 19th]; Radiological Society of North America radiology resource for patients]. Available from: http://www.radiologyinfo.org.

3. Kassis, A.I. and S.J. Adelstein, *Radiobiologic principles in radionuclide therapy.* J Nucl Med, 2005. **46 Suppl 1**: p. 4S-12S.

4. Volkert, W.A. and T.J. Hoffman, *Therapeutic radiopharmaceuticals.* Chemical Reviews, 1999. **99**(9): p. 2269-2292.

5. Vose, J.M., *Bexxar((R)): Novel radioimmunotherapy for the treatment of low-grade and transformed low-grade non-Hodgkin's lymphoma.* Oncologist, 2004. **9**(2): p. 160-172.

6. *Health Canada website (Bexxar).* 2005 [cited; Available from: http://www.hc-sc.gc.ca/dhp-mps/prodpharma/activit/proj/sbd-smd/nd_ad_2005_bexxar_084518_e.html.

7. Borjesson, P.K.E., et al., *Radioimmunodetection and radioimmunotherapy of head and neck cancer.* Oral Oncology, 2004. **40**(8): p. 761-772.

8. Britton, K.E., *Radioimmunotherapy of non-Hodgkin's lymphoma.* Journal of Nuclear Medicine, 2004. **45**(5): p. 924-925.

9. Brouwers, A.H., et al., *Optimization of radioimmunotherapy of renal cell carcinoma: Labeling of monoclonal antibody cG250 with I-131, Y-90, Lu-177, or Re-186.* Journal of Nuclear Medicine, 2004. **45**(2): p. 327-337.

10. Wesley, J.N., et al., *Systemic radioimmunotherapy using a monoclonal antibody, anti-Tac directed toward the alpha subunit of the IL-2 receptor armed with the alpha-emitting radionuclides Bi-212 or At-211.* Nuclear Medicine and Biology, 2004. **31**(3): p. 357-364.

11. Behr, T.M., et al., *Therapeutic advantages of Auger electron- over beta-emitting radiometals or radioiodine when conjugated to internalizing antibodies.* European Journal of Nuclear Medicine, 2000. **27**(7): p. 753-765.

12. vanGog, F.B., et al., *Monoclonal antibodies labeled with rhenium-186 using the MAG3 chelate: Relationship between the number of chelated groups and biodistribution characteristics.* Journal of Nuclear Medicine, 1996. **37**(2): p. 352-362.

13. Colnot, D.R., et al., *Phase I therapy study of 186Re-labeled chimeric monoclonal antibody U36 in patients with squamous cell carcinoma of the head and neck.* J Nucl Med, 2000. **41**(12): p. 1999-2010.

14. *National Nuclear Data Center Chart of the Nuclides.* 2006 [cited; Available from: http://www.nndc.bnl.gov/chart.

15. Zhang, Z.Y., et al., *Preparation of Re-186 and Re-188 with high specific activity by the Szilard-Chalmers effect.* Journal of Labelled Compounds & Radiopharmaceuticals, 2000. **43**(1): p. 55-64.

16. Colnot, D.R., et al., *Phase I therapy study of Re-186-labeled chimeric monoclonal antibody U36 in patients with squamous cell carcinoma of the head and neck.* Journal of Nuclear Medicine, 2000. **41**(12): p. 1999-2010.

17. Postema, E.J., et al., *Dosimetric analysis of radioimmunotherapy with Re-186-labeled bivatuzumab in patients with head and neck cancer.* Journal of Nuclear Medicine, 2003. **44**(10): p. 1690-1699.

18. Kinuya, S., et al., *Radioimmunotherapy with Re-186-labeled monoclonal antibody to treat liver metastases of colon cancer in nude mice.* Cancer Biotherapy and Radiopharmaceuticals, 2002. **17**(6): p. 681-687.

19. Shigeta, N., et al., *Production method of no-carrier-added Re-186.* Journal of Radioanalytical and Nuclear Chemistry-Articles, 1996. **205**(1): p. 85-92.

20. Zhang, X.D., et al., *Excitation functions for W-nat(p,xn)Re181-186 reactions and production of no-carrier-added Re-186 via W-186(p,n) Re-186 reaction.* Radiochimica Acta, 1999. **86**(1-2): p. 11-16.

21. Lapi, S., et al., *Production cross-sections of 181-186Re isotopes from proton bombardment of natural tungsten.* Appl Radiat Isot, 2007. **65**(3): p. 345-9.

22. Moustapha, M.E., et al., *Preparation of cyclotron-produced Re-186 and comparison with reactor-produced Re-186 and generator-produced Re-188 for the labeling of bombesin.* Nuclear Medicine and Biology, 2006. **33**(1): p. 81-89.

Chapter 2

Radioimmunotherapy

2.1 Introduction

Radioimmunotherapy (RIT) is targeted radiotherapy using antibodies as the targeting agent. Antibodies that are specific for certain types of receptors which are typically overexpressed on cancerous cells, are labeled with radionuclides which emit cell damaging radiation, thus enabling delivery of high doses of radiation to cancer sites, while sparing normal tissue.

Antibodies are proteins which are secreted by the body and bind specifically to foreign antigens [1]. Immunoglobulin G (IgG) antibodies are typically composed of one light chain and one heavy chain connected by disulphide bridges in a typical Y shape. The shape consists of two domains, the Fab domain (so named because it is the fragment that contains the antigen

binding site) and the Fc domain (so named because it is the fragment that remains constant) [1]. A generic antibody structure is shown below in Figure 2.1.

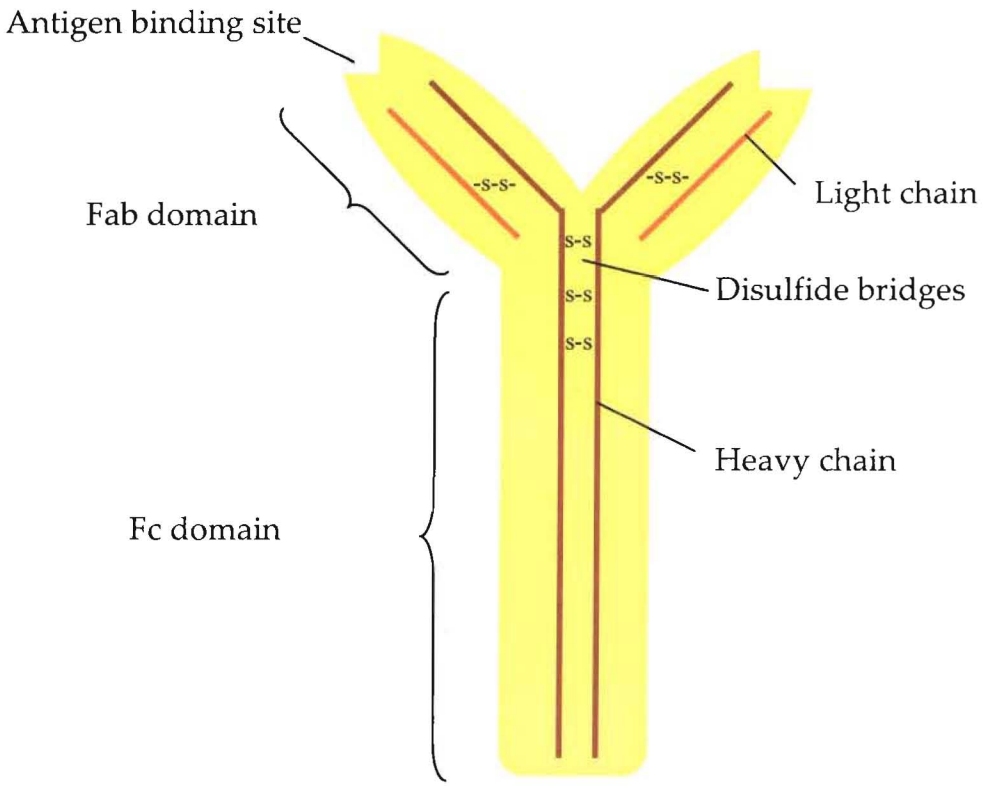

Figure 2.1
Schematic drawing of a generic IgG antibody

At the turn of the 19th century, Paul Ehrlich came up with the idea that antibodies could act as "magic bullets" which would target specific sites of disease [2]. In the 1950's the first antibody-radionuclide conjugate was produced, but the United States FDA and Health Canada have only approved the first radioimmunotherapeutics in the last few years (see sections 2.3 and 2.4

Appendix 2

Documents Concerning the

Rhenium Ion Source Test Stand

for details). The use of antibodies in radioimmunotherapy is still evolving with investigations into new radionuclides, radiochemistry, and host toxicities contributing to the field. The only currently approved radioimmunotherapeutics in the United States and Canada are for Non-Hodgkin's Lymphoma (NHL). While there have been some investigations into translating this technology into a therapeutic for solid tumors, recent efforts have focused mainly on hematologic malignancies.

2.2 Non-Hodgkin's Lymphoma

Non-Hodgkin's Lymphoma is the sixth most common cause of cancer deaths. More than 80 % of NHLs are of B-cell origin and a substantial number of these tumors will be of follicular histology [3]. Although generally treatable, these tumors are typically incurable. This type of cancer is a good candidate for radioimmunotherapy for several reasons. (1) Lymphomas are highly radiosensitive[1]. (2) A variety of antibodies exist which are known to target lymphoid specific antigens (3). Several of these unlabeled antibodies exhibit antitumor activity in some patients with NHL [5].

[1] Cells are most sensitive to radiation in the mitotic phase due to the possibility of multiple double strand breaks, which can lead to chromosomal aberrations during the mitotic process [4]. Because lymphoma cells are rapidly dividing the percentage of cells in m-phase is higher than normal tissue.

The CD20 antigen is densely expressed on the surface of nearly all B-cell lymphomas. This antigen is ideal for targeting as it is not shed from the cell surface or internalized (and therefore not metabolized by the cell) [6]. Although CD20 is expressed on some normal B-cells, it is not expressed by pre-B cells in the bone marrow or by mature plasma cells and hence the targeted dose will spare the bone marrow and other target tissues. An expression profile of CD20 expression is shown in Figure 2.2.

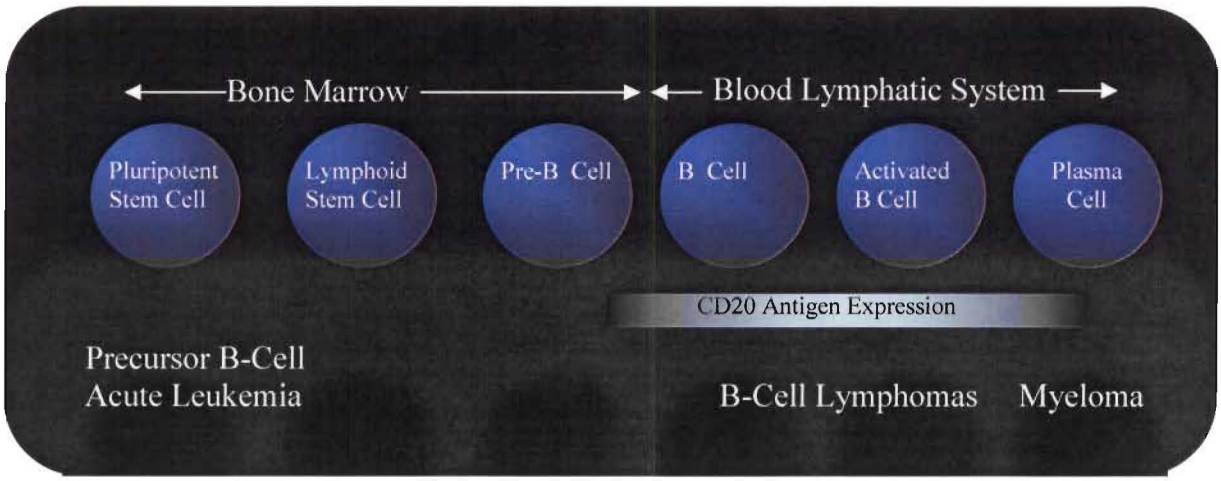

Figure 2.2
B-cell maturation and CD20 expression (adapted from [3])

Currently there are two radiopharmaceuticals approved by both the FDA and Health Canada which target the CD20 antigen on mature B-cells.

2.3 Bexxar®

^{131}I-tositumab (Bexxar®; Corixa/GlaxoSmithKline) was approved by Health Canada in August, 2005 for the treatment of follicular Non-Hodgkin's Lymphoma. In Canada, Bexxar® is indicated for the "treatment of patients with CD20 positive relapsed or refractory, low grade, follicular or transformed Non-Hodgkin's Lymphoma" [7]. Bexxar® is composed of a ^{131}I- labeled murine monoclonal antibody which targets the CD20 antigen [8].

Treatment with Bexxar® consists of two steps: a dosimetric step followed by a therapeutic step. The dosimetric step involves administration of a combination of unlabeled antibody followed by a small dose of antibody labeled with ^{131}I (typically 5mCi) [6]. The dosimetric step allows for the therapeutic dose to be varied according the rate of clearance of the radioactivity from the body of the patient. Patients that have a rapid clearance are given a higher amount of the radioactive drug than patients with a slow clearance in order to achieve a predetermined dose [3]. Because ^{131}I has an imagable gamma emission (365 keV, 81.5 %), the distribution of the labeled antibody can also be determined in the dosimetric step with Single Photon Emission Computed Tomography (SPECT) imaging. If the distribution of the radioactivity looks normal (high uptake in the tumor sites and low uptake in the spleen and liver), a week later the patient will receive a therapeutic dose (typically ~30 mCi). The patient is

again given a dose of unlabeled antibody followed by a dose of ^{131}I labeled antibody. The predose of unlabeled antibody (in both the dosimetric and therapeutic steps) improves tumor targeting by binding to accessible B-cells in the blood and spleen, thus allowing the subsequently administered antibody to reach more distant tumor sites [3].

Results from trials with Bexxar® have been extremely promising, with many patients that have been refractory (unresponsive) to standard chemo- or radiotherapy responding favorably to this treatment. Figure 2.3 shows the efficacy of Bexxar® within various patient populations (newly diagnosed, relapsed following chemo- or radiotherapy and refractory to chemo- or radiotherapy) with low grade B-cell Non-Hodgkins Lymphoma. Partial Responders (darks bars) are patients that have some sign of response (for example tumor shrinkage), while Complete Responders (light bars) are patients that have no sign of the disease after treatment. The Partial Responder numbers also include the Complete Responders as an indication of total patient response.

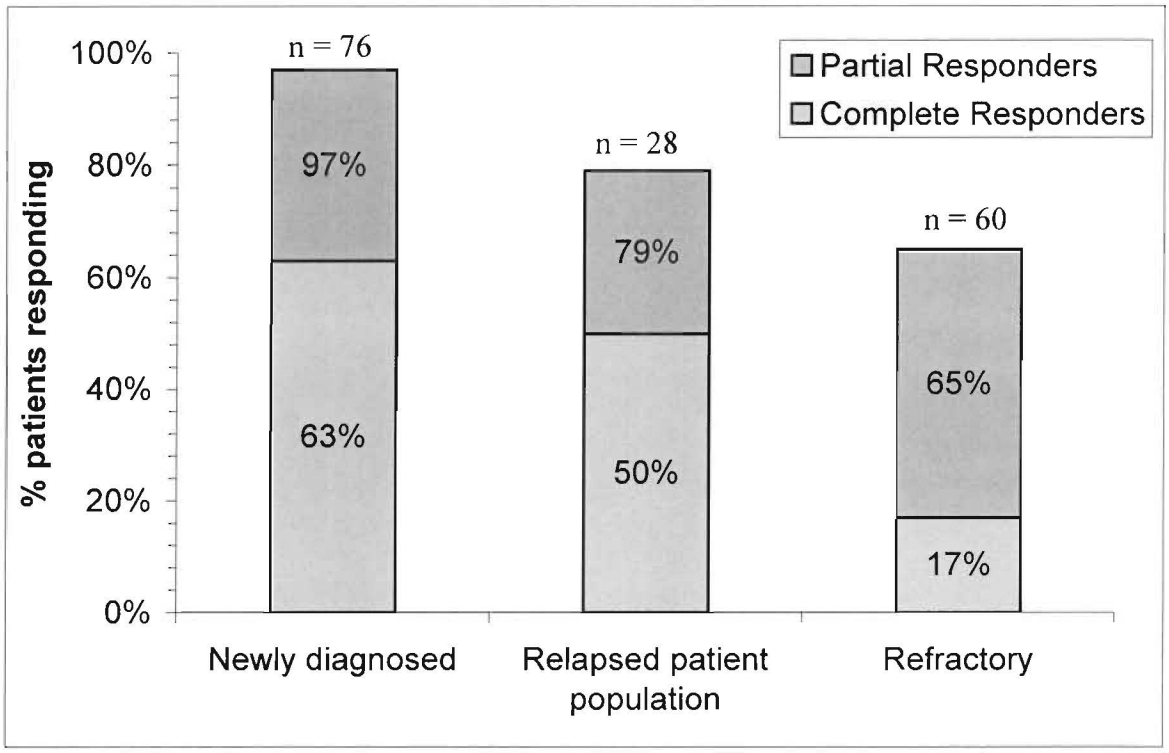

Figure 2.3
Evaluation of Bexxar® within various patient populations (data from [6])

Because of the possibility of ^{131}I-release from Bexxar®, which is known to target the thyroid, blockade with a saturated solution of potassium iodide is given from day one through fourteen of treatment. Despite this treatment, some 5-10 % of patients will develop hyperthyroidism. With thyroid blockade, the majority of free ^{131}I is excreted through the kidneys. Also, many patients experience low platelet and hemoglobin counts, as with most therapeutic radioactive treatments, as the bone marrow is very radiation sensitive. Because ^{131}I is also a gamma emitter, patients may (in some cases) present a radiation risk for other family members, in particular young children, but in most cases

patients are treated on an outpatient basis. Currently Bexxar® is approved for only a single-dose treatment, but clinical trials suggest that repeated doses may be well tolerated and beneficial.

2.4 Zevalin®

^{90}Y-ibritumomab tiuxetan (Zevalin®, Biogen Idec, Inc.) was approved by Health Canada in May, 2005 [9]. It is approved for "the treatment of relapsed or refractory low grade, follicular, or transformed B-cell non-Hodgkin's lymphoma" [9]. Similar to Bexxar®, it is a labeled murine monoclonal antibody which targets the CD20 antigen on mature B-cells; however, it differs from Bexxar® in several ways. First, Zevalin® consists of an antibody labeled with ^{90}Y ($t_{1/2}$ = 2.7 d). As this isotope is a pure β emitter, imaging must be done using an ^{111}In labeled antibody as a surrogate. In Canada this imaging step is not required, and the amount of radioactivity administered to the patient is simply calculated by weight (dose is administered on a per kilogram basis up to a maximum of 32 mCi). As with Bexxar® a predose with an unlabeled antibody is performed in order to increase tumor cell targeting.

Zevalin® is also showing promising results. In a phase III randomized trial consisting of 143 patients, 80 % of patients achieved an overall response and 34 % achieved a complete response [10].

Side effects from Zevalin® are similar to those with Bexxar® including hemalogical effects such as low platelet (thrombocytopenia) and white blood cell (neutropenia) counts [10]. As free ^{90}Y is excreted by the kidneys, thyroid blockage is not necessary. Also, as ^{90}Y is a pure β emitter with no γ emissions, it has fewer environmental radiation restrictions. For this reason, treatment with Zevalin® may be preferable in cases where close proximity to family members (as in the case with small children) is unavoidable.

2.5 Other Radioimmunotherapy Drugs

Many other radionuclides are becoming of interest for this type of therapy. Although β emitters have been the most common radioisotopes, α emitters and Auger electron emitters are starting to be explored for this type of therapy. A short list of radionuclides of interest for radioimmunotherapy can be found in table 2.1 [11].

Table 2.1
Characteristics of radionuclides of interest for radioimmunotherapy

Isotope	Symbol	Half-life (h)	Emission (for therapy)	Maximum particle energy (keV)	Maximum particle range in water (mm)
Iodine-131	^{131}I	193	β	610	2.0
Yttrium-90	^{90}Y	64	β	228	12.0
Lutetium-177	^{177}Lu	161	β	496	1.5
Copper-67	^{67}Cu	62	β	577	1.8
Rhenium-186	^{186}Re	89	β	1080	5.0
Rhenium-188	^{188}Re	17	β	2120	11.0
Astatine-211	^{211}At	7.2	α	7450	0.08

When considering a radionuclide that may be appropriate for radioimmunotherapy, there are several things to consider:

1) method of production and availability (accelerator, reactor, generator)

2) chemical (ease of incorporation into the antibody complex) and decay properties

3) chemical and radiochemical purity.

^{186}Re and ^{188}Re are emerging as good candidates for this type of therapy due to their favorable half-lives (89 h and 17 h respectively) and decay properties.

^{188}Re is commercially available as a generator isotope. The parent radionuclide, ^{188}W, is produced by double neutron capture on stable tungsten ^{186}W. The tungsten is loaded onto a silica column in the form of tungstate and

the decay product, ^{188}Re, is eluted as perrhenate with a saline solution. This is similar to the common ^{99m}Mo/^{99m}Tc generator found in most nuclear medicine departments. ^{188}Re-labeled antibodies have been used in several animal studies [12, 13]. Despite the availability of ^{188}Re, ^{186}Re appears to be gaining popularity as a therapeutic isotope possibly due to the shorter path length (and hence dose spared to surrounding tissues) of the emitted beta particle.

^{186}Re is commonly produced by neutron capture on stable ^{185}Re. ^{186}Re-labeled antibodies have to date been used in several phase I clinical trials [14-16] with initial promising results. During one study conducted to determine the maximum tolerated dose of ^{186}Re-U36 (a chimeric monoclonal antibody against the CD44 antigen) in patients with head and neck squamous cell carcinoma, a marked reduction on tumor size was observed in two of the thirteen subjects [15]. In a Phase 1 study with ^{186}Re-eprauzumab (a monoclonal antibody directed against the CD22 antigen on B-cells), an objective response was observed in five out of fifteen patients, with one patient in complete remission for four months [16].

While Bexxar® and Zevalin® have both proven to be efficacious therapeutics, research into other isotope/antibody combinations is necessary for several reasons:

1) Other antibodies which target overexpressed receptors on different types of cancer are clearly required if this type of therapy is to gain importance for non-hematological malignancies.

2) The energy difference in emitted β particles from varying isotopes will lead to different ranges in tissue, and thus the range can be tuned to match the size of the tumor.

3) The difference in half-lives of various isotopes allows for antibodies (or fragments) of varying residence time in the body to be used [17].

2.6 References

1. Harlow, E. and D. Lane, *Antibodies: a laboratory manual.* 1988, Cold Spring Harbor, NY: Cold Spring Harbor Laboratory. xiii, 726 p.

2. Sharkey, R.M. and D.M. Goldenberg, *Perspectives on cancer therapy with radiolabeled monoclonal antibodies.* J Nucl Med, 2005. **46 Suppl 1**: p. 115S-27S.

3. Wahl, R.L., *Tositumomab and I-131 therapy in non-Hodgkin's lymphoma.* Journal of Nuclear Medicine, 2005. **46**: p. 128S-140S.

4. Pawlik, T.M. and K. Keyomarsi, *Role of cell cycle in mediating sensitivity to radiotherapy.* International Journal of Radiation Oncology Biology Physics, 2004. **59**(4): p. 928-942.

5. Kaminski, M.S., et al., *Radioimmunotherapy with iodine I-131 tositumomab for relapsed or refractory B-cell non-Hodgkin lymphoma: updated results and long-term follow-up of the University of Michigan experience.* Blood, 2000. **96**(4): p. 1259-1266.

6. Vose, J.M., *Bexxar((R)): Novel radioimmunotherapy for the treatment of low-grade and transformed low-grade non-Hodgkin's lymphoma.* Oncologist, 2004. **9**(2): p. 160-172.

7. *Health Canada website (Bexxar).* 2005 [cited; Available from: http://www.hc-sc.gc.ca/dhp-mps/prodpharma/activit/proj/sbd-smd/nd_ad_2005_bexxar_084518_e.html.

8. Seldin, D.W., *Techniques for using Bexxar for the treatment of non-Hodgkin's lymphoma.* J Nucl Med Technol, 2002. **30**(3): p. 109-14.

9. *Health Canada website (Zevalin).* 2005 [cited; Available from: http://www.hc-sc.gc.ca/dhp-mps/prodpharma/activit/proj/sbd-smd/nd_ad_2005_zevalin_076192_e.html.

10. Borghaei, H. and R.J. Schilder, *Safety and efficacy of radioimmunotherapy with yttrium 90 ibritumomab tiuxetan (Zevalin).* Semin Nucl Med, 2004. **34**(1 Suppl 1): p. 4-9.

11. Goldenberg, D.M., *Targeted therapy of cancer with radiolabeled antibodies.* J Nucl Med, 2002. **43**(5): p. 693-713.

12. Li, G., et al., *The experimental study on the radioimmunotherapy of the nasopharyngeal carcinoma overexpressing HER2/neu in nude mice model with intratumoral injection of 188Re-herceptin.* Nucl Med Biol, 2005. **32**(1): p. 59-65.

13. Schmidt, P.F., S.V. Smith, and P.G. Bundesen, *188Re DD-3B6/22 Fab' for use in therapy of ovarian cancer: labelling and animal studies.* Nucl Med Biol, 1998. **25**(7): p. 639-49.

14. Borjesson, P.K., et al., *Phase I therapy study with (186)Re-labeled humanized monoclonal antibody BIWA 4 (bivatuzumab) in patients with head and neck squamous cell carcinoma.* Clin Cancer Res, 2003. **9**(10 Pt 2): p. 3961S-72S.

15. Colnot, D.R., et al., *Phase I therapy study of 186Re-labeled chimeric monoclonal antibody U36 in patients with squamous cell carcinoma of the head and neck.* J Nucl Med, 2000. **41**(12): p. 1999-2010.

16. Postema, E.J., et al., *Final results of a phase I radioimmunotherapy trial using (186)Re-epratuzumab for the treatment of patients with non-Hodgkin's lymphoma.* Clin Cancer Res, 2003. **9**(10 Pt 2): p. 3995S-4002S.

17. Jain, M., G. Venkatraman, and S.K. Batra, *Optimization of radioimmunotherapy of solid tumors: biological impediments and their modulation.* Clin Cancer Res, 2007. **13**(5): p. 1374-82.

Chapter 3

Cross-section Measurements and Production of High Specific Activity ^{186}Re

3.1 Introduction

High specific activity ^{186}Re can be produced by proton bombardment of enriched tungsten targets [1-3] . However, there are large discrepancies in the literature for the excitation function of the ^{186}W(p,n)^{186}Re reaction [1, 2, 4]. In order to better assess the feasibility of producing multi-mCi levels of ^{186}Re for therapeutic applications via the ^{186}W(p,n)^{186}Re reaction, the excitation function was measured in our laboratory. Cross sections for the production of ^{181}Re, ^{182m}Re, ^{182g}Re, ^{183}Re ^{184}Re, and ^{186}Re from natural tungsten were measured using the stacked foil technique for proton energies up to 17.6 MeV [5]. By examining

the production of a range of Re isotopes, multiple comparisons between the current work and previous results can be drawn. This provides for a check on the estimates derived for the reaction of primary interest in this study, the production of ^{186}Re. In addition, the experimental values were compared to excitation functions as calculated by the EMPIRE-II nuclear reaction code [6].

High specific activity ^{186}Re was produced by proton bombardment of enriched tungsten target material. A dry distillation technique was employed to separate the ^{186}Re from the target material with high recoveries.

3.2 Cross-section Measurements

3.2.1 Materials and Methods

High purity tungsten foils (99.998%, EPSI products, Ashland, OR, USA) of natural isotopic composition, each of thickness 0.025 ± 0.002 mm (48 ± 4 mg/cm^2), were loaded into a helium-cooled target body for irradiation. The isotopic composition of natural tungsten is given in Table 3.1.

Table 3.1
Isotopic composition of natural tungsten foil

Isotope	^{180}W	^{182}W	^{183}W	^{184}W	^{186}W
Percent Abundance	0.12 %	26.50 %	14.31 %	30.64 %	28.43 %

The stack of foils consisted of tungsten foils with two copper foils (0.025 ± 0.002 mm; 22 ± 2 mg/cm^2 thickness) inserted in the stack for beam monitoring purposes. Foils were irradiated on the TR13 cyclotron located at TRIUMF in Vancouver BC, on a TR19 Cyclotron at the Edmonton PET Center (EPC) within the Cross Cancer Institute in Edmonton Alberta, and on a TR19 Cyclotron at Brookhaven National Laboratory (BNL), Upton, NY. The incident energy was 13 MeV from the TR13 cyclotron and ranged from 15-18 MeV for the TR19 cyclotrons (EPC and BNL) (See Table 3.2).

Table 3.2.
The incident proton energy on the W foils as calculated for the primary extracted beam (through the Al vacuum isolation foil) and subsequently through the W/Cu stack

Cyclotron	Primary Energy (MeV)	Degraded Energy (MeV)[a]
EPC TR19	18.0	17.6, 16.6, 15.5, 14.8, 14.1, 13.3, 12.6
	18.0	17.2, 16.2, 15.5, 14.8, 14.1, 13.3, 12.6
BNL TR19	18.0	17.0
	17.5	16.5, 15.4
	16.0	14.9, 13.8
	15.0	13.9, 12.7
	13.0	11.7, 10.3
TRIUMF TR13	13.0	11.1, 9.7, 8.7, 7.6, 6.5

[a]As calculated by SRIM-2003 [7].

Irradiations were typically 5 μA for 5-30 minutes. The same target body was used for all irradiations. An aluminum target body was designed for the irradiation of foils of 1 cm in diameter. A drawing of the target body is show in Figure 3.1.

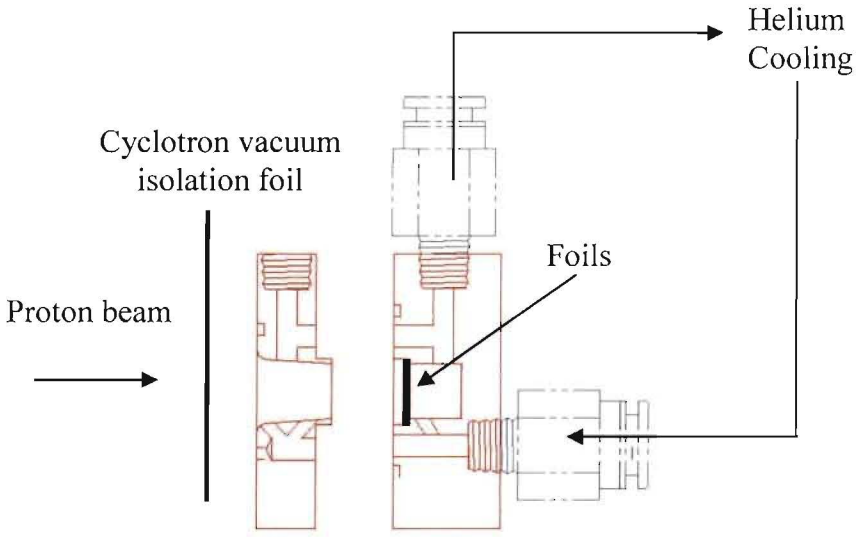

Figure 3.1
Target holder for the irradiation of 1 cm diameter foils

The foil stack was helium-cooled as shown (He flow 90 L/min at 10 psi) and separated from the cyclotron vacuum by a 0.025 ± 0.002 mm thick aluminum foil.

For the irradiations in Edmonton and Upton, the target assembly was shipped to the site, irradiated and shipped back to Vancouver for processing. Due to the time delay in the return of the assembly, radioisotopes with short half-lives were not observed in these irradiations.

Radioactivity measurements were made on an energy and efficiency calibrated high purity germanium (HPGe) gamma-ray detector (Canberra, 15 % efficiency, 2.0 keV (FWHM) at 1.33 MeV). The detector was calibrated by measurement of an ^{152}Eu source at the same distance from the detector as the foils. Analysis of the peaks and a plot of the natural logarithm of detector efficiency vs the natural logarithm of energy gives rise to a straight line as shown in Figure 3.2.

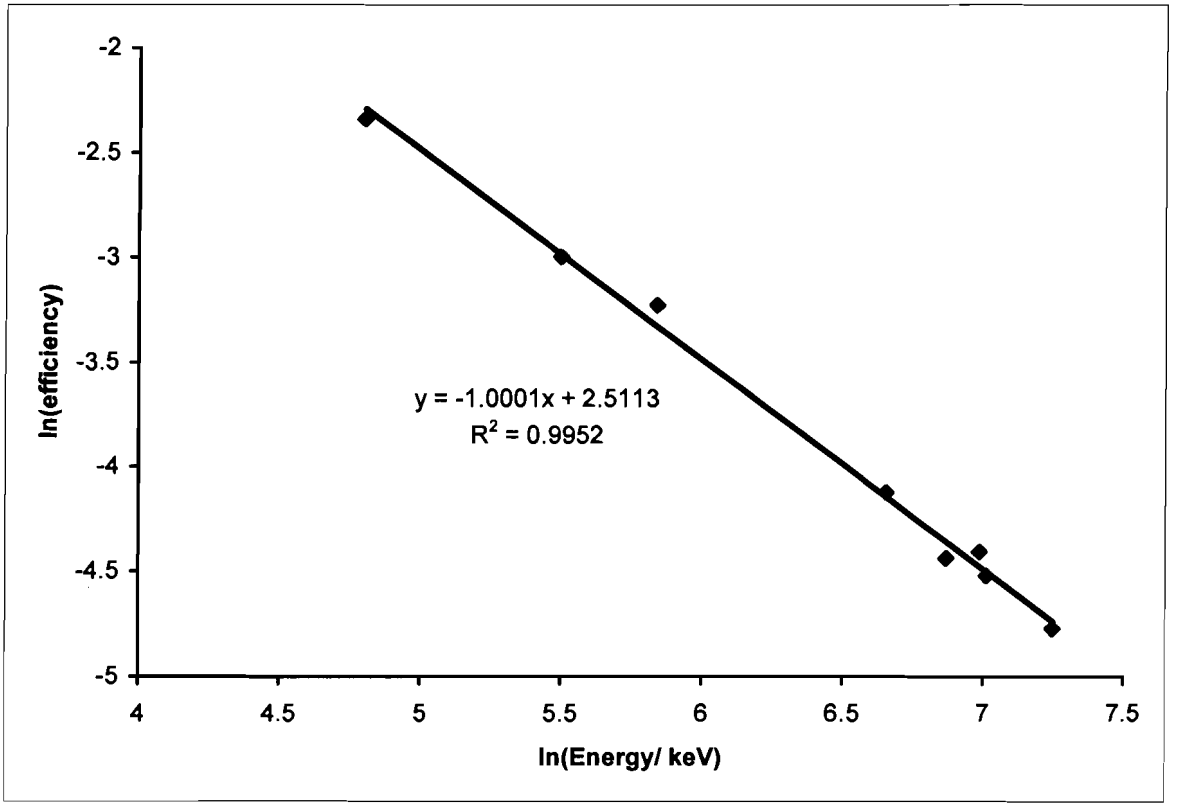

Figure 3.2
Efficiency calibration curve of HPGe detector

The γ emissions and branching ratios used for cross-section analysis are given in Table 3.3. All peaks were individually fit using a gamma-ray spectroscopy fitting program (GF3) [8]. No isotopes produced in the copper foils were observed in the spectra of the irradiated tungsten foils, indicating that knockouts from one foil to the next were negligible. In addition to this, in preliminary experiments Aluminium catcher foils were placed between each target foil to determine to probability of knockouts. In these experiments, no knockouts were observed. Energy degradation in each foil (including the Al vacuum isolation foil) was calculated by the computer code Stopping and Range of Ions in Matter (SRIM) [7]. In all cases the midpoint proton energy in each foil was used.

Table 3.3.
Gamma ray energies and branching ratios used in this study

Reaction	Calculated Threshold /MeV	Half-life[a]	γ-ray energy in keV and abundance[a]
$^{182}W(p,2n)^{181}Re$	10.65	20 h	365.5 (56.4 %)
$^{182}W(p,n)^{182m}Re$	3.60	12.7 h	1121.4 (31.9 %)
			1221.5 (25.1 %)
$^{182}W(p,n)^{182g}Re$	3.60	2.67 d	169.2 (12.2 %)
			351.1 (11.2 %)
$^{183}W(p,n)^{183}Re$	1.35	70.0 d	162.3 (23.3 %)
			291.7 (3.2 %)
$^{184}W(p,n)^{184}Re$	2.28	38.0 d	792.1 (37.4 %)
			903.3 (37.8 %)
$^{186}W(p,n)^{186}Re$	1.37	3.72 d	137.2 (9.2 %)
$^{65}Cu(p,n)^{65}Zn$	2.17	244 d	1116.0 (50.6 %)

[a] from [9]

For all measurements, beam flux was determined from the average of two Cu foils placed in the stack using the $^{nat}Cu(p,n)^{65}Zn$ monitor reaction [10]. This was calculated using the equation:

$$A = n\phi\sigma(1-e^{-\lambda t}) \qquad \textbf{[eq. 1]}$$

where: ϕ = incident proton flux (particles s^{-1} cm^{-2})

A = radioactivity present in the foil at the end of irradiation (Bq)

n = number of target nuclei per cm

σ = cross section in cm^2

λ = decay constant in s^{-1}

t = time of irradiation in s

The difference between beam flux determinations from the two Cu monitor foils was <5 %.

The uncertainty in each cross-section measurement results from statistical error in the observed counts (1-3 %), error in the proton beam flux (5 %), error in the foil thickness (8 %) and error in the detector efficiencies (5 %). The errors were summed in quadrature. In general errors were typically 8-10 %. The uncertainty in of the proton energy results from uncertainty in the Al, Cu and W foil thicknesses as well as the energy spread from energy degradation on the foil stack.

Theoretical values were calculated by the nuclear reaction model code EMPIRE-II [6]. Empire is a modular system of nuclear reaction codes, which

combines various nuclear models for the calculation of various theoretical reaction parameters. The only modification to EMPIRE's default parameter library was the extension of calculations over the level scheme of ^{182}Re up to the first 1$^-$ excitation, in order to better separate the excitation functions of ^{182g}Re and ^{182m}Re (EMPIRE default considers only the ground state of this nucleus).

3.2.2 Results and Discussion

Cross sections (σ) as a function of proton energy were calculated using equation **1**. The measured excitation functions are shown in Figures 3.3-3.8, together with the literature values. For clarity the error bars have been omitted from these graphs. The numerical values with errors, however, are presented in Table 3.4. Where possible, two γ-rays were used for each cross-section measurement and the average value is presented.

Table 3.4.
Measured cross-sections for the production of ^{181}Re, ^{182m}Re, ^{182g}Re, ^{183}Re ^{184g}Re, ^{186}Re nuclides.

Proton Energy /MeV	Cross-section/mb					
	^{181}Re	^{182m}Re	^{182g}Re	^{183}Re	^{184}Re	^{186}Re
17.6 ±0.2[a]			49.9 ± 3.6	457 ± 33	119 ± 9	8.98 ± 0.64
17.2 ±0.2[a]	289 ± 21		44.4 ± 3.2		77.9 ± 5.6	10.4 ± 0.7
17.0 ±0.2[b]				401 ± 29	122 ± 9	9.93 ± 0.71
16.6 ±0.2[a]	245 ± 18		41.6 ± 3.0	461 ± 33	32.6 ± 2.3	9.02 ± 0.64
16.5 ±0.2[b]				435 ± 31	78.5 ± 5.6	12.6 ± 0.9
16.2 ±0.2[a]	204 ± 15			442 ± 32	18.3 ± 1.3	8.78 ± 0.63
15.5 ±0.2[a]	202 ± 14		36.9 ± 2.6	471± 34	16.4 ± 1.2	9.81 ± 0.70
15.4 ±0.3[b]				399 ± 28	47.4 ± 3.4	11.9 ± 0.9
14.9 ±0.2[b]				383± 27	20.0 ± 1.5	11.3 ± 0.8
14.8 ±0.3[a]	162 ± 12		31.6 ± 2.3	399 ± 28	18.3 ± 1.3	10.1 ± 0.7
14.1 ±0.4[a]	133 ± 9		28.1 ± 2.0	331 ± 24	21.2 ± 1.5	11.3 ± 0.8
13.9 ±0.2[b]				347 ± 25	26.6 ± 1.9	13.0 ± 0.9
13.8 ±0.3[b]				396 ± 28	27.4 ± 2.0	11.2 ± 0.8
13.3 ±0.4[a]			33.2 ± 2.4	277 ± 20	31.3 ± 2.2	12.4 ± 0.8
12.7 ±0.3[b]				271 ±19	35.6 ± 2.5	12.3 ± 0.9
12.6 ±0.6[a]			30.9 ± 2.2	249 ± 18	42.0 ± 3.0	15.2 ± 1.1
12.4 ±0.2[c]	89.3 ± 6.4	167 ± 12	29.0 ± 2.1	252 ± 18	27.6 ± 2.0	14.0 ± 1.0
11.7 ±0.2[b]					48.7 ± 3.5	16.3 ± 1.2
11.1 ±0.3[c]	4.5 ± 0.3	125 ± 9	16.8 ± 1.2	145 ± 10	36.9 ± 2.6	18.5 ± 13
10.3 ±0.3[b]				191 ± 14	105 ± 8	24.8 ± 1.8
9.7 ±0.3[c]		40.1 ± 2.9	4.8 ± 0.3	32.1 ± 2.3	50.0 ± 3.6	22.0 ± 1.6
8.7 ±0.4[c]		14.2 ± 1.0	1.3 ± 0.1	0.82 ± 0.06	19.7 ± 1.4	14.9 ± 1.1
7.6 ±0.6[c]		2.9 ± 0.2	0.40 ± 0.04		3.8 ± 0.3	3.17 ± 0.23
6.5 ±0.9[c]		0.20 ± 0.02			0.20 ± 0.02	0.19 ± 0.02

[a]Measured at Edmonton PET Centre [b]Measured at Brookhaven National Lab
[c]Measured at TRIUMF

^{181}Re.

The theoretical and experimental data for the production of ^{181}Re, via the ^{182}W(p,2n) reaction can be found in Figure 3.3. Excellent agreement was found with the data from Zhang, as well as with the theoretical calculations, while the Tárkányi data appears systematically high in comparison

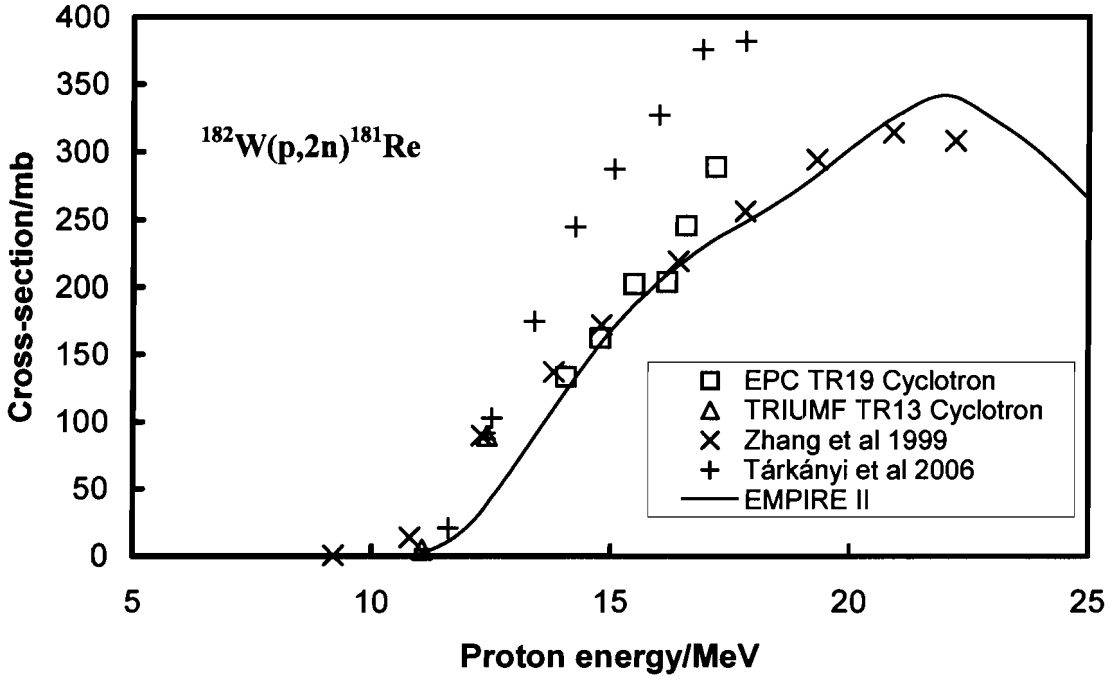

Figure 3.3
Excitation function of the ^{182}W(p,2n)^{181}Re reaction

^{182m}Re.

The theoretical and experimental data for the production of ^{182m}Re, via the ^{182}W(p,n) and ^{183}W(p,2n) reactions can be found in Figure 3.4. The agreement with Zhang and the theoretical data is reasonably good up to 10 MeV. However, both the experimental data and the data from Tárkányi et al. appear systematically high at higher energies.

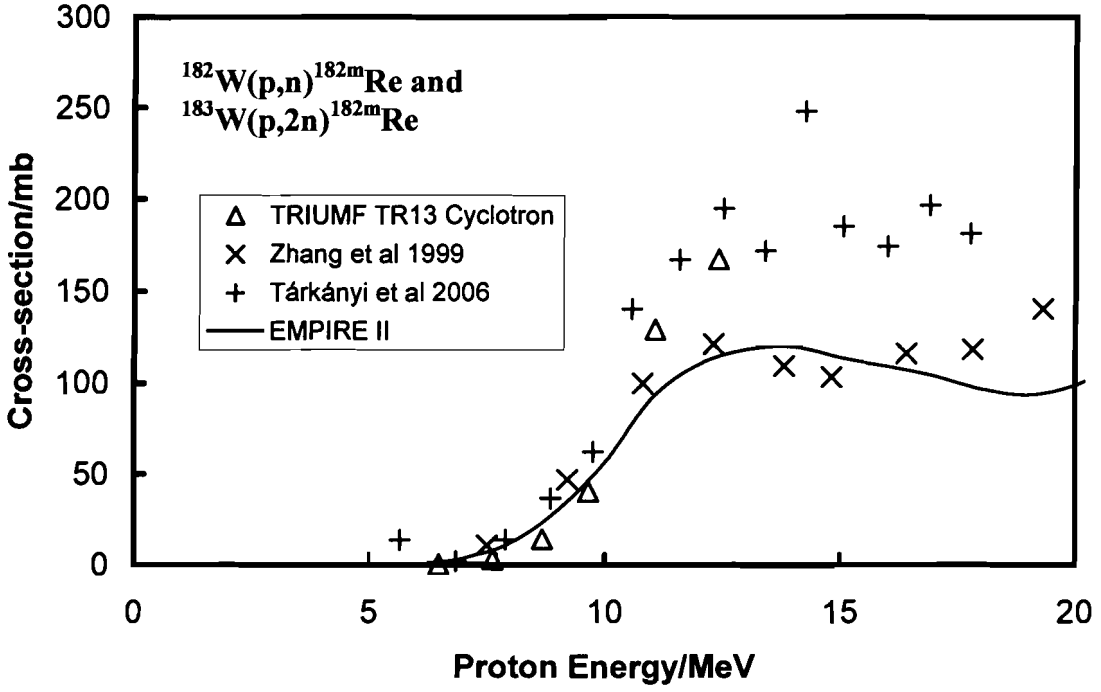

Figure 3.4
Excitation function of the ^{182}W(p,n)^{182m}Re and ^{183}W(p,2n)^{182m}Re reactions

^{182g}Re.

For ^{182g}Re (Figure 3.5) via the ^{182}W(p,n) and ^{183}W(p,2n) reactions, there is reasonable agreement of the measured values with Tárkányi and Zhang and theoretical values up to 13 MeV. At 15 MeV the excitation function for ^{182m}Re is about 3 times that of ^{182g}Re. This is most likely due to the low angular momentum of the proton, which makes the population of the 2+ metastable state of ^{182}Re more likely than the 7+ ground state. This is supported by the theoretical calculations.

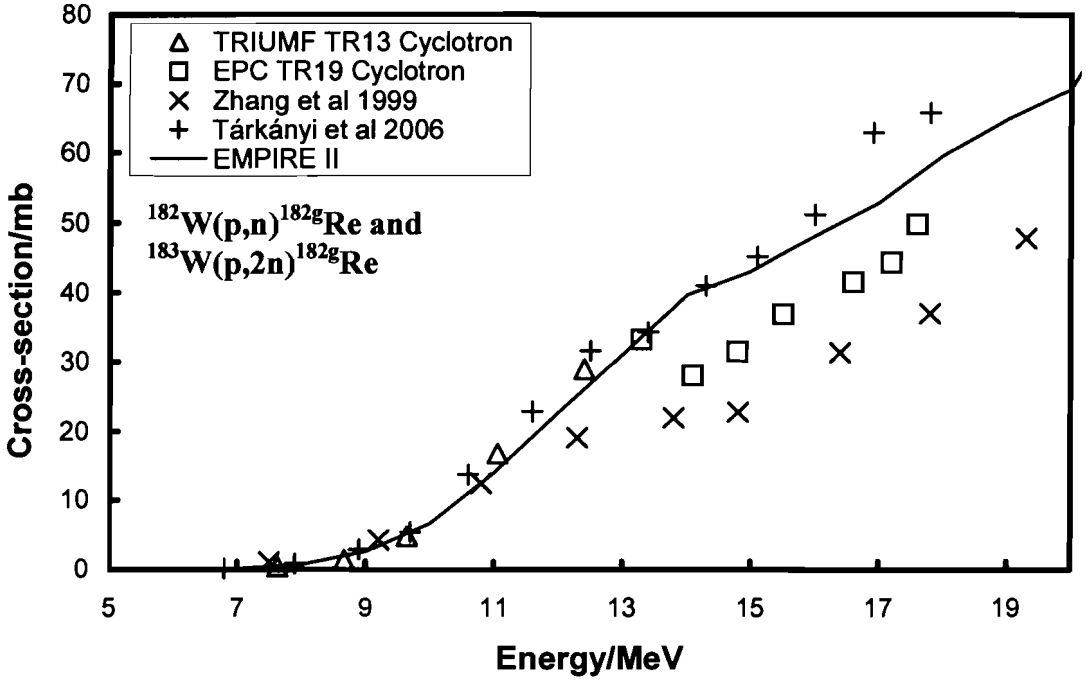

Figure 3.5
Excitation function of the ^{182}W(p,n)^{182g}Re and ^{183}W(p,2n)^{182g}Re reactions

^{183}Re.

For ^{183}Re (Figure 3.6) via the ^{183}W(p,n) and ^{184}W(p,2n) reactions, there is some agreement of the measured values with the current work, the theoretical data as well as the previously published data at lower energies; however, at higher energies (>10 MeV) the theory and data values from Tárkányi et al. lie in between the Zhang data and our new findings. The reasons for this discrepancy are unknown at this time.

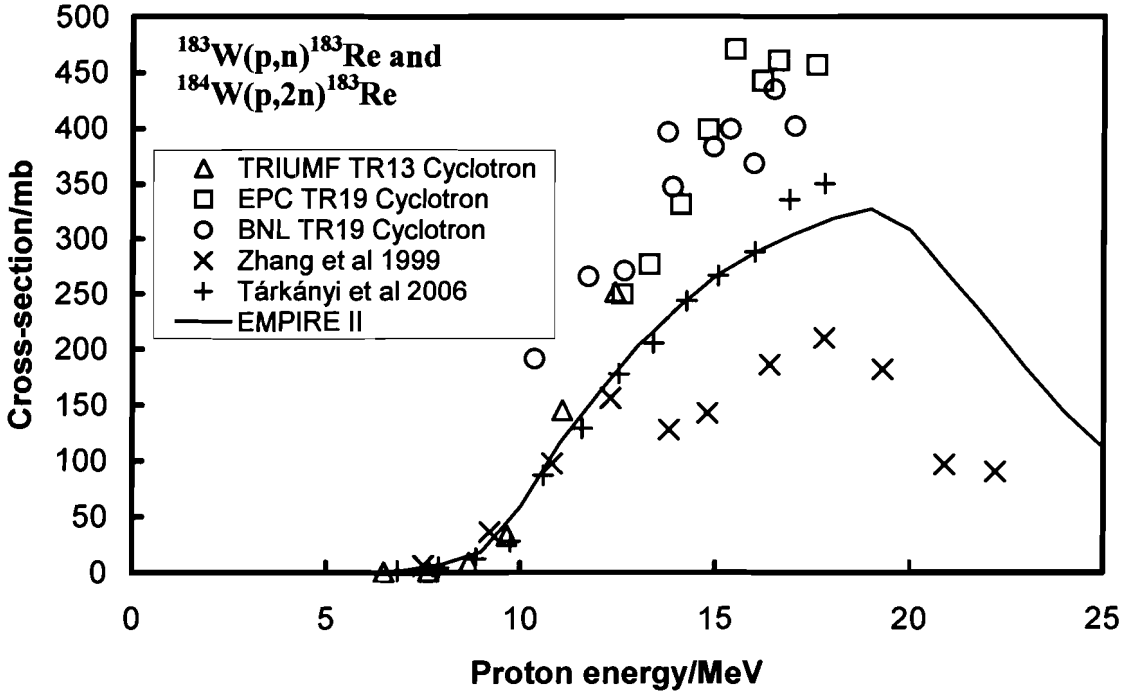

Figure 3.6
Excitation function of the ^{183}W(p,n)^{183}Re and ^{184}W(p,2n)^{183}Re reactions

^{184}Re.

For ^{184}Re (Figure 3.7) via the ^{184}W(p,n) reaction, the experimental data is in reasonable agreement with Tárkányi , Zhang and the theoretical values, although all sets of experimental values are slightly higher than predicted by theory in the energy range of 16 to 20 MeV.

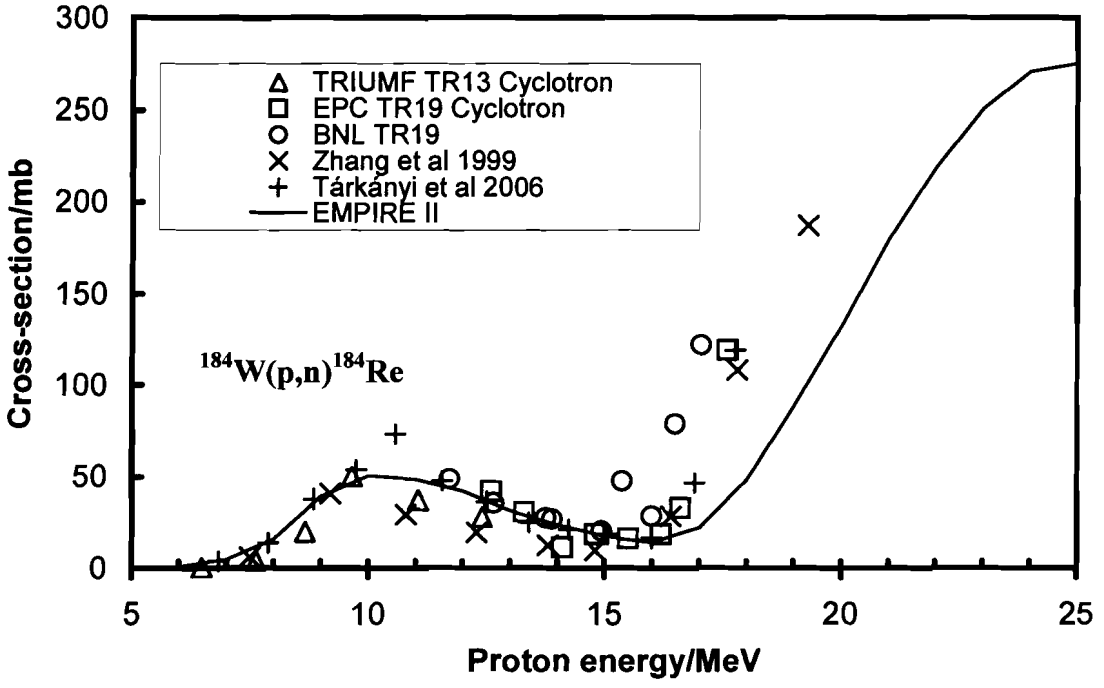

Figure 3.7
Excitation function of the ^{184}W(p,n)^{184}Re reaction

^{186}Re.

In comparison with Tárkányi, as well as the theoretical values, the ^{186}Re (Figure 3.8) data are in strong agreement. For ^{186}Re, the results of Shigeta are for the most part consistent with the present work except for relatively high values around 10 MeV, while the results of Zhang are consistently low when compared to the current work.

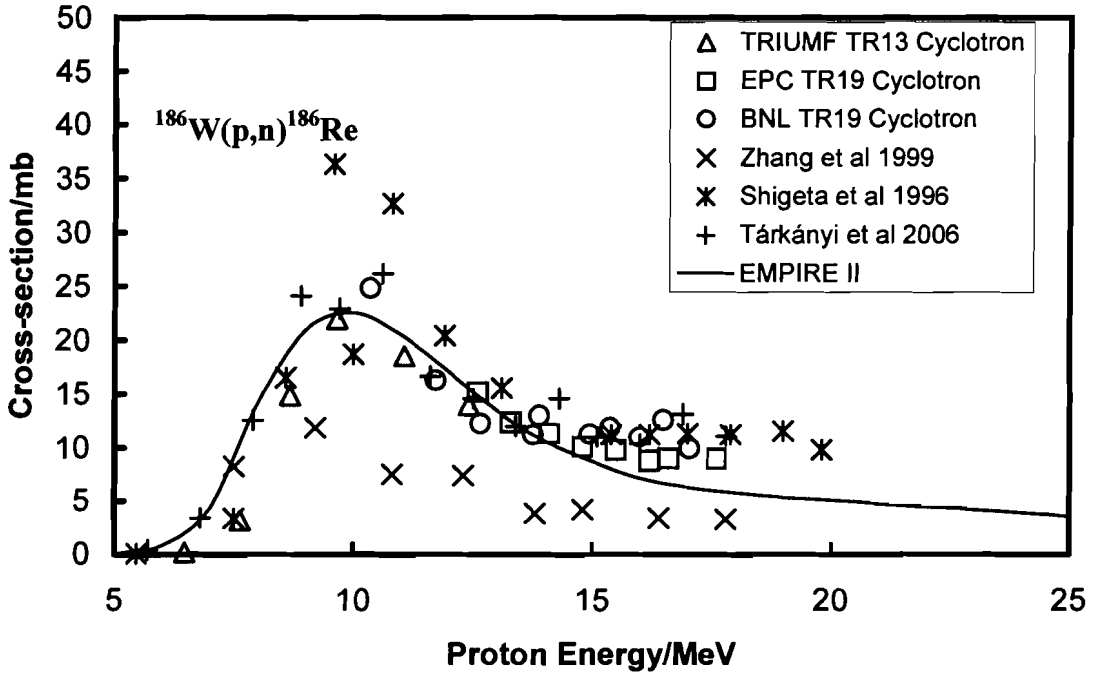

Figure 3.8
Excitation function of the ^{186}W(p,n)^{186}Re reaction

^{186}Re Cumulative Yields.

Cumulative yields for the production of ^{186}Re from an enriched ^{186}W target from a 24 h irradiation were calculated by integrating the cross-section over the energy range using the present data; results are shown in Figure 3.9. Based on our excitation function for the ^{186}W(p.n)^{186}Re reaction (Figure 3.8), a 50 μA, 24 hour irradiation with 18 MeV protons yields approximately 5.5 GBq of ^{186}Re at the end of bombardment. The target thickness for this irradiation would be 850 mg/cm^2 (~0.4 mm). This amount of radioactivity would be approximately enough to treat two patients [11]. From these estimates it is obvious that the (p,n) reaction on tungsten may not be a cost-effective viable route for the routine production of therapeutic doses of ^{186}Re (at $500 per hour the cyclotron time cost alone would be $12,000) [12].

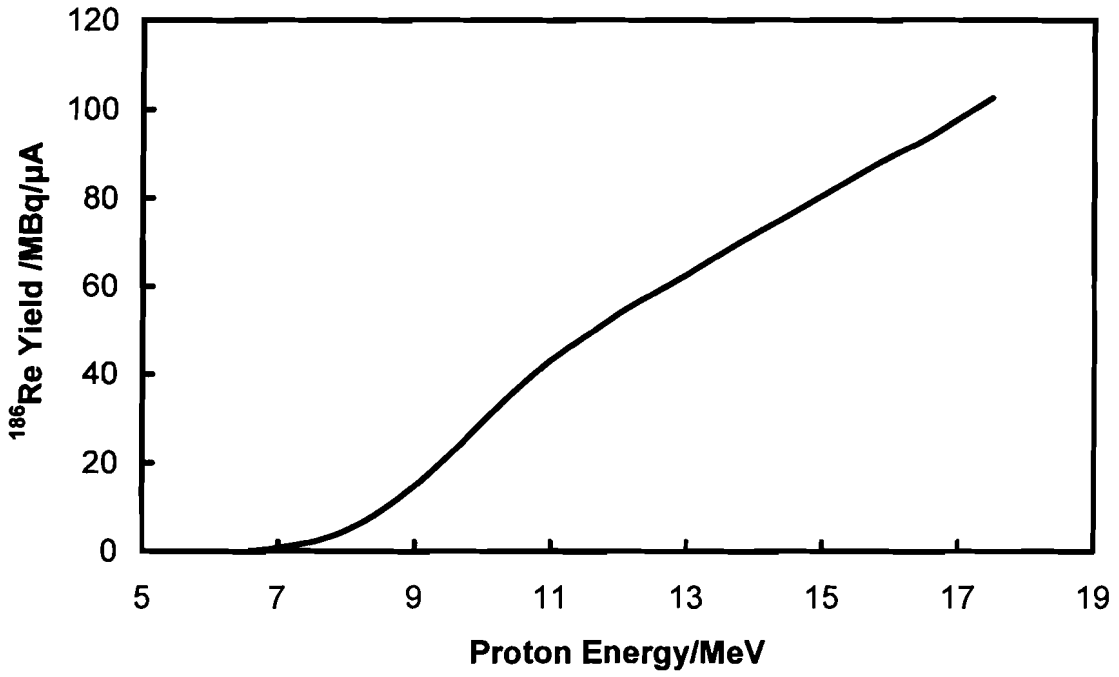

Figure 3.9
Calculated thick target yields of ^{186}Re from enriched ^{186}W target per μA for a 24 hr irradiation

3.3 Production of High Specific Activity ^{186}Re via Proton Irradiation of an Enriched Tungsten Powder Target

3.3.1 Materials and Methods

^{186}Re in high specific activity was produced by 13 MeV proton bombardment of enriched tungsten powder (96.7%, Isoflex isotopes, USA). Elemental analysis indicated that the content of rhenium metal in this powder was below detection limits. An aluminum target body was designed with water-cooling on the back and helium-cooling on the front. The target material is positioned in the target body in a removable aluminum cup, which can be easily

removed after irradiation in order to maintain low radiation exposure rates to personnel. The powder was isolated from a helium-cooling chamber by a 0.025 ± 0.002 mm thick aluminum foil, which was in turn separated from the cyclotron vacuum by a 0.025 ± 0.002 mm thick aluminum foil. A drawing of the target body is given in Figure 3.10.

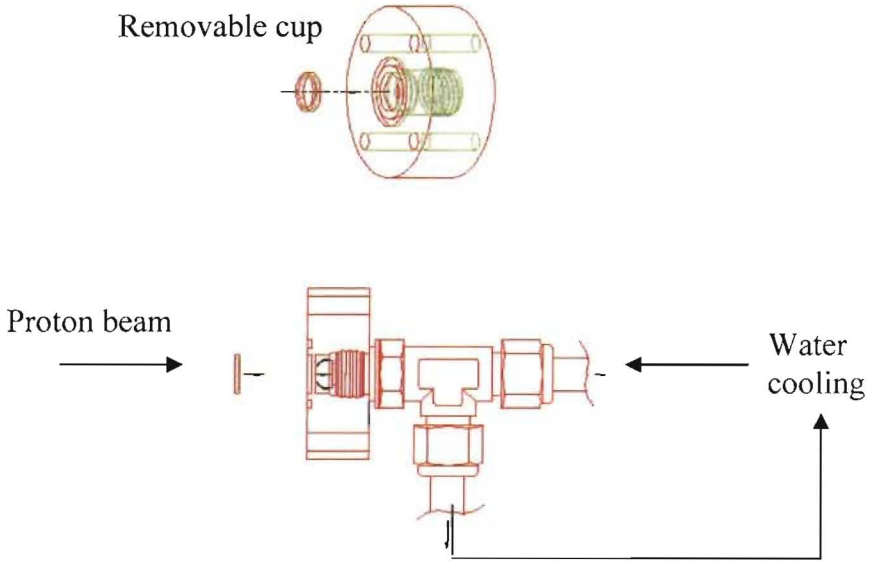

Figure 3.10
Target body for the production of ^{186}Re via proton bombardment of tungsten powder

The target was initially tested for short irradiations with natural tungsten powder. Irradiations were typically 5 μA for 30 minutes to test the durability of the target. The tungsten powder was loaded into the target body under an argon

atmosphere to prevent oxidation (and hence expansion) of the target material, which would rupture the isolation foils as it did in one preliminary experiment (see Appendix 1 for incident details).

Enriched powder irradiations were typically 25-30 hours in fragmented (8-10 hours) time periods to allow for reasonable operating times.

3.3.2 Results and Discussion

A gamma–ray spectrum of the irradiated natural tungsten powder is shown in Figure 3.11.

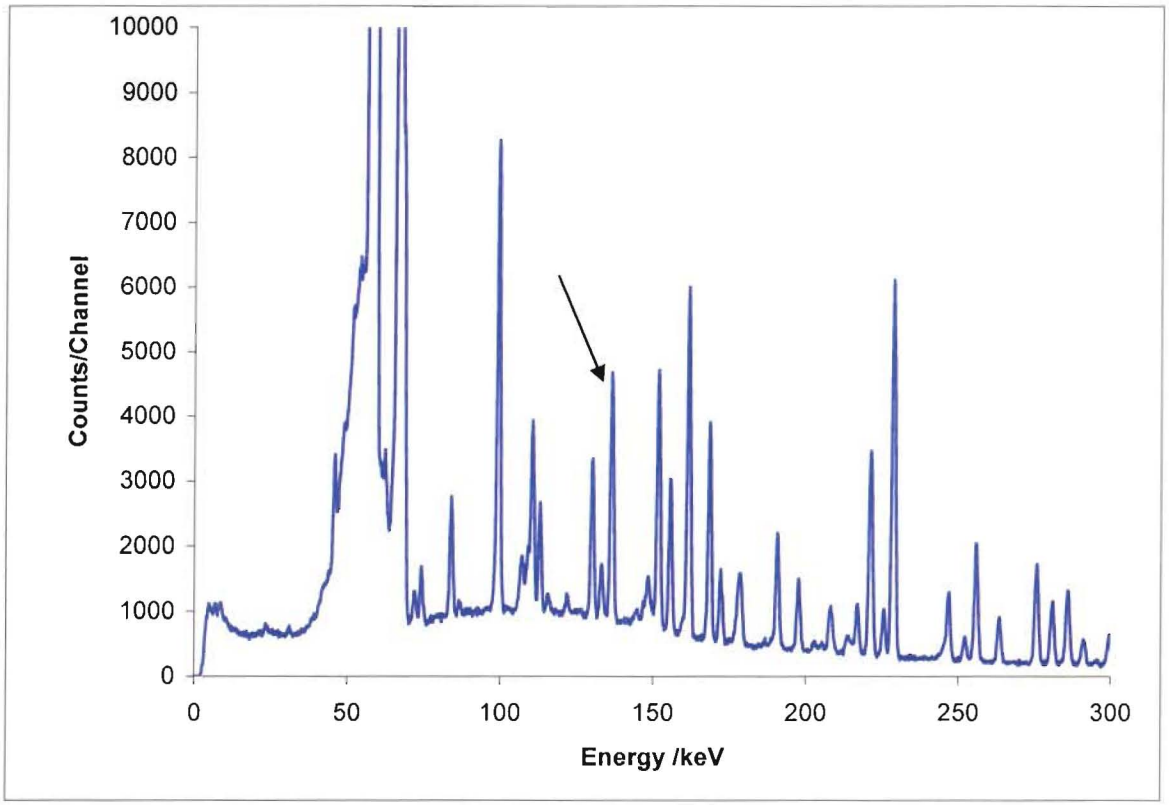

Figure 3.11
Gamma ray spectrum of irradiated natural tungsten powder

As can be observed from Figure 3.11, the gamma spectrum from an irradiated natural tungsten target is very complex. The arrow in the diagram indicates the position of the 137 keV gamma ray, which is characteristic of ^{186}Re decay. Natural tungsten irradiations resulted in an average of 2.0 MBq of ^{186}Re per 30 minute, 5 μA irradiation, which accounted for 6.0 % of the total activity at the end of bombardment.

A gamma–ray spectrum of the irradiated enriched tungsten powder is shown in Figure 3.12.

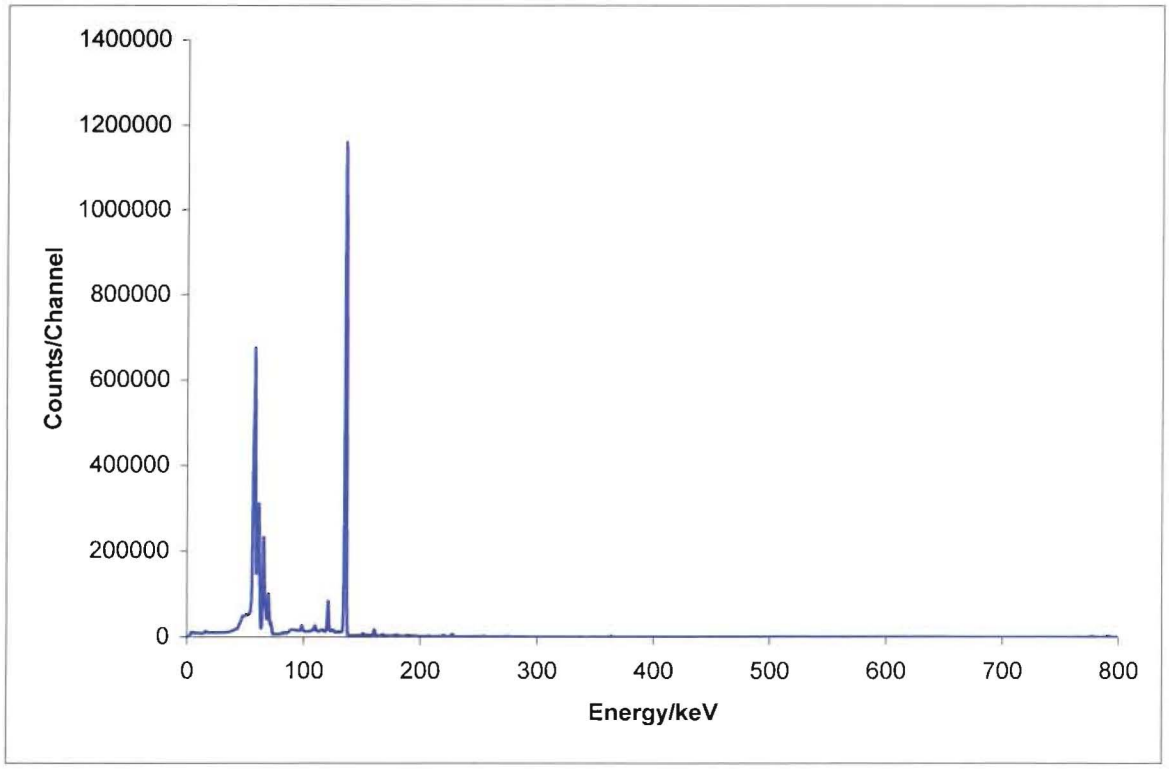

Figure 3.12
Gamma ray spectrum of an irradiated enriched ^{186}W powder target.

The 137 keV and 122 keV peaks are due to decay of ^{186}Re and all peaks below 100 keV are X-rays from the de-excitation of the daughter nucleus ^{186}W. Enriched tungsten irradiations resulted in an average of 670 MBq of ^{186}Re with a small contamination of ^{184}Re (740 Bq). This represents 59% of theoretical yield. The loss may be due to the settling of the powder during irradiation resulting in a thin target. Losses may also have occurred during transfer of the target powder material from the target body for processing.

3.4 Dry Distillation Separation of ^{186}Re from Irradiated Tungsten Powder

3.4.1 Materials and Methods

A previously developed technique for the separation of trace rhenium from tungsten targets was utilized. The separation uses a dry distillation technique [13]. A dry distillation oven was constructed by wrapping nichrome wire around a grooved 2.5 cm diameter ceramic tube and sealing with kiln cement. Insulation was accomplished by the addition of a 2 cm thick layer of kiln cement. A temperature profile of the oven at two different operating voltages, measured along the central axis with a standard K-type thermocouple is shown in Figure 3.13.

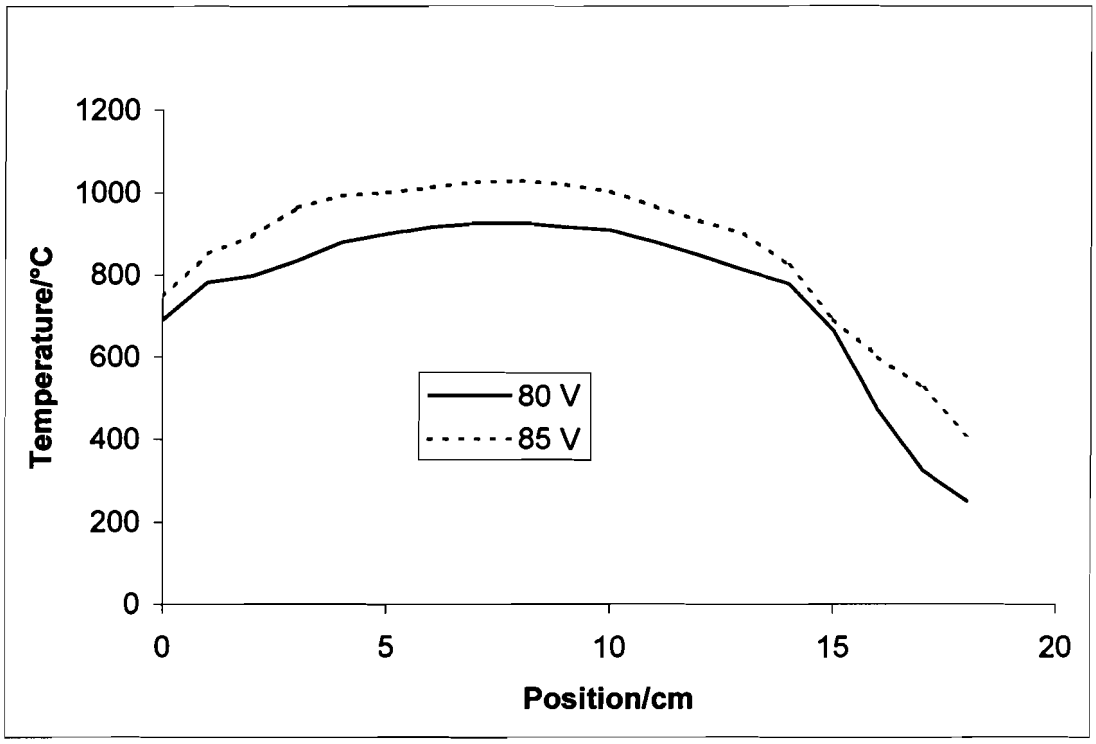

Figure 3.13
Temperature profile of oven used for dry distillation

After irradiation the powder was carefully transferred to a quartz boat. The tungsten target material was heated to 1000° C under an air stream inside a quartz tube, which was placed in the oven. The Re isotopes form oxides (most likely ReO_3 – b.p. 400 °C) which are volatile at this temperature. The Re isotopes travel down the tube and condense on a quartz plug outside the oven. A schematic of the distillation apparatus is given in Figure 3.14.

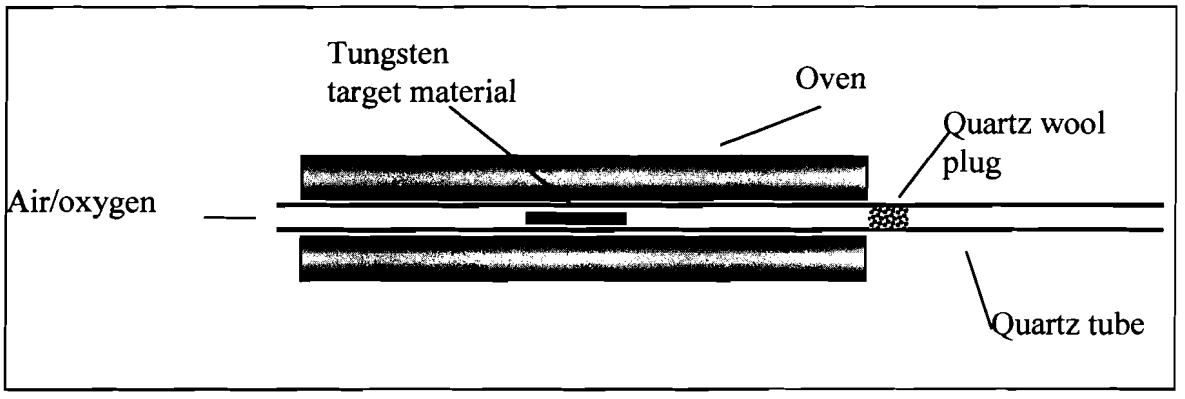

Figure 3.14
Distillation apparatus for the separation of ^{186}Re from irradiated tungsten targets.

After the distillation procedure the quartz wool plug was removed from the oven and the rhenium was rinsed off with saline with more than 99 % recovery from the quartz.

The partially oxidized tungsten powder was reduced back to tungsten metal by heating at 800° under an argon atmosphere containing 5% hydrogen.

3.4.2 Results and Discussion

Figure 3.15 shows the recovery of Re isotopes as a function of distillation time as determined by radioactivity analysis of the saline rinse.

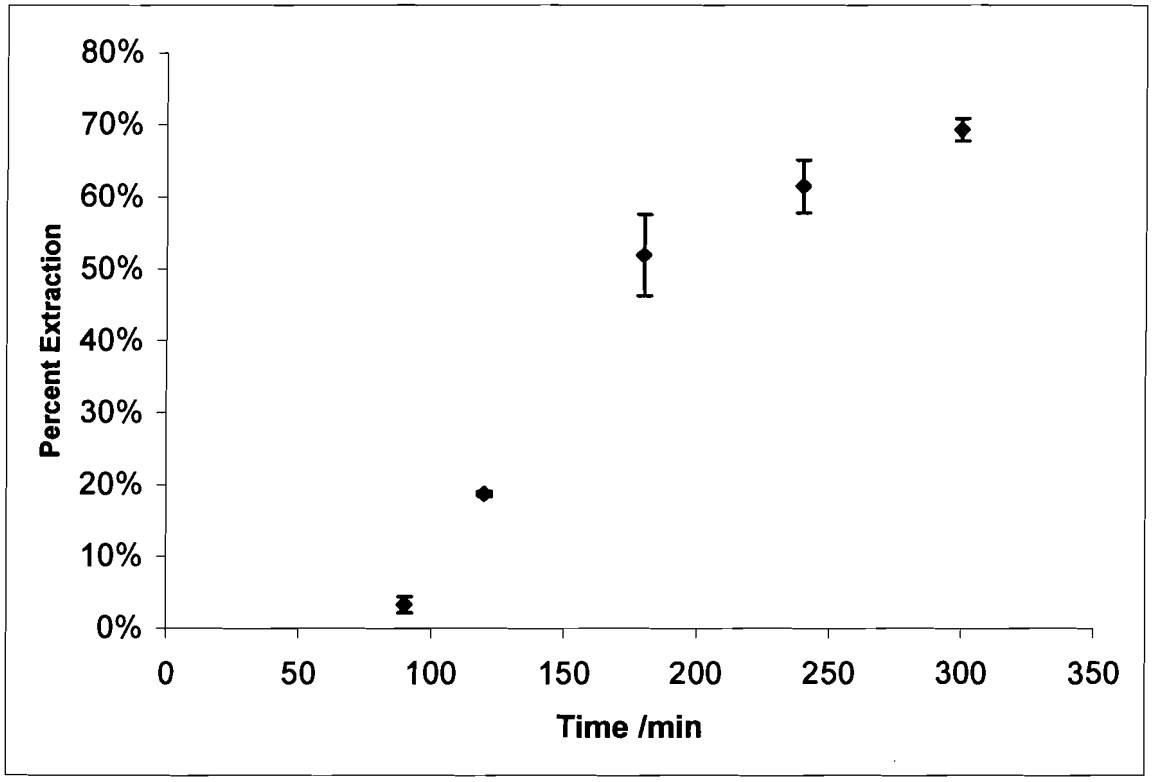

Figure 3.15
Recovery vs. distillation time for powder target distillations

As can be determined from the above graph, recoveries of 70% were obtained by distillation times of 6 hours. Due to the long half-life of ^{186}Re, this distillation time is appropriate for recovery of this isotope from irradiated tungsten targets.

3.5 References

1. Zhang, X.D., et al., *Excitation functions for W-nat(p,xn)Re181-186 reactions and production of no-carrier-added Re-186 via W-186(p,n) Re-186 reaction.* Radiochimica Acta, 1999. **86**(1-2): p. 11-16.

2. Shigeta, N., et al., *Production method of no-carrier-added Re-186.* Journal of Radioanalytical and Nuclear Chemistry-Articles, 1996. **205**(1): p. 85-92.

3. Moustapha, M.E., et al., *Preparation of cyclotron-produced Re-186 and comparison with reactor-produced Re-186 and generator-produced Re-188 for the labeling of bombesin.* Nuclear Medicine and Biology, 2006. **33**(1): p. 81-89.

4. Tarkanyi, F., et al., *Excitation functions of proton induced nuclear reactions on natural tungsten up to 34 MeV.* Nuclear Instruments & Methods in Physics Research Section B-Beam Interactions with Materials and Atoms, 2006. **252**(2): p. 160-174.

5. Uddin, M.S., et al., *Experimental studies on excitation functions of the proton-induced activation reactions on yttrium.* Appl Radiat Isot, 2005. **63**(3): p. 367-74.

6. *EMPIRE-II Nuclear Reaction Model code (version 2.19).* 2005 [cited; Available from: http://www.nndc.bnl.gov/empire219/index.html.

7. Ziegler, J.F., Biersalc, J.P., Littmark, U. *The Stopping and Range of Ions in Matter SRIM-2003.26.* 2003 [cited; Available from: www.SRIM.org.

8. Radford, D.C. *GF3 software.* 2000 [cited December 1, 2006]; Available from: http://radware.phy.ornl.gov/gf3/gf3.html.

9. *National Nuclear Data Center Chart of the Nuclides.* 2006 [cited; Available from: http://www.nndc.bnl.gov/chart.

10. *IAEA cross-section database for medical radioisotope production.* 2006 [cited; Available from: http://www-nds.iaea.or.at/medical/.

11. Colnot, D.R., et al., *Phase I therapy study of Re-186-labeled chimeric monoclonal antibody U36 in patients with squamous cell carcinoma of the head and neck.* Journal of Nuclear Medicine, 2000. **41**(12): p. 1999-2010.

12. Buckley, K.R., *personal communication*. 2007.

13. Novgorodov, A.F., et al., *Thermochromatographic separation of no-carrier-added Re-186 or Re-188 from tungsten targets relevant to nuclear medical applications*. Radiochimica Acta, 2000. **88**(3-4): p. 163-167.

Chapter 4

Synthesis of S-benzoylmercaptoacetyltriglycine and Re-MAG3 Antibody Labeling

4.1 Introduction

Several techniques have been developed for the labeling of antibodies with Re isotopes, with both direct and indirect methods being published [1, 2]. The direct method involves directly reducing disulfide bonds within the antibody and coordinating the rhenium directly. The indirect method involves chelating the rhenium first followed by conjugation to the biomolecule. There are advantages and disadvantages to both of these techniques. The direct

method is simpler, while the chelation approach typically yields a more stable conjugate. For our purposes an indirect technique using a mercaptoacetyltriglycine (MAG3) chelating agent was chosen [2, 3].

4.2 Materials

Thioglycolic acid (>98%), benzoyl chloride (ACS grade, 99%), N-hydroxysuccimide (>97%), dicyclohexylcarbodiimide (>99%), and tin (II) chloride (>95%) were purchased from Sigma-Aldrich Canada (Oakville, Ontario). 1-ethyl-3-(3-dimethlyaminopropyl)carbodiimide hydrochloride (>98%), tetrafluorophenol (>98%) and glycylglycylglycine (>98%) were purchased from TCI America (Portland, Oregon). Reference S-benzoylmercaptoacetylglycylglycylglycine was purchased from ABX Advanced Biochemical Compounds (Radeberg, Germany). All solvents used were HLPC grade unless otherwise stated. PD10 desalting columns were purchased from GE Healthcare Canada (Mississauga, Ontario). LSA ^{186}Re was purchased from the Missouri University Research Reactor (MURR) and had a specific activity of 500 mCi/mg at the time of shipping (shipping times varied from 2-5 days).

4.3 Synthesis of S-benzoylmercaptoacetylglycylglycylglycine

S-benzoylmercaptoacetylglycylglycylglycine was synthesized according to the procedure of Brandau *et al* [4] with modifications by Zhang *et al* [5].

4.3.1 Synthesis of S-benzoylthioglycolic acid

.

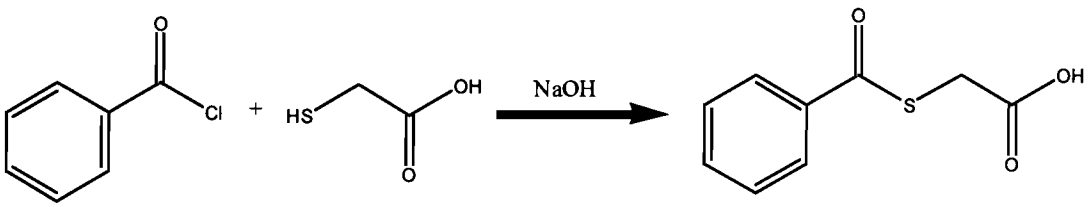

Figure 4.1
Reaction scheme for the synthesis of S-benzoylthioglycolic acid

9.26 grams (0.10 mol) of thioglycolic acid and 8.82 grams (0.22 mol) of sodium hydroxide was dissolved in a mixture of 75 ml toluene and 75 ml water and placed in an ice bath. 14.05 grams (0.10 mol) of benzoyl chloride was added over 30 minutes while stirring. The mixture was stirred at 0 °C for another 30 minutes and then for 45 minutes at room temperature. The aqueous layer was removed and set aside. The organic layer was extracted 3 times with 20 ml of deionized water. The aqueous phases were combined and acidified to pH 1 with concentrated HCl, which resulted in the precipitation of a white solid. The mixture was filtered and carefully dried under vacuum. Recrystallization in

ethyl acetate resulted in 13.16 grams (0.067 mol, 67 %) of clear needle-like crystals. ^{1}H NMR (400 MHz, $CDCl_3$) showed the following peaks, which are in excellent agreement with published values [5]:

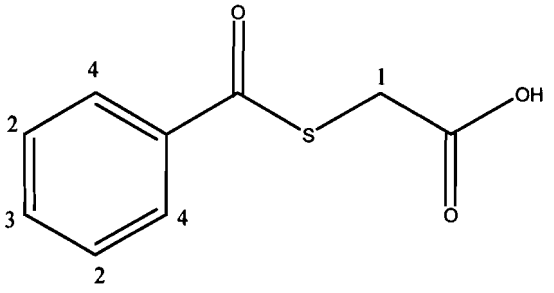

Figure 4.2
Assignment of protons for NMR spectrum of S-benzoylthioglycolic acid

Table 4.1
NMR peaks of S-benzoylthioglycolic acid

Position	Integral	Shift (ppm)	Multiplicity	J values
1	2	3.93	singlet	N/A
2	2	7.48	triplet*	7.7 Hz
3	1	7.61	triplet	7.4 Hz
4	2	7.98	doublet	8.4 Hz

* Theoretically the multiplicity of this peak should be a doublet of doublets, however, due to the close J-values, it appears as a triplet. On a higher resolution machine, this would likely be resolved.

4.3.2 Synthesis of Succinimidyl-S-benzoylthioglycolate

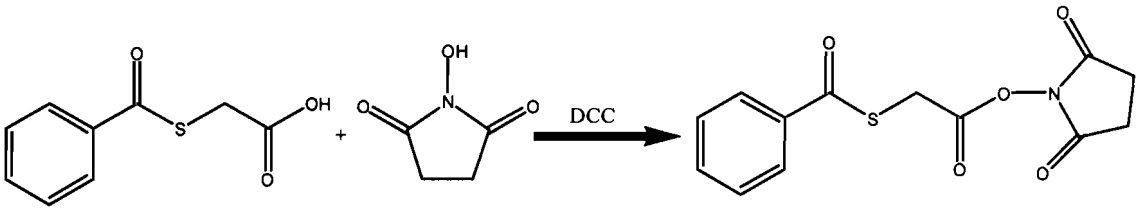

Figure 4.3
Reaction scheme for the synthesis of succinimidyl-S-benzoylthioglycolate

9.87 grams (0.050 mol) of S-benzoylthioglycolic acid and 5.72 grams (0.050 mol) of N-hydroxysuccinimide were dissolved in 60 ml dry-distilled absolute tetrahydrofuran. The reaction mixture was placed in an ice bath under argon. 13.39 grams of dicyclohexylcarbodiimide was dissolved in 20 ml dry-distilled absolute tetrahydrofuran and was added to the mixture over 20 minutes. The mixture was stirred on ice for another 90 minutes and at room temperature for another 3 hours. The mixture was filtered* and the filtrate was evaporated to dryness yielding a yellowish residue. Recrystallization in ethyl acetate gave 6.31 grams (0.022 mol, 43%) of colorless crystals. Silica thin layer chromatography (TLC) in a mixture of $CHCl_3$:CH_3OH:glacial acetic acid 60:40:1 showed an R_f of 1.0 in agreement with the literature value [5]. ^1H NMR (400 MHz, $CDCl_3$)

* Note: extraction of the filter cake with boiling tetrahydrofuran at this stage as in (1,2) extracted significant quantities of the byproduct N,N'-dicyclohexylurea. Recovery was sacrificed for purity by omitting this step.

showed the following peaks, which are in excellent agreement with published values [5]:

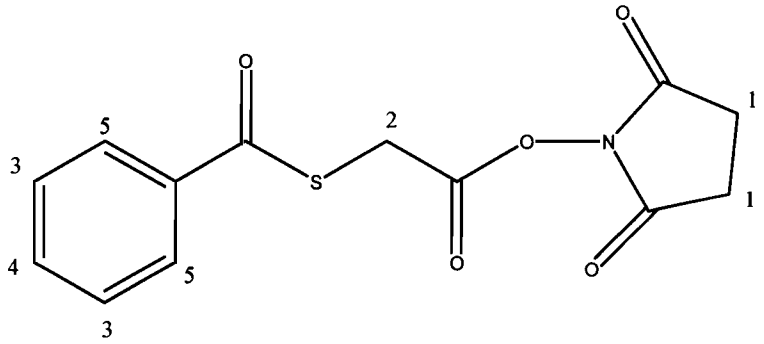

Figure 4.4
Assignment of protons for NMR spectrum of succinimidyl-S-benzoylthioglycolate

Table 4.2
NMR peaks of succinimidyl-S-benzoylthioglycolate

Position	Integral	Shift (ppm)	Multiplicity	J values
1	4	2.85	singlet	N/A
2	2	4.18	singlet	N/A
3	2	7.48	triplet*	7.8 Hz
4	1	7.62	triplet	7.4 Hz
5	2	7.99	doublet	8.4 Hz

* Theoretically the multiplicity of this peak should be a doublet of doublets, however, due to the close J-values, it appears as a triplet. On a higher resolution machine, this would likely be resolved.

4.3.3 Synthesis of S-benzoylmercaptoacetylglycylglycylglycine

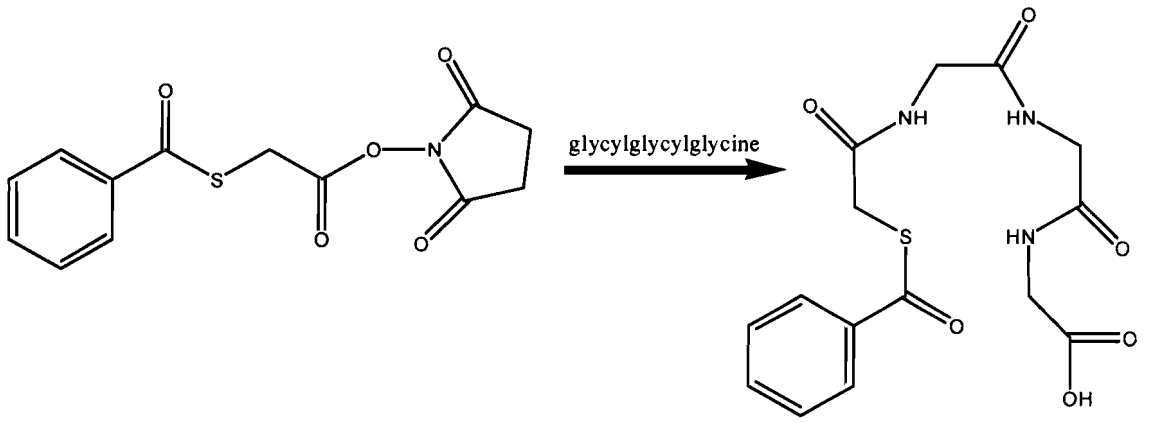

Figure 4.5
Reaction scheme for the synthesis of S-benzoylmercaptoacetylglycylglycylglycine

2.93 grams (0.010 mol) of succinimidyl-S-benzoylthioglycolate was dissolved in 25 ml acetonitrile at 60° C. 1.42 grams (0.0075 mol) of glycylglycylglycine* dissolved in 7.5 ml of 1M NaOH was added to the solution. The mixture was stirred at 60 °C for 3 hours and then at room temperature for an additional 16 hours. The mixture was acidified to pH 2 with 1 M HCl. The precipitate was filtered and dried. Recrystallization in isopropanol resulted in 1.100 grams (0.003 mol, 40%) of small white crystals. Silica TLC in a mixture of $CHCl_3$:CH_3OH:glacial acetic acid 60:40:1 showed an R_f of 0.2 which differs significantly from the literature value of 0.45 [5]. ^1H NMR (400 MHz, d_6-DMSO) showed the following peaks, which are in excellent agreement both with

* Note: the chemical reagent glycylglycylglycine is not equivalent to the chemical reagent triglycine. Some confusion arose at this stage as these two names are commonly used interchangeably in the literature.

published values [5] and to commercially purchased s-benzoyl-mercaptoacetoglycylglycylglycine:

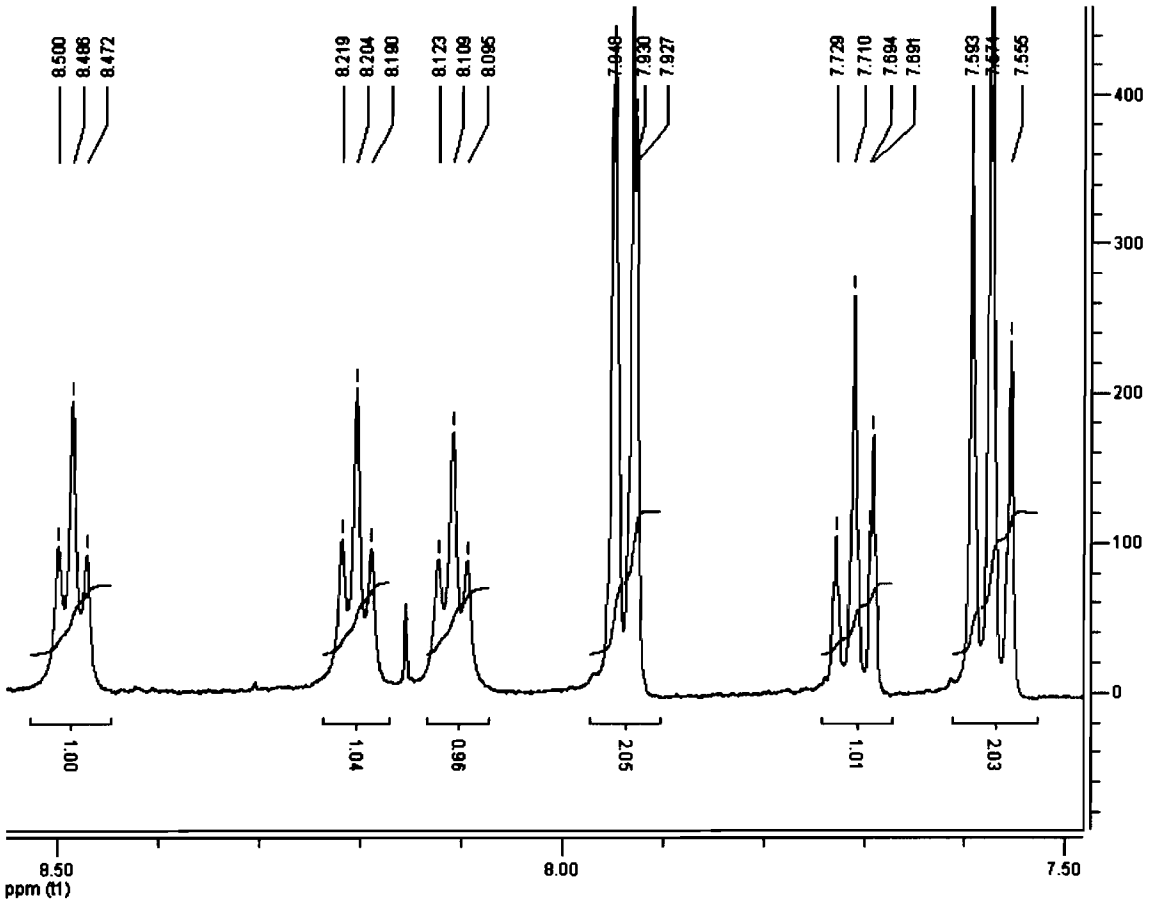

Figure 4.6
NMR spectrum of aromatic region of S-benzoylmercaptoacetylglycylglycylglycine

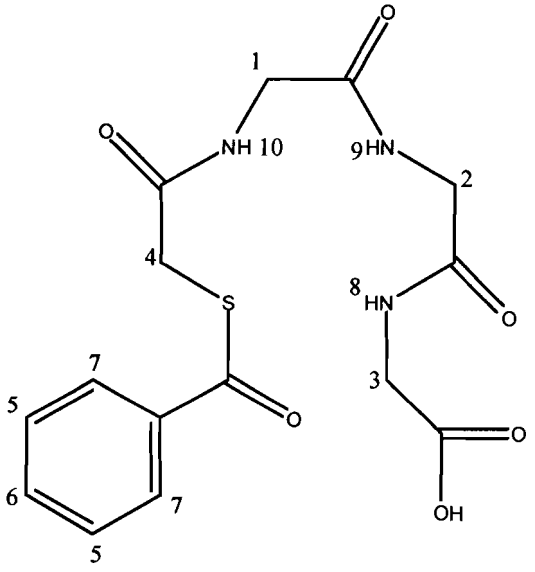

Figure 4.7
Assignment of protons for NMR spectrum of S-benzoylmercaptoacetylglycylglycylglycine

Table 4.3
NMR peaks of S-benzoylmercaptoacetylglycylglycylglycine

Position	Integral	Shift (ppm)	Multiplicity	J values
1	2	3.72	doublet	6.2 Hz
2	2	3.74	doublet	6.4 Hz
3	2	3.78	doublet	5.7 Hz
4	2	3.88	singlet	N/A
5	2	7.57	triplet*	7.7 Hz
6	1	7.71	triplet	7.4 Hz
7	2	7.94	doublet	8.5 Hz
8	1	8.11	triplet	5.7 Hz
9	1	8.20	triplet	5.9 Hz
10	1	8.49	triplet	5.6 Hz

* Theoretically the multiplicity of this peak should be a doublet of doublets, however, due to the close J-values, it appears as a triplet. On a higher resolution machine, this would likely be resolved.

4.4 Preparation of a Re-MAG3-Antibody Conjugate

Several references are available for the chelation of rhenium with mercaptoacetyltriglycine and subsequent bioconjugation [2, 3], with various buffer systems and pH values used for each step. After several attempts the following method (based on Crudo *et al.* [3].) was deemed to be the most successful.

4.4.1 Preparation of a Rhenium-mercaptoacetyltriglycine Complex

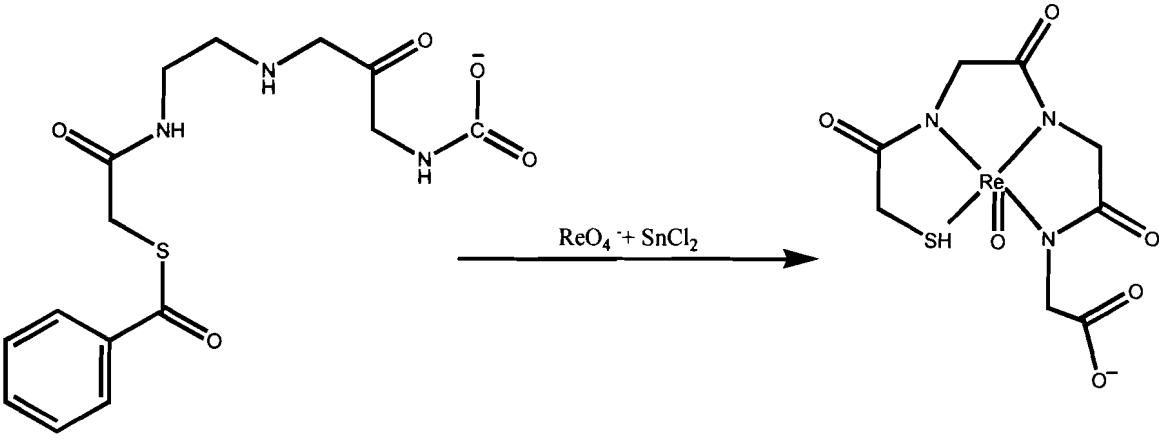

Figure 4.8
Reaction scheme for the preparation of a rhenium-mercaptoacetyltriglycine complex

LSA ^{186}Re (Specific activity = 200-500 mCi/mg or 7.4-18.5 GBq/mg) or in house produced HSA (theoretical specific activity = 189 Ci/mg or 7.0 TBq/mg) ^{186}Re solution was taken to dryness at 90 degrees C under a stream of N_2. When the rhenium had reached room temperature, 50 µl of s-benzoyl-

mercaptoacetoglycylglycylglycine solution (3 mg/ml in 60:40 acetonitrile and water) and 125 μl of $SnCl_2$ solution (12 mg/ml in 0.1 M citric acid buffer pH 5.5) was added. The vial was flooded with nitrogen, capped and heated at 80-90 °C for 45 minutes.

RadioTLC on silica with an acetone mobile phase yielded an R_f of 0.45 (>99% yields were typical). This reaction was found to be very sensitive to oxygen, thus it was critical that the vial be well purged with nitrogen to avoid re-oxidation of the rhenium.

4.4.2 Preparation of a Rhenium-mercaptoacetyltriglycine Activated Ester

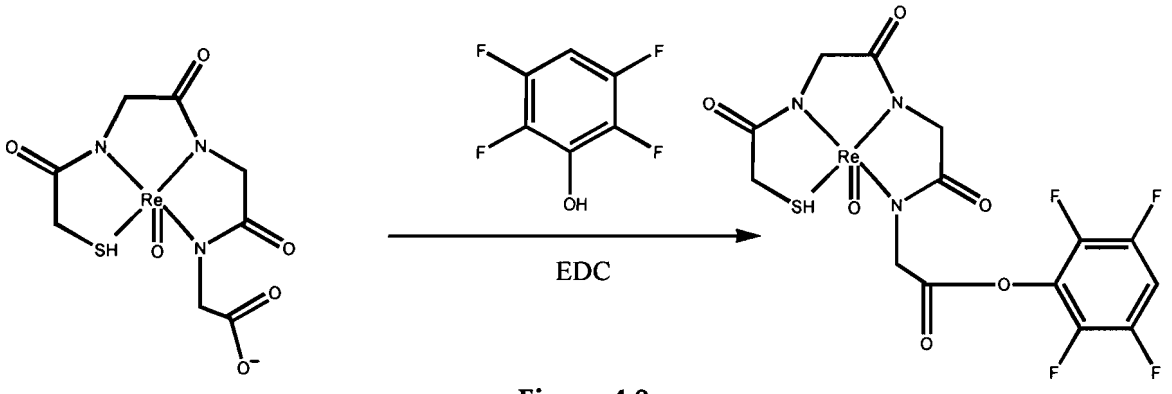

Figure 4.9
Reaction scheme for the preparation of a rhenium-mercaptoacetyltriglycine activated ester

100 μl of tetrafluorophenol solution (100 mg/ml in 9:1 Acetonitrile in water) and 50 mg 1-ethyl-3-(3-dimethlyaminopropyl)carbodiimide (EDC) as a solid were added to the solution. The reaction mixture was agitated and left to

react at room temperature for one hour. RadioTLC on silica with an acetone mobile phase yielded an R_f of 1.0 (>99% yields were typical). A SepPak® C18 cartridge was prepared by washing with 5 ml ethanol and 5 ml water. The reaction mixture was loaded onto the cartridge, washed with 5 ml water and the activated ester was eluted with 2 ml acetonitrile. The acetonitrile fraction was taken to dryness under nitrogen.

4.4.3 Preparation of a Rhenium-mercaptoacetyltriglycine Labeled Antibody

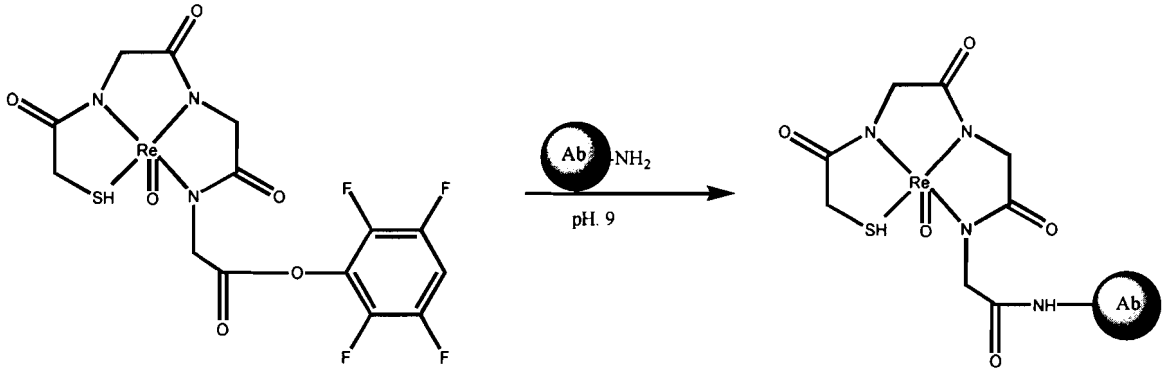

Figure 4.10
Reaction scheme for the preparation of a rhenium-mercaptoacetyltriglycine labeled antibody

The antibody preparation (200 μg in 0.1 ml azide-free, phosphate buffered saline) was added to the dried ester and the pH was adjusted to 9 using pH strips by addition of 0.1 M Na_2CO_3. Initial experiments with antibody preparations containing sodium azide as a preservative resulted in no bioconjugation. The mixture was left to react at room temperature for 1 hour. RadioTLC on silica

with an acetone mobile phase yielded an R_f of 0 (30 % yields were typical, with the remainder of the radioactivity in the Re-MAG3 form). The antibody was purified by passage through a pre-equilibriated PD10 desalting column in phosphate buffered saline. Silica radioTLC using acetone as the mobile phase yielded an R_f of 0 and SE-HPLC confirmed the radiopurity of the product (Phenomenex Biosep-2000, mobile phase: 50 mM phosphate buffer, pH 6.8, flow rate 1ml/min, ret time: 6.9 min).

The 1H7 antibody (see chapter 5) was labeled with HSA and LSA ^{186}Re in final specific activities ranging from $7.5 \times 10^5 - 8.5 \times 10^6$ Bq/μg. A clear correlation between specific activity of the ^{186}Re and specific activity of the antibody preparation was not observed.

4.5 References:

1. John, E., et al., *Rhenium-186-Labeled Monoclonal-Antibodies for Radioimmunotherapy - Preparation and Evaluation.* Journal of Nuclear Medicine, 1993. **34**(2): p. 260-267.

2. Visser, G.W.M., et al., *Labeling of Monoclonal-Antibodies with Re-186 Using the Mag3 Chelate for Radioimmunotherapy of Cancer - a Technical Protocol.* Journal of Nuclear Medicine, 1993. **34**(11): p. 1953-1963.

3. Crudo, J.L., et al., *Optimization of antibody labeling with rhenium-188 using a prelabeled MAG(3) chelate.* International Journal of Pharmaceutics, 2002. **248**(1-2): p. 173-182.

4. Brandau, W., et al., *Technetium-99M Labeled Renal-Function and Imaging Agents.3. Synthesis of Tc-99M-Mag3 and Biodistribution of by-Products.* Applied Radiation and Isotopes, 1988. **39**(2): p. 121-&.

5. Zhang, X.L., et al., *An improved synthesis of S-benzoyl mercaptoacetyltriglycine as BFCA and the labeling of IgG with carrier-free Re-188.* Journal of Radioanalytical and Nuclear Chemistry, 2003. **256**(2): p. 339-343.

Chapter 5

In Vitro Cell Studies

5.1 Introduction

The goal of this section of research was to determine if ^{186}Re-conjugated antibodies retain immunoreactivity after conjugation and to determine whether enough radiation dose could be delivered to cells via specific binding to a receptor of interest with this method to inflict biological damage.

To this end, cells that do and do not express receptors for the Insulin-like Growth Factor Receptor-1 (IGF-1R) were cultured and an antibody for this receptor was labeled as described in Chapter 4. Baseline studies to determine binding of the unconjugated antibody to the receptor and saturation levels were conducted using these cell lines. Studies to determine the intrinsic radiosensitivity of these cell lines were also conducted using both external beam

radiation and free ^{186}Re. Finally, a method to determine specific binding of the labeled antibody to the cell line, which expresses the IGF-1R, was developed and determination of the immunoreactive fraction of the labeled antibody preparation was investigated.

5.2 Role of the Insulin-like Growth Factor Receptor in Radiation Therapy

To assess the feasibility of ^{186}Re-labeled antibodies as possible therapeutics, a receptor target and antibody system of biological interest was required. A survey of the literature resulted in the decision to use the well-studied Insulin-like Growth Factor Receptor-1 (IGF-1R) as a model for the labeled antibody receptor studies. The IGF-1R is normally involved in the regulation of cell proliferation, differentiation and motility, and has also been strongly implicated in regulation of tumor transformation (metastasis) and cancer cell survival [1]. The IGF-1R is overexpressed by several cancer cell lines including carcinomas of the breast, lung, colon and prostate [2]. This receptor has been shown to be associated with an increase in growth in cancer cells and there are several drugs, including humanized antibodies, which target this receptor and are currently undergoing clinical trials as potential anti-cancer agents [2-5]. It has been previously demonstrated that the presence of the IGF-1R

is required for transformation and that inhibition of this receptor leads to increased apoptosis in vitro [2, 6]. In addition, it has been determined that blockade of this receptor (with antibodies or small molecules) may also enhance tumor cell radiosensitivity and sensitivity to chemotherapeutic agents [7, 8].

The IGF (insulin-like growth factor) system consists mainly of six IGF binding proteins, two receptors (IGF-1R, IGF-IIR) and their associated ligands (IGF-I, IGF-II) [2]. In this system, the IGF-IR is the primary responder. Activation of the IGF-IR results in activation of the tyrosine kinase of the receptor, which in turn results in phosphorylation of the insulin receptor substrates [2]. This initiates a signaling cascade, the result of which is the promotion of proliferation and suppression of apoptosis.

The IGF-1R is a transmembrane tyrosine kinase consisting of two extracellular α subunits which are involved in ligand binding and two transmembrane β subunits which are involved in enzymatic activity [1]. These subunits are linked together by disulfide bonds which give rise to the tertiary structure [2].

There are several antibodies available that have high binding affinities to the extracellular domain of the IGF-1R. In these studies, I have chosen to use the 1H7 antibody, which is a mouse monoclonal antibody (MAb) raised against IGF-1R purified from human placenta [9]. MAb 1H7 is an IgG class 1 antibody,

which binds to the α subunit of the IGF-1R and is known to antagonize IGF binding. This antibody is also known to inhibit IGF-I-induced DNA synthesis [9]. In these proof-of-principle studies, using MAb 1H7 as a targeting agent for ^{186}Re would therefore combine directing the radiotherapeutic nuclide to specific cells with the known activity of 1H7 to block receptor activation by IGFs and sensitize the cells to cytotoxic stress.

5.3 Materials and Methods

5.3.1 Materials

The MAb 1H7 antibody and IGF-1Rβ (C-20), an affinity purified polyclonal rabbit antibody against the β subunit of the IGF-1R, were purchased from Santa Cruz Biotechnology (California, U.S.A.). IRDye® 800CW conjugated affinity purified goat anti-rabbit IgG was purchased from Rockland (Pennsylvania, U.S.A.). Goat anti-mouse fluorescein isothiocyanate (FITC) conjugated affinity purified IgG was purchased from BD Canada. Recombinant Protein G Agarose beads (Invitrogen), Trypsin, Fetal Bovine Serum (FBS), Dubelcco's Modified Eagle's Medium (DMEM), Phosphate Buffered Saline (PBS), eosin and A.C.S. grade EDTA were purchased from Fisher Scientific. All plasticware (petri dishes, pipettes and centrifuge tubes) was purchased from Fisher Scientific.

5.3.2 Cells and Cell Culture

Immortalized mouse embryonic fibroblasts (MEFs) from IGF-1R knock out mice (R-) [10] were obtained from the Cox Laboratory (Prostate Center, Vancouver General Hospital, Vancouver, B.C.). A lineage-derived line in which the human IGF-1R is re-expressed (R+) [11] was obtained from P. Sorenson (B.C. Cancer Center, Vancouver, B.C.). Both cell lines were cultured in Dulbecco's Modified Eagle's Medium (DMEM) containing 10% Fetal Bovine Serum (FBS) and passed as required. Both of these cell lines have been fully characterized previously [11-13]. It is interesting to note that the R- cells grew at a markedly slower rate than did the R+, with doubling times of 12 hours and 20 hours for the R+ and R- cell lines respectively, thus further enforcing the idea that the IGF-1R is important for cell proliferation.

In order to use ^{186}Re in our cell culture experiments, a small cell culture laboratory was set up at TRIUMF (due to licensing restraints, the level of ^{186}Re required for experiments was not permitted in the Cox Laboratory). Supported by funding secured from an NSERC Idea to Innovation grant, a previously used radiochemistry lab was outfitted with a flow-through CO_2 incubator (Lab-line, model 315), laminar flow hood (Labconco vertical clean bench), centrifuge, inverted microscope (Motic model AE21), autoclave, refrigerator, freezer and associated equipment for this purpose.

5.3.3 Treatments

Determination of R+ versus R- Binding Affinity for 1H7

To assess specificity of MAb 1H7 binding to IGF-1R expressing cells, a live cell Fluorescence-Activated Cell Sorting (FACS) method was used. R+ and R- cells were seeded into 6 well plates in serum-free media and allowed to adhere for 24 hours. In this medium the cells can adhere to the plate, but the lack of FBS significantly slows down the proliferation rate so as to keep cell numbers consistent without disrupting cell function. The cells were detached from the petri dish with 10 mM EDTA in PBS and treated with 3 μg/ml of 1H7 antibody (or PBS) for 15 minutes. The cells next were treated with 20 μg/ml of goat anti-mouse FITC conjugated affinity purified IgG (excluding blanks – see section 5.4.1), and incubated for a further 15 min. The purpose of the secondary (goat) antibody is to bind to the primary (1H7) antibody and thus qualitatively visualize the amount of primary antibody via fluorescence analysis [14]. The cells were washed twice with PBS and then analyzed for fluorescence intensity.

Determination of Antibody Binding to R+ cells as a Function of 1H7 Concentration

For the determination of differential binding as a function of antibody concentration, R+ cells were seeded onto 6 well plates and allowed to attach for

24 hours. They were incubated in serum free media for 24 hours prior to being detached from the petri dish with 10 mM EDTA in PBS and treated with varying concentrations of 1H7 antibody for 15 minutes. The wells were treated with 20 μg/ml of goat anti-mouse FITC conjugated affinity purified IgG (excluding controls), and incubated for a further 15 min. The cells were washed twice with PBS and then analyzed for fluorescence intensity.

Determination of Cell Line Radiosensitivity

For the determination of cell line radiosensitivity to external beam irradiation, R+ and R- cells were allowed to grow to 50-75% confluence on 100 mm diameter petri dishes (~10^6 cells per dish) in 10 % FBS in DMEM before exposure to external beam radiation. The cells were exposed to X-rays at a dose rate of 5 Gy/min via a 300 kV, 10 mA linear accelerator (linac) at the B.C. Cancer Agency in Vancouver, British Columbia. This linac works in typical fashion by bombarding a tungsten target with electrons, thus creating X-rays in a range of energies (up to 300 keV).

For the determination of cell line radiosensitivity to exposure to free ^{186}Re, approximately 10^5 R+ and R- cells were seeded into 35 mm petri dishes in 10% FBS in DMEM and allowed to adhere for 48 hours in a 5 % CO_2, 37 °C atmosphere. The dishes were treated with increasing concentrations of ^{186}Re

radioactivity in a total volume of 1.5 ml for an exposure period of 48 hours. This small volume ensured that the cell medium would not attenuate the radiation significantly. Each radioactive treated dish was shielded with in-house made plastic beta shields so as to shield neighboring petri dishes from the β radiation. Dose rates were calculated using Varskin3, a beta skin dose program, available from Oak Ridge National Laboratory [15]. The cells were washed with serum-free media and cultured for a further 5 days, passing as necessary so as to keep cell density consistent. For viability measurements the cells were detached from the petri dish with trypsin, stained with a 0.1 % eosin solution in PBS and manually counted with an inverted microscope with the aid of a phase contrast hemacytometer.

Radiolabeled Antibody Studies

The MAb 1H7 was labeled and purified as described in Chapter 4. Approximately 10^5 R+ and R- cells were plated in 10% FBS in DMEM onto 35 mm diameter petri dishes and allowed to adhere for 24 hours in a 5% CO_2, 37 °C atmosphere. The medium was aspirated and cells were exposed to treatment solutions consisting of 33 μg/ml of ^{186}Re-labeled 1H7 antibody and incubated in a 5% CO_2, 37 °C atmosphere for 20 to 60 minutes. The cells were rinsed with PBS, detached from the petri dish with a 10 mM EDTA in PBS solution, centrifuged

and separated from the supernatant liquid and assayed for bound radioactivity with a High Purity Germanium (HPGe) detector. Binding of the rhenium to the EDTA was not suspected due to the stability of the Re-MAG3 complex.

Further investigation was performed to determine the functionality of the 1H7 antibody after exposure to labeling conditions. For this experiment, immunoprecipitation/western blot analysis of IGF-1R from the LNCaP human prostate cancer cell line was used. This is a human cancer cell line in which IGF-1R expression has been studied previously [16]. Cell lysates (1 mg) prepared in Radioimmunoprecipitation Assay (RIPA) buffer, were incubated with 1 μg of either 3B7 (a control anti-IGF-1R antibody), untreated 1H7 and 1H7 that had been exposed to labeling chemical conditions as described in Chapter 4. The IGF-1 receptor-antibody complex was immunoprecipitated using recombinant protein G agarose beads, and separated by Sodium Dodecyl Sulfate PolyAcrylamide Gel Electrophoresis (SDS-PAGE). The protein was transferred to nitrocellulose membranes and blocked with bovine serum albumin to prevent non-specific binding to the nitrocellulose in the subsequent steps. Total IGF-1R was determined by immunoblotting using an IGF-1Rβ (C-20), an affinity purified polyclonal rabbit antibody against the β subunit of the IGF-1R, which was then stained with IRDye® 800CW conjugated affinity purified goat anti-rabbit IgG for fluorescent detection.

5.3.4 Mortality Assays

Clonogenic Assays

Clonogenicity is a determination of the cell's ability to undergo division and form visible colonies and is one of the most sensitive assessments of cell viability. For clonogenicity, cells were dissociated from the petri dish with trypsin immediately after external beam irradiation and counted with a Coulter cell counter. $5 \times 10^5 - 5 \times 10^6$ cells were plated in 10 cm diameter petri dishes with higher numbers of cells plated for higher radiation doses so as to obtain statistically significant numbers of colonies for each treatment level. The plated cells were allowed to grow in a 5% CO_2, 37 °C atmosphere in 10% FBS in DMEM media over a 14 day period. The medium was aspirated from the colonies, which were stained with methyl green (0.1 mol/L in pH 7.4 acetate buffer) and counted by visual inspection.

Fluorescence-Activated Cell Sorting (FACS)

FACS analysis was also used to assess cell cycle distribution and cell viability by DNA content. For the FACS analysis, cells were detached from the petri dish with trypsin 7 days after exposure, rinsed with PBS and fixed in ice-

cold ethanol. Cells were stained with propodium iodide (50 μg/ml in PBS) and analyzed on a flow cytometer at the Jack Bell Research Center. Propidium iodide binds to intact DNA by intercalating between the bases. Cells that are undergoing apoptosis (programmed cell death) have fragmented DNA, which will leave the cell and thus will have a lower cellular fluorescence with this method than do viable cells. The peaks in the viable section of the fluorescence are due to the cell cycle (i.e. diploid G_0/G_1 interphase cells, S-phase cells undergoing DNA replication, and G_2/M-phase cells undergoing division will have respectively higher DNA content and thus a higher fluorescence signal). An example of a typical propidium iodide FACS graph with explanations of the characteristics is shown in Figure 5.1.

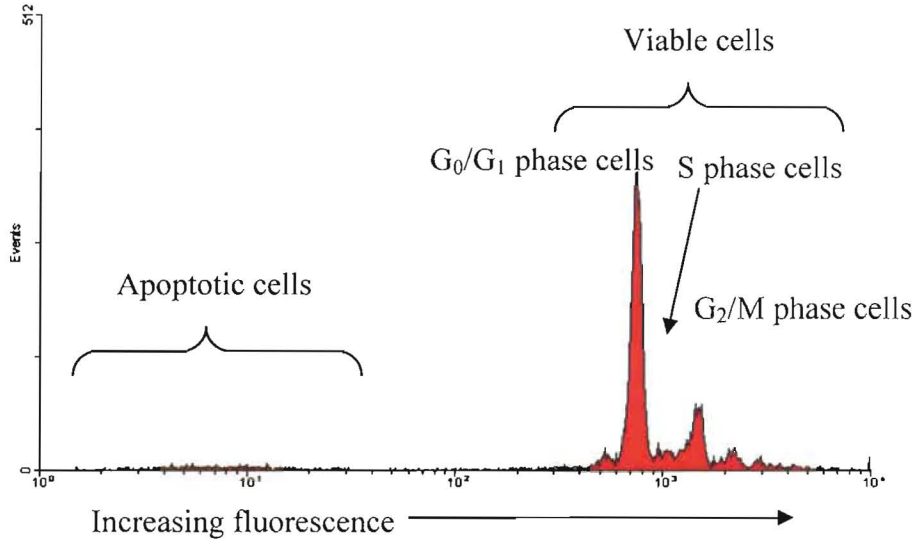

Figure 5.1
Typical propidium iodide FACS analysis of a healthy cell population.
(R+ cells grown 10% FBS in DMEM, in 5 % CO_2, at 50% confluence)

Vital dye exclusion

Vital dye exclusion is a measurement of cell viability via its metabolic processes. This assay is also the simplest used to assess cell viability as it consists of simply visually assessing dye uptake by the cells. Viable cells with intact membranes actively exclude the red eosin dye while the non-viable cells with compromised membranes are unable to. For vital dye exclusion, cells were detached from the petri dish with trypsin and stained with a 0.1 % eosin in PBS solution 7 days after exposure. Viable vs. non-viable cells were manually counted by observation through an inverted microscope. An example of a viable vs. non-viable cell colour is shown below in Figure 5.2. The crenulated cell

morphology and cytoplasmic apoptotic bodies are also visible in the non-viable cell in the photograph, indicating that this cell is undergoing programmed cell death.

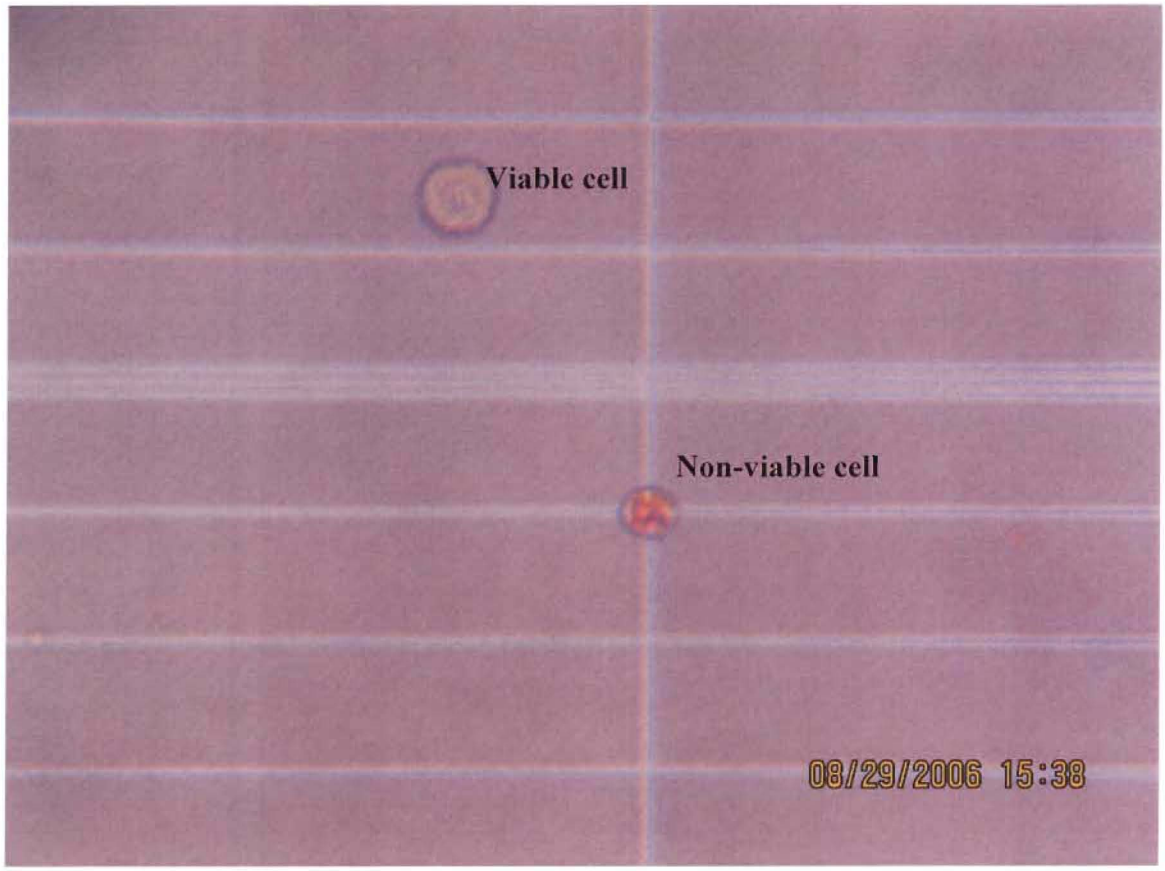

Figure 5.2
Photograph showing the visual difference during a vital dye exclusion assay for a viable vs. non-viable cell. Shown are trypsinized untreated R+ cells in 10% FBS in DMEM at 200X magnification.

5.4 Experimental Design and Results

5.4.1 Determination of Antibody-Receptor Binding

R+ and R- cells were plated and allowed to adhere for 24 hours. The medium was aspirated and R+ and R- cells were treated in duplicate with the treatments given in Table 5.1. The results are shown in Table 5.2

Table 5.1
Treatments to determine specific binding of 1H7 to the R+ cell line

Well Number	Treatment 1	Treatment 2
1	Serum-free media only	Serum-free media only
2	Serum-free media only	2° FITC Antibody
3	1H7 antibody	Serum-free media only
4	1H7 antibody	2° FITC Antibody
5	Normal mouse IgG	Serum-free media only
6	Normal mouse IgG	2° FITC Antibody

Table 5.2
Results of FACS analysis to determine specific binding of 1H7 to the R+ cell line

Well Number	R+ RFI[a]	R- RFI[a]
1	<2	<2
2	2	2
3	<2	<2
4	10	2
5	<2	<2
6	2	2

[a]peak Relative Fluorescence Intensity

R+ and R- cells had peak fluorescence values ~2 RFI (see Figure 5.3 for comparison). The R+ cell line bound significantly more 1H7 antibody than the R- cell line as indicated by the >5-fold increased fluorescence intensity of the 1H7 and FITC 2° antibody-stained R+ cells in the FACS analysis. Fluorescence intensity from well 4 for R+ and R- cells is shown in Figure 5.3.

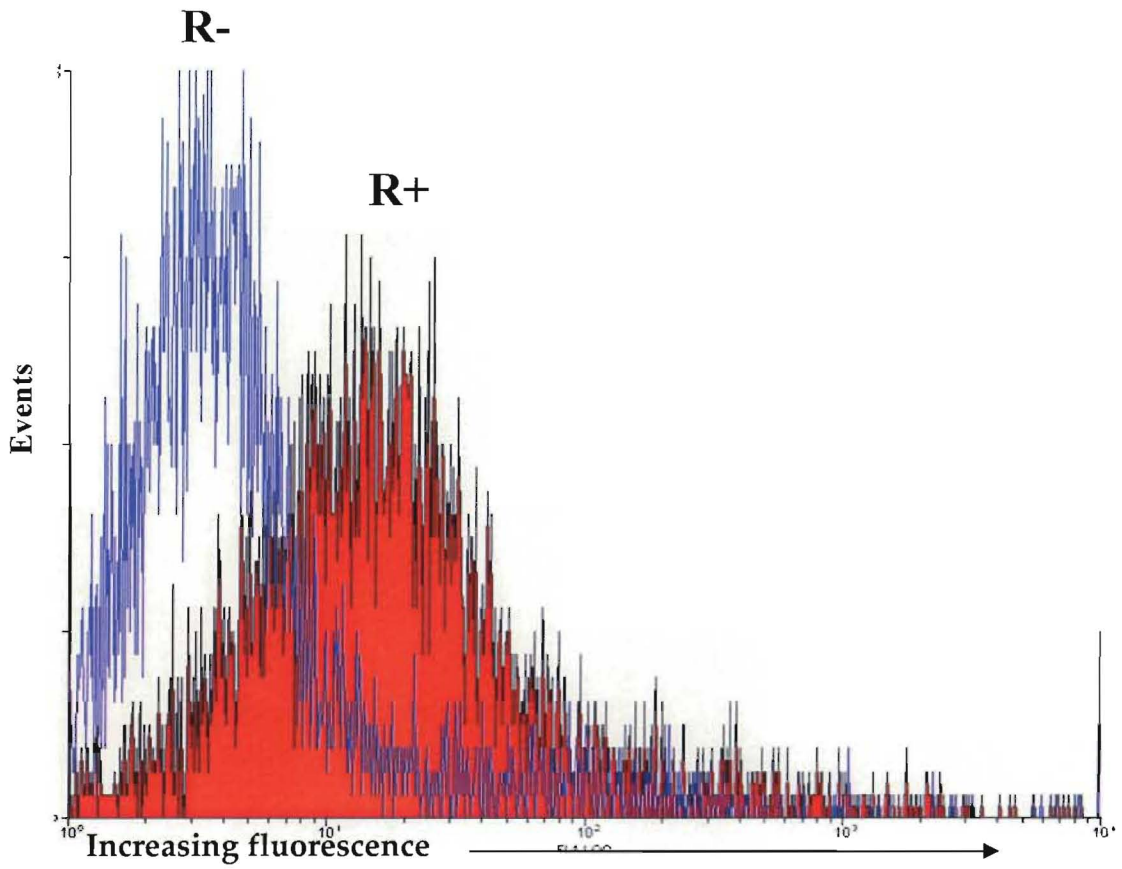

Figure 5.3
Fluorescence-Activated Cell Sorting (FACS) analysis illustrating preferential binding of the 1H7 antibody to the R+ cell line

Determination of Binding to R+ as a Function of 1H7 Concentration

An increased fluorescence signal per cell was achieved when the R+ cell line was incubated with increasing MAb 1H7 concentrations as determined by FACS analysis. This is illustrated in Figure 5.4.

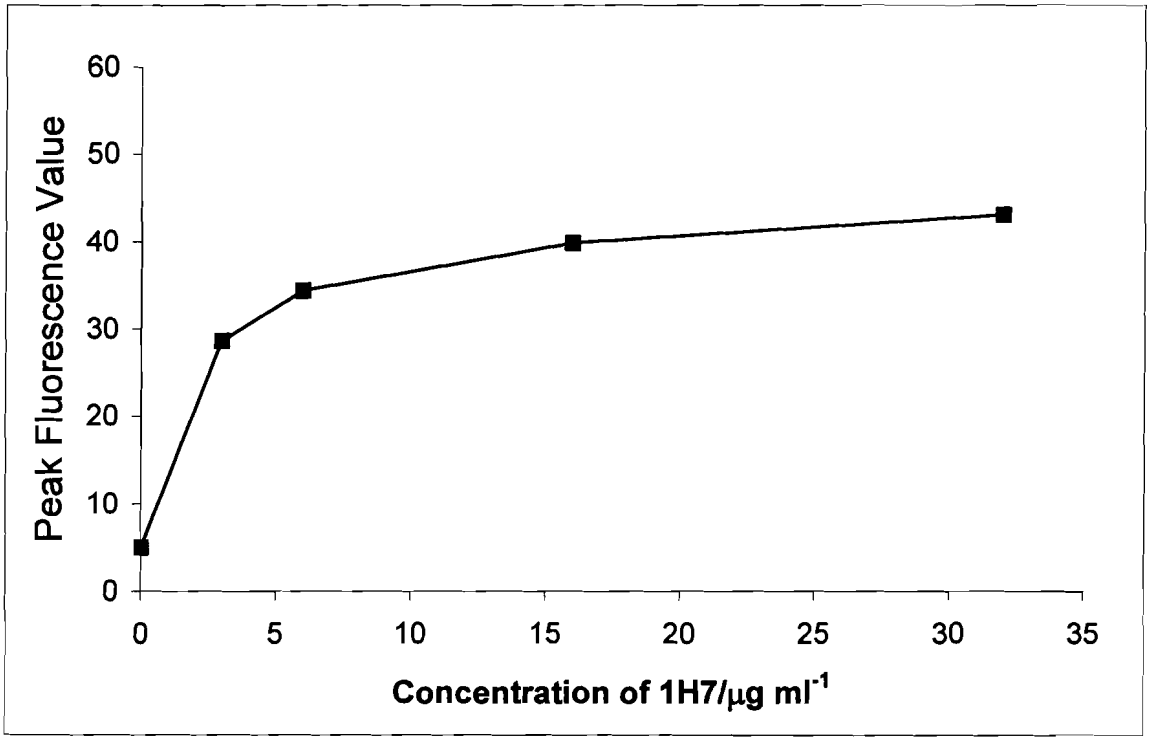

Figure 5.4
Plot of peak fluorescence value as a function of 1H7 antibody concentration. Shown are the maximum intensity fluorescent values for R+ cells incubated with increasing concentrations of MAb 1H7 and stained with FITC 2° antibody.

It is clear that an increased antibody concentration leads to increased antibody binding, with a concentration of 35 μg/ml being essentially a saturating value. Concentrations of 30-35 μg/ml MAb 1H7 were used in subsequent experiments.

5.4.2 Characterization of Cell Line Radiosensitivity Using External Beam Irradiations

In order to determine the intrinsic radiosensitivity of the cell lines and the potential for differential radiosensitivity of the R + and R- cell lines, viability of

R+ and R- cells were analyzed for clonogenicity, by FACS analysis, and by vital dye exclusion after exposure to external beam radiation. The purpose of using many different analyses was to confirm the validity of the vital dye exclusion as a measurement of cell viability. Although the experiments involving external beam radiation were perform jointly at the BC Cancer Agency and the Jack Bell Research Center, which are fully equipped cell biology facilities, all subsequent experiments involving ^{186}Re were performed on-site at TRIUMF for radioactive licensing reasons. For experimental purposes a small cell lab was outfitted, but access to complex equipment (i.e. flow cytometer etc.) was not available. For these reasons, the results of the free radioactivity exposure (as detailed in section 5.3.3) were determined by vital dye exclusion only.

Clonogenic Assays

The results of the clonogenic assays are shown in Figure 5.5. The R- cells exhibited an LD50 (dose which achieves a cell mortality of 50%) of ~4 Gy and an essential LD100 of 9 Gy, whereas the R+ cells exhibited an LD50 of ~5 Gy and an essential LD100 of 12 Gy. This suggests that the R+ cells are intrinsically slightly more resistant to ionizing radiation than R- cells. At high doses (>12 Gy for the R+ cell line and >9 Gy for the R- cell line) cell colonies became very sparse and

diffuse, and thus it was not possible to obtain an accurate estimate of the total number of cell colonies.

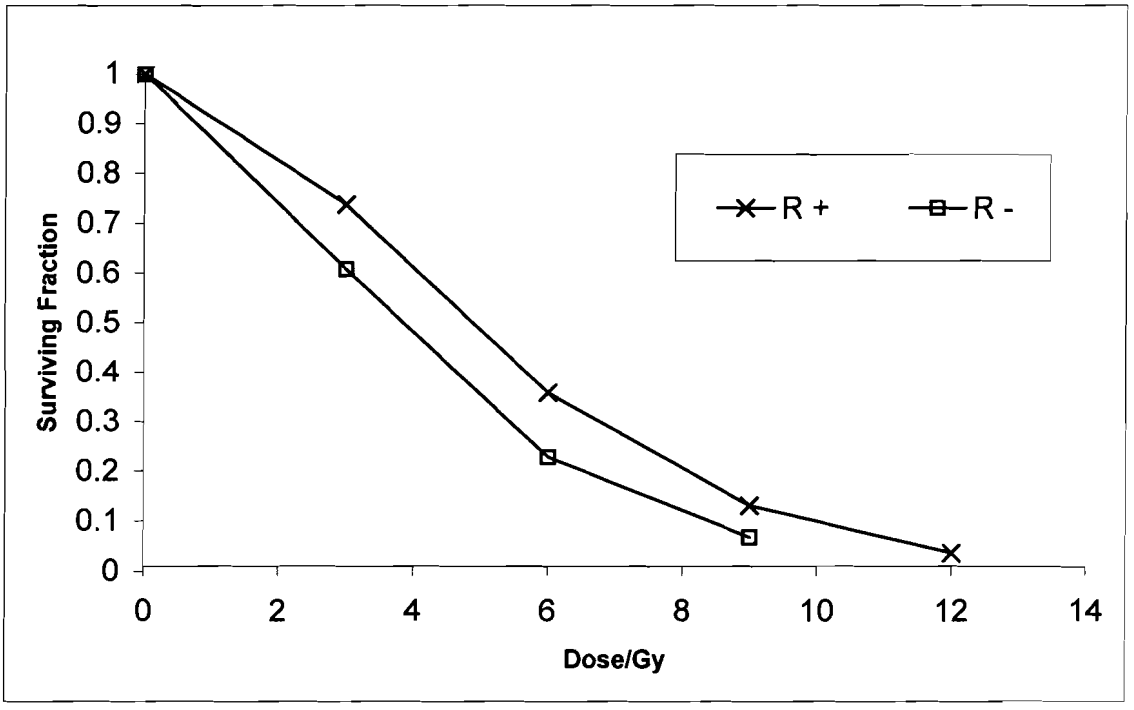

Figure 5.5
Results of external beam irradiation as determined by clonogenic assay. Shown are the number of cells colonies per cell plated, normalized to the plating efficiency as determined by unexposed cells.

Fluorescence-Activated Cell Sorting (FACS)

Figures 5.6 and 5.7 show the results of the FACS analysis for R+ and R- cells at escalating dose rates from 0 to 12 Gy. Again, by this assay, the R- cells exhibited an intrinsic increased sensitivity to radiation exposure (LD50 = ~12 Gy; LD100 = 15 Gy) than R- cells (LD50 = ~6 Gy; LD100 = 12 Gy) though the

magnitude of the difference was greater by FACS (almost 2 fold) than by clonogenicity (~20%).

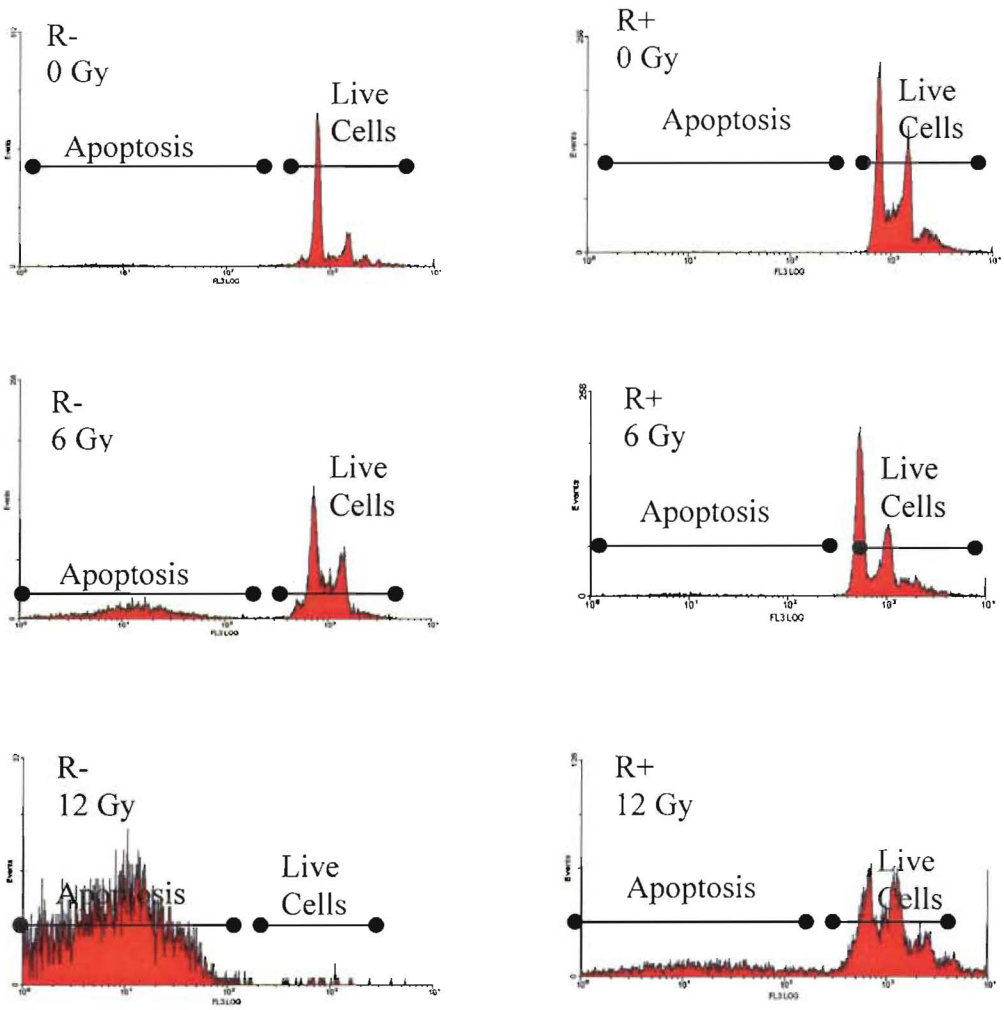

Figure 5.6
FACS analysis of R- (left) and R+ (right) cells exposed to external beam irradiation

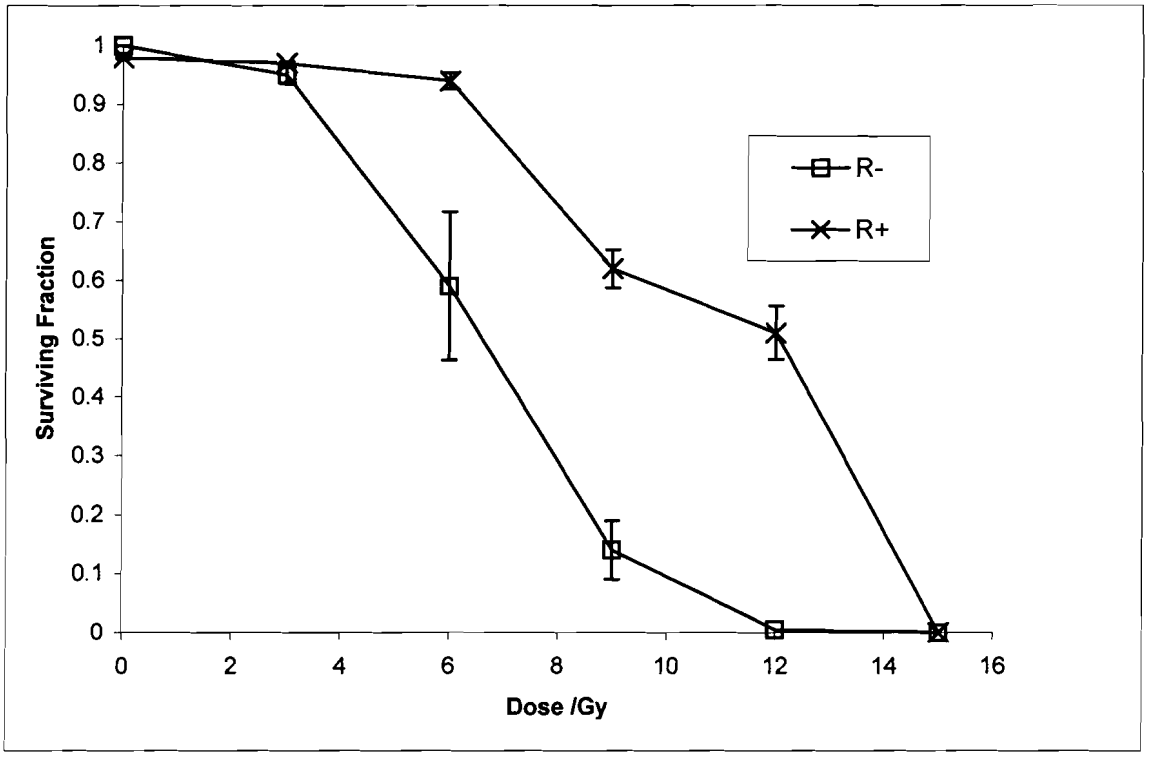

Figure 5.7
Graphical representation of survival of cells exposed to escalating external beam irradiation as analyzed by FACS. Surviving fraction was calculated by dividing number of live cells by the total number of cells (see Figure 5.6).

As can be determined from the preceding figures, the FACS analysis indicates that the R+ cell line has a higher tolerance to radiation than does the R- cell line. In addition, analysis of the FACS profile indicates a severe disruption in the cell cycle distribution of the R+ and R- populations. At the higher dose rates for both cell lines there is an increase in the ratio of cells in M-phase to cells in G-phase. This may indicate a disruption in the natural cell cycle due to the radiation exposure. Similar G_2 arrest has been observed in several cell lines exposed to ionizing radiation [17]. This apparent cell cycle disruption may also be due to cells in the G_0/G_1 phase being preferentially eliminated.

Vital Dye Exclusion

The results of the vital dye exclusion analysis are shown below in Figure 5.8. Initial sensitivity of R+ and R- cells to ionizing radiation by dye exclusion was reminiscent of the responses seen by FACS analysis. While in response to higher doses (>18 Gy for R+ and >12 Gy for R-) the cells began to break up causing the petri dishes to be full of debris, lower doses did allow for calculation of approximate LD50s (15 Gy and 11 Gy for R+ and R- cells, respectively). This result confirms that the dye exclusion assay is a viable alternative to the FACS and clonogenicity assays, which were not feasible to implement on the TRIUMF site.

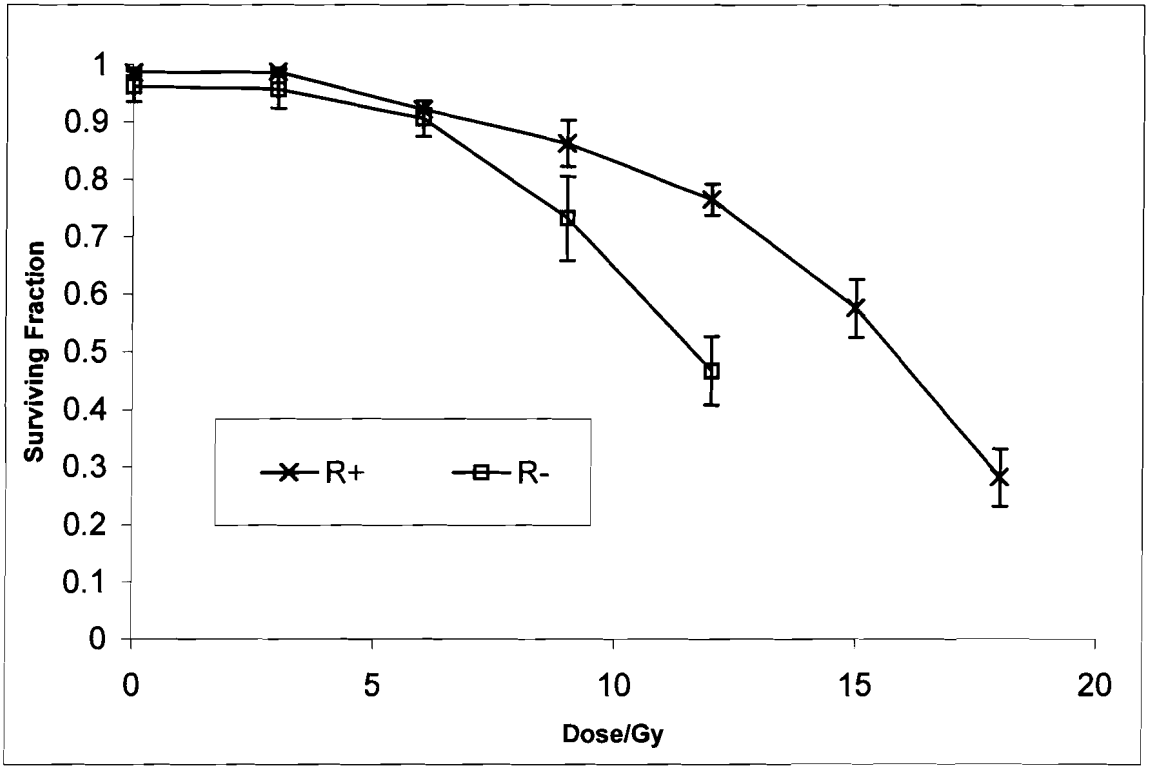

Figure 5.8
Response to external beam irradiation as determined by vital dye exclusion

Comparison of viability analysis

Results of the clonogenic, FACS analysis, and dye exclusion show similar trends indicating that loss of IGF-1R expression radio-sensitizes the fibroblasts to external beam irradiation. This observation has been demonstrated recently by other groups [8]. The LD50 for external beam irradiation for both cell lines as determined by all three methods of analysis can be found below in Table 5.3

Table 5.3
LD50 for R+/R- cells as analyzed by FACS, vital dye exclusion and clonogenicity

	FACS	Vital Dye Exclusion	Clonogenicity
R+	12.0 Gy	15.0 Gy	5.0 Gy
R-	6.0 Gy	11.0 Gy	4.0 Gy

As can be determined from comparative assays, the sensitivity of these tests varies greatly with the sensitivity of clonegenicity > FACS > vital dye exclusion. Since the capacity of the cells to continue to propagate is the strictest measure of survival to radiation damage, results from vital dye exclusion should only be thought of as a rough estimate of cell viability, with cell damage (in a propagation sense) most likely occurring at lower doses. The lack of direct comparability between the clonogenicity assay with the FACS and dye exclusion assays likely results from cell to cell variability in the time to breakdown of

cellular metabolism such that observation of fractions of cells undergoing apoptosis (FACS) or losing membrane pump integrity (dye exclusion) represent only a snapshot of the response of that fraction at a given point in time.

5.4.3 Characterization of Cell Line Radiosensitivity Using Exposure to Free ^{186}Re

R+ and R- cells were next exposed to escalating doses of free ^{186}Re to determine the relative sensitivity of cells to beta vs. X-ray ionizing radiation. Using dye exclusion as an end point, concentrations from 50 μCi/ml to 300 μCi/ml were required to achieve cell kill comparable to that achieved with external beam radiation. Dose rates were calculated as in section 5.3.3 in order to make a comparison between external beam irradiations and exposure to free ^{186}Re. Attempts were made to experimentally confirm these values using Thermo Luminescent Dosimeter (TLD) chips, which were affixed to the bottom of the petri dishes. While quantitative numerical dose estimates were not obtained for these TLD chips, confirmation of the ratios of doses between treatments was achieved (the TLD chips exhibited a linear response to β irradiation). All numerical doses shown for dose from ^{186}Re are those calculated by Varskin3 [15].

A photograph of the transfected (R+) adherent cells prior to exposure to ^{186}Re is shown below in Figure 5.9.

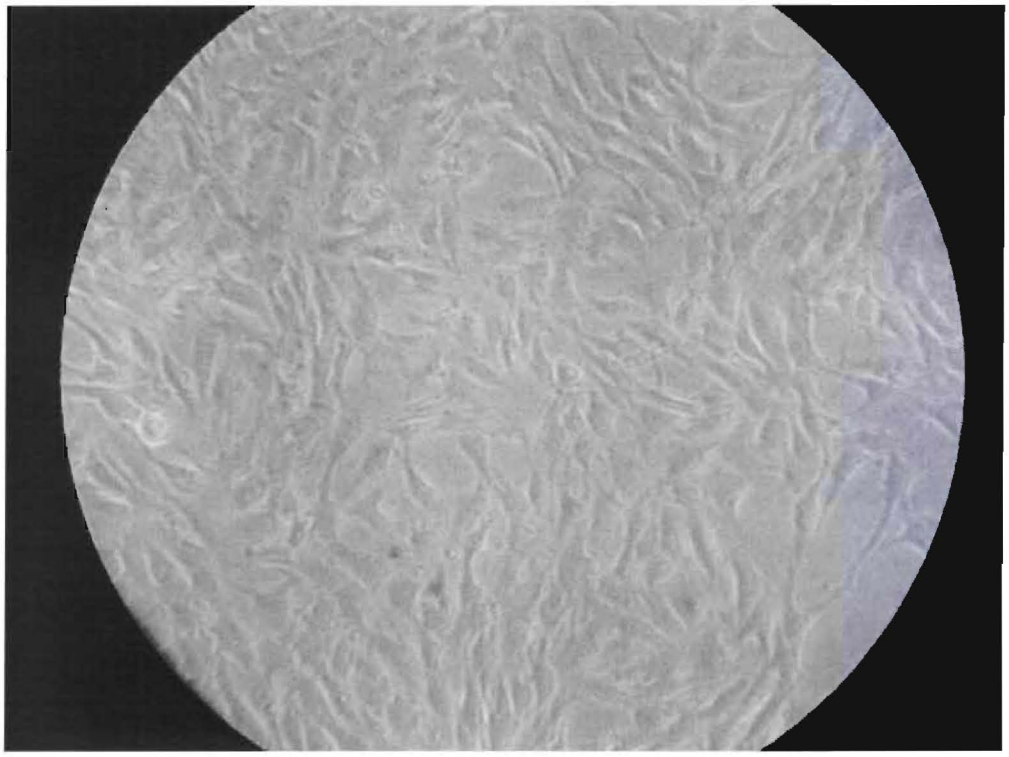

Figure 5.9
Photograph of R+ cells used in the study.
Shown are untreated R+ cells in 10% FBS in DMEM at 100X magnification

The R+ and R- cell lines are phenotypically indistinguishable by visual inspection.

Cells exposed to beta irradiation underwent morphological changes with many of them lifting from the surface of the petri dish. A photograph of R+ cells exposed to 300 μCi/ml free ^{186}Re for 48 hours can be found below in Figure 5.10.

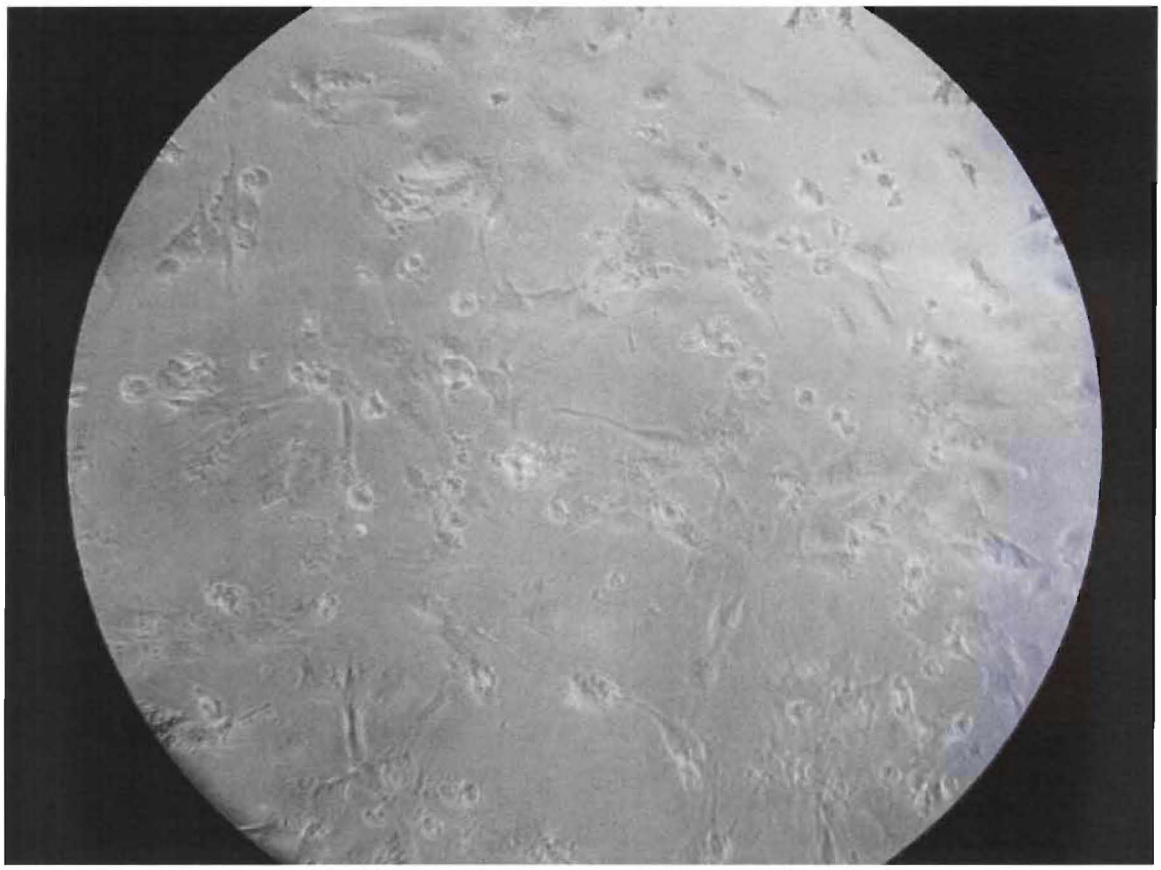

Figure 5.10
Photograph of R+ cells exposed to ^{186}Re. Shown are R+ cells in 10% FBS in DMEM exposed to 300 μCi/ml free ^{186}Re for 48 hours at 100X magnification.

The results of cell kill by exposure to free ^{186}Re are shown below in Figure 5.11. In this case no differential radiosensitivity between the R+ and R- cells was observed, with LD50 for both cell lines ~30 Gy.

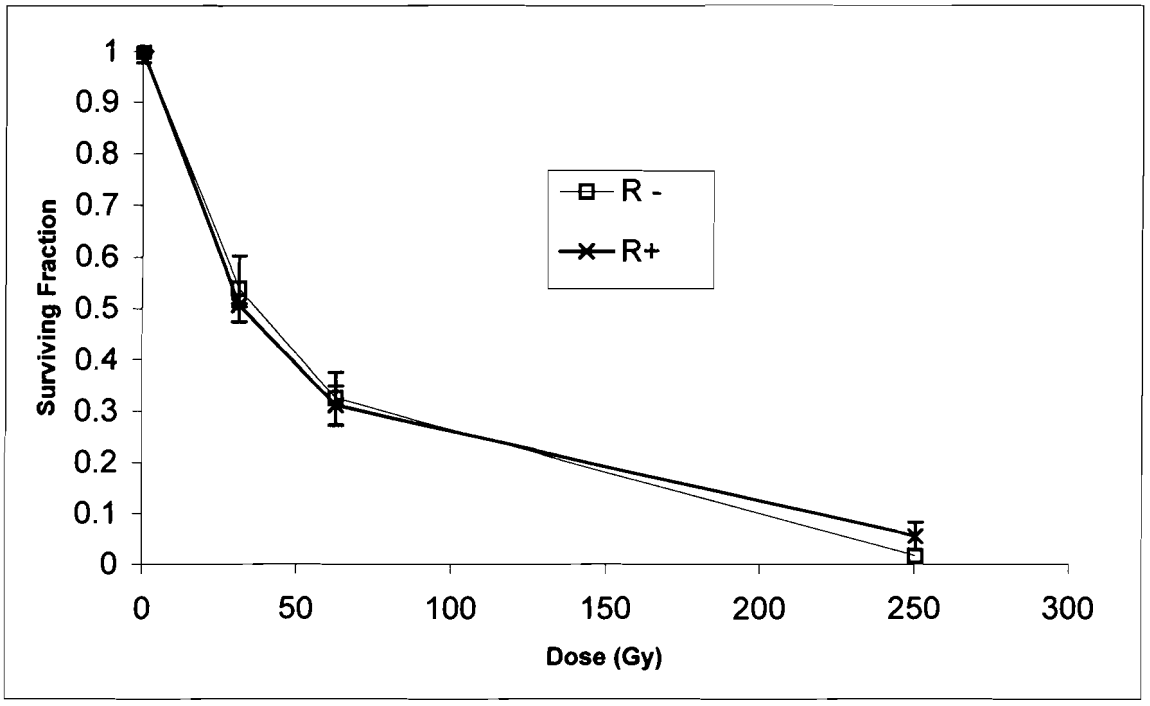

Figure 5.11
Dose-response curve of R+ and R- cells exposed to ^{186}Re as determined by vital dye exclusion.

Two things can be noted from the preceding figure: (1) Much higher doses are needed to achieve the same percentage of cell kill when using free ^{186}Re as compared to external beam irradiation (>2 fold for the LD50 as assayed by vital dye exclusion); (2) there does not appear to be a difference in R+ vs. R- cell kill with respect to exposure to free ^{186}Re. Interpretations of this effect are covered in more detail in the next section.

Dose Rates and Linear Energy Transfer

It is of value to note the difference in cell kill at varying dose rates and types of ionizing radiation. This is illustrated in Figure 5.12

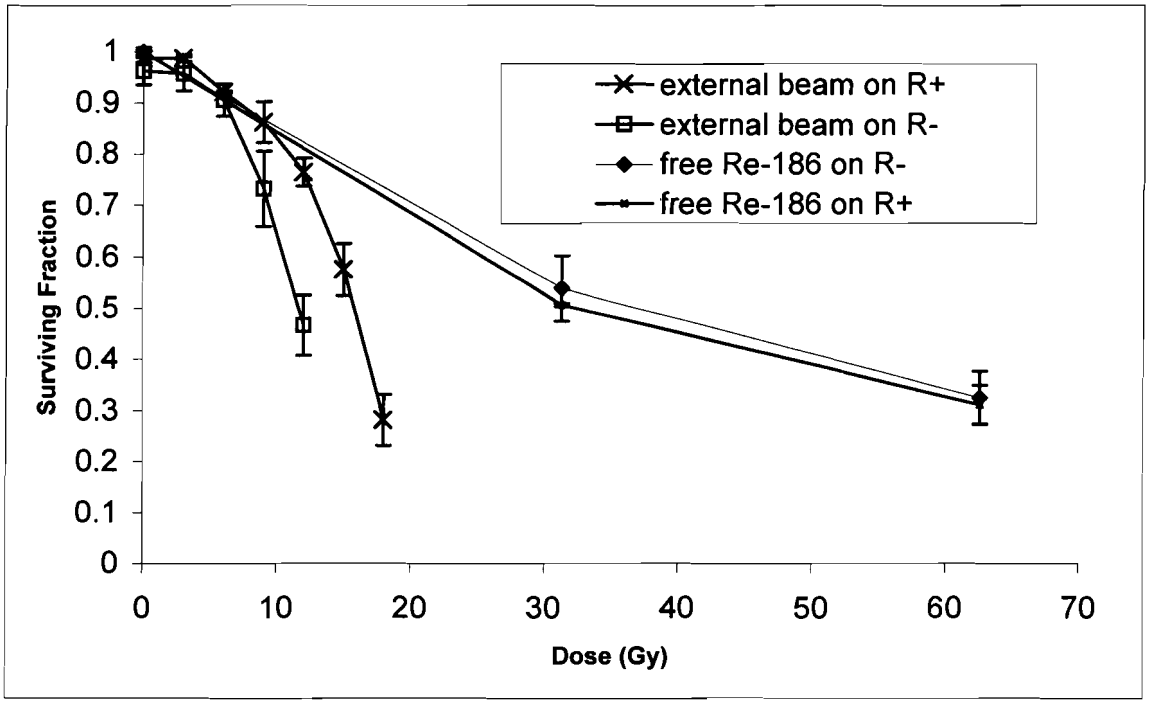

Figure 5.12
Comparison of dose-response curves to external beam radiation and free ^{186}Re

This may be due to differences amongst various repair mechanisms. It has been recently observed that certain agents can radiosensitize cells to low linear energy transfer (LET) radiation (gamma rays) but not high LET radiation (such as beta or alpha particles) [18]. It is thought that the breaks in DNA caused by high LET radiation are more complex and slowly repaired than those due to low LET radiation, and thus radiosensitization agents may interfere with repair mechanisms concerning damage from low LET radiation [18]. In addition, the lower dose rates (initial dose rate 0.46 Gy/hour) for the free ^{186}Re experiments provide longer time for cell DNA repair, thus possibly accounting for the much

higher doses required to achieve the same cell kill with free ^{186}Re, than as for the external beam radiation, although the effects of low dose rates on apoptosis are variable [17]. This observation is important as comparisons are often made between therapeutic effects of external beam irradiation and targeted molecular radiotherapy despite vast differences in dose rates and types of cellular damage [17].

5.4.4 Radiolabeled Antibody Studies

After several attempts using a variety of methods detailed in Table 5.4, specific binding to IGF-1R in the R+ cell line of the labeled MAb 1H7 was observed. Figure 5.13 shows typical results of a radiolabeled 1H7 binding assay.

Table 5.4
Unsuccessful attempts to determine 1H7 binding to R+ and R- cell lines

Attempt	Method	Results
1	Treat cells, wash cells in PBS and assay cells for bound radioactivity while adhered to petri dishes.	Discovered preferential binding of the 1H7 antibody to the petri dish rather than cells leads to excessive background. Further literature research indicated that this problem had been reported previously.
2	Treat cells, wash cells in PBS and lift cells with trypsin. Assay suspended cells for bound radioactivity.	Trypsin treatment detached all radiolabeled antibody and thus radioactivity from cells.
3	Trypsinize cells and treat while suspended. Centrifuge, wash cells with PBS and assay for radioactivity.	No radioactivity bound to cells. We suspect this may be because the trypsin treatment causes the R+ cells to shed the receptor.
4	Treat cells. Gently scrape cells off petri dish without the aid of trypsin. Centrifuge, wash with PBS and assay for radioactivity.	Inconsistent results. Suspect clumping of cells led to poor rinsing of loose radioactivity.

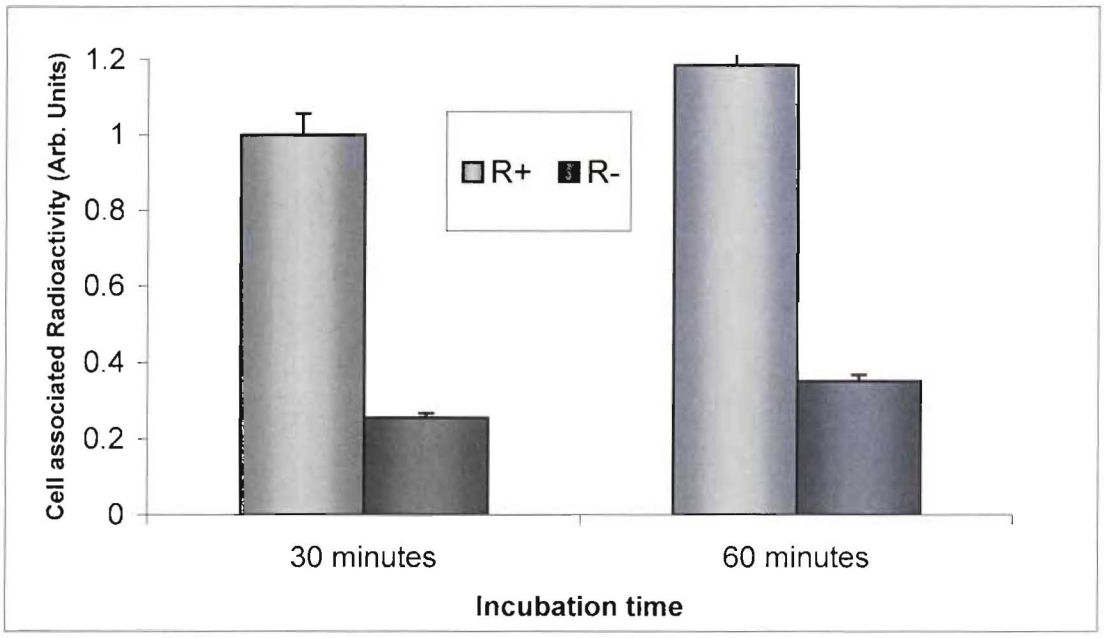

Figure 5.13
Cell associated radioactivity for R+ and R- cells incubated with labeled 1H7 antibody

While results varied, average bound radioactivity indicated that approximately 10^5-10^6 antibodies were bound to each R+ while approximately 30% of this was bound to each R- cell through non-specific binding. This 30% seemed to be consistent even though total antibody binding to each cell line varied by an order of magnitude. This may be the result of the final bioconjugation step, which variably denatured some portion of the antibody mixture. In addition, the amount of radioactivity bound to each cell was orders of magnitude lower than that required to achieve even 10% cell kill. No binding difference was found between cells incubated with radiolabeled preparation for high as opposed to low specific activity ^{186}Re. It may be the case that this model

is not sensitive enough to determine the difference in binding affinity between these two preparations.

Further analysis determined that the 1H7 antibody does undergo significant denaturization during the labeling process. The result of the IP-western blot analysis is shown below, in Figure 5.14.

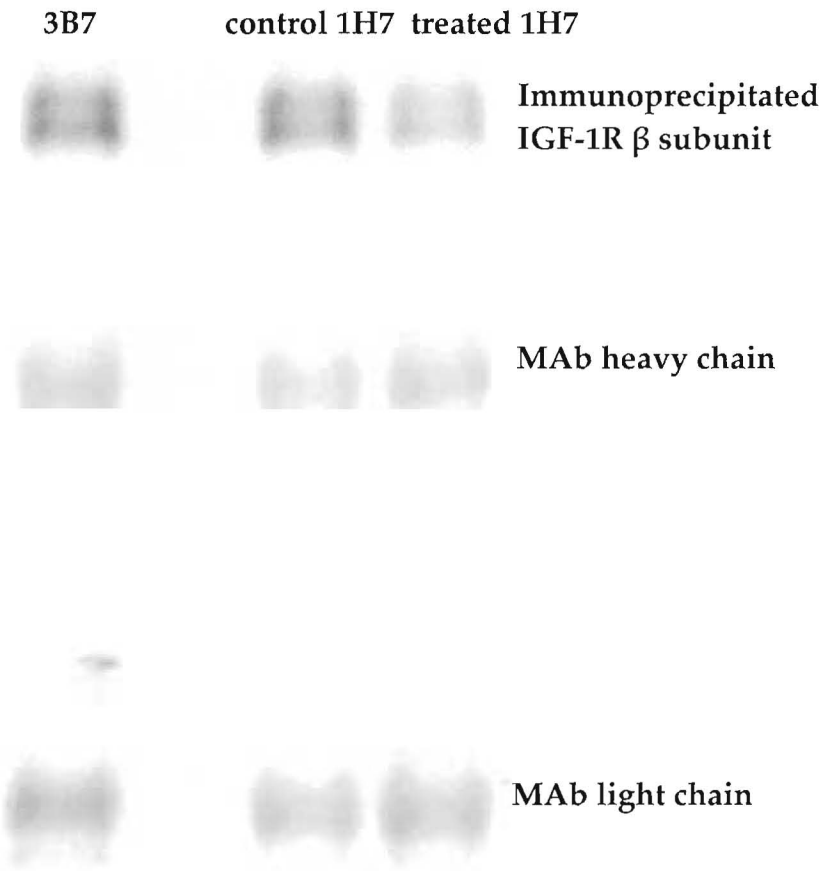

Figure 5.14
SDS PAGE Western Blot analysis of immunoreactivity of labeled 1H7.

The Western Blot analysis indicated that the treated 1H7 has approximately 50% of the immunoreactivity as compared to the untreated 1H7

as the fluorescence of the treated 1H7 immunoprecipitated IGF-1R β subunit band is 50% that of the native 1H7 immunoprecipitated IGF-1R β subunit band . This is shown by the decreased intensity in the IGF-1R band detected in the treated 1H7 lane. It appears that the total amount of antibody was consistent as indicated by the similarities in intensity of the heavy and light chains (the secondary antibody used also bound to the light and heavy chains of the 1H7 and 3B7). These results indicate a loss of immunoreactivity. It is suspected that this change in immunoreactivity may be responsible for the inconsistent results from the labeled 1H7 binding studies.

5.5 Conclusions

The IGF-1R was investigated as a possible target for radioimmunotherapy. Cells that do and do not express the IGF-1R, were exposed to external beam radiation and to free ^{186}Re. Differential radiosensitivity was observed between the R+ and R- cell lines when exposed to external beam radiation indicating that the IGF-1R may have a radioprotectant effect. This difference was not observed during exposure to free ^{186}Re, indicating that the mechanism of cell damage from these two types of radiation is different and that various repair mechanisms involving the IGF-1R may be responsible for this differential effect. The 1H7 antibody was labeled with both HSA and LSA ^{186}Re as described in Chapter 4.

Although specific binding to the R+ cell line was observed with the labeled antibody, no difference was observed between the HSA and LSA preparations. In addition, a significant portion of the 1H7 antibody was denatured during the labeling process as determined by an immunoprecipitation Western Blot analysis.

5.6 References

1. Larsson, O., A. Girnita, and L. Girnita, *Role of insulin-like growth factor 1 receptor signalling in cancer.* British Journal of Cancer, 2005. **92**(12): p. 2097-2101.

2. Wang, Y. and Y. Sun, *Insulin-like growth factor receptor-1 as an anti-cancer target: blocking transformation and inducing apoptosis.* Current Cancer Drug Targets, 2002. **2**(3): p. 191-207.

3. Krueckl, S.L., et al., *Increased insulin-like growth factor I receptor expression and signaling are components of androgen-independent progression in a lineage-derived prostate cancer progression model.* Cancer Research, 2004. **64**(23): p. 8620-8629.

4. LeRoith, D., et al., *The role of the insulin-like growth factor-I receptor in cancer.* Receptor Activation by Antigens, Cytokines, Hormones, and Growth Factors, 1995. **766**: p. 402-408.

5. Cohen, B.D., et al., *Combination therapy enhances the inhibition of tumor growth with the fully human anti-type 1 insulin-like growth factor receptor monoclonal antibody CP-751,871.* Clinical Cancer Research, 2005. **11**(5): p. 2063-73.

6. Granerus, M. and W. Engstrom, *Effects of insulin-like growth factor-binding protein 2 and an IGF-type I receptor-blocking antibody on apoptosis in human*

teratocarcinoma cells in vitro. Cell Biology International, 2001. **25**(8): p. 825-8.

7. Benini, S., et al., *Inhibition of insulin-like growth factor I receptor increases the antitumor activity of doxorubicin and vincristine against Ewing's sarcoma cells.* Clinical Cancer Research, 2001. 7(6): p. 1790-7.

8. Cosaceanu, D., et al., *Modulation of response to radiation of human lung cancer cells following insulin-like growth factor 1 receptor inactivation.* Cancer Letters, 2005. **222**(2): p. 173-181.

9. Li, S.L., et al., *Two new monoclonal antibodies against the alpha subunit of the human insulin-like growth factor-I receptor.* Biochem Biophysics Research Communications, 1993. **196**(1): p. 92-8.

10. Coppola, D., et al., *A functional insulin-like growth factor I receptor is required for the mitogenic and transforming activities of the epidermal growth factor receptor.* Molecular and Cellular Biology, 1994. **14**(7): p. 4588-95.

11. Martin, M.J., et al., *The insulin-like growth factor I receptor is required for Akt activation and suppression of anoikis in cells transformed by the ETV6-NTRK3 chimeric tyrosine kinase.* Molecular and Cellular Biology, 2006. **26**(5): p. 1754-69.

12. Morrison, K.B., et al., *ETV6-NTRK3 transformation requires insulin-like growth factor 1 receptor signaling and is associated with constitutive IRS-1 tyrosine phosphorylation.* Oncogene, 2002. **21**(37): p. 5684-95.

13. Liu, J.P., et al., *Mice carrying null mutations of the genes encoding insulin-like growth factor I (Igf-1) and type 1 IGF receptor (Igf1r).* Cell, 1993. **75**(1): p. 59-72.

14. Harlow, E. and D. Lane, *Antibodies: a laboratory manual.* 1988, Cold Spring Harbor, NY: Cold Spring Harbor Laboratory. xiii, 726 p.

15. RSICC, *Varskin3, Beta point-kernal Software.* 2004: Oak Ridge, TN.

16. Krueckl, S.L., et al., *Increased insulin-like growth factor I receptor expression and signaling are components of androgen-independent progression in a lineage-*

derived prostate cancer progression model. Cancer Research, 2004. **64**(23): p. 8620-9.

17. Pouget, J.P. and S.J. Mather, *General aspects of the cellular response to low- and high-LET radiation.* European Journal Nuclear Medicine, 2001. **28**(4): p. 541-61.

18. Supiot, S., et al., *Gemcitabine radiosensitizes multiple myeloma cells to low LET, but not high LET, irradiation.* Radiotherapy and Oncology, 2007. **83**(1): p. 97-101.

Chapter 6

Ion Source Experiments

6.1 Introduction

^{186}Re is typically produced by neutron capture on stable ^{185}Re. As the product element is the same as the target element, these species cannot be separated chemically and thus this reaction yields a product with low specific activity. As mentioned in Chapter 1, this is not optimal for site-specific radiotherapy. The goal of this section of research was to investigate the feasibility of using an ionization and mass separation technique for the production of high specific activity ^{186}Re from neutron irradiated reactor targets. A similar technique has been demonstrated previously to purify ^{81}Rb for nuclear medicine applications [1]. The first step in this process is to investigate a means of producing an ionized species of rhenium. To this end, experiments were

conducted at both Oak Ridge National Laboratory with an electron beam plasma ion source and at TRIUMF with a proof-of-principle cusp ion source test stand.

Although progress has been made towards improving the specific activity of ^{186}Re from reactor targets via a Szilard-Chalmers reaction, this method requires wet chemical processing of the neutron irradiated target, is not capable of achieving specific activities near theoretical values and/or has reduced recoveries of ^{186}Re from the target material [2, 3].

6.2 Experiments with an Electron Beam Plasma Ion Source at Oak Ridge National Laboratory

6.2.1 Overview

Several experiments were conducted at Oak Ridge National Lab to determine the feasibility of producing a rhenium radioactive ion beam via proton irradiation of a natural abundance tungsten oxide (WO_3) target material. Offline studies were conducted in order to determine the percent release of rhenium isotopes from the target material and online studies were conducted to determine the ionization efficiency in an electron beam positive ion source.

6.2.2 Pressing Pellets, Loading and Off-line Irradiation of the Target Material

Attempts to press target pellets from pure WO_3 were unsuccessful. Addition of 3% albumin as a binder resulted in more successful pellets but the composite pellets were still quite friable and thus required careful handling. Pellets were loaded into aluminum holders for irradiation. As a safety precaution the back of the aluminum holders containing the WO_3 powder were covered with a tantalum foil to prevent contamination of the irradiation apparatus. Due to the low beam currents throughout these experiments (see Table 6.1) no cooling was necessary.

The pellets were irradiated with 25 MeV protons accelerated by the tandem accelerator at Oak Ridge National Lab. A photograph of the tandem accelerator building is shown in Figure 6.1 and irradiation details can be found in Table 6.1.

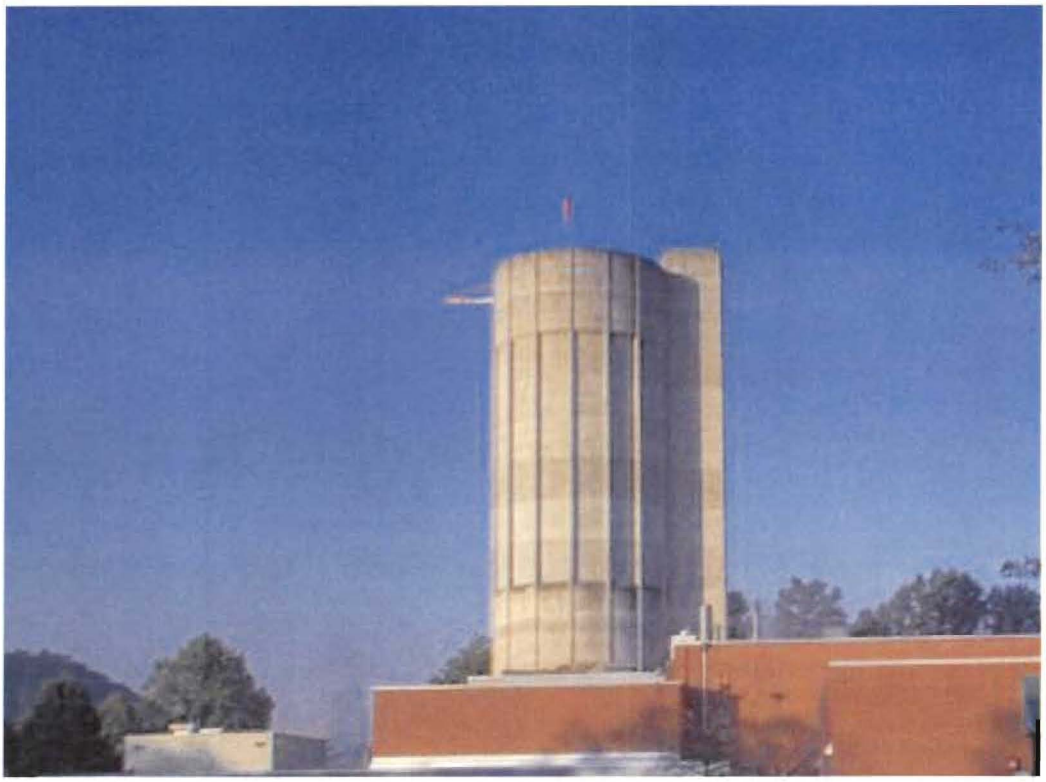

Figure 6.1.
Oak Ridge tandem accelerator building

Table 6.1
Tungsten oxide sample irradiation parameters

Sample	Irradiation Time (min)	Current	Comments
WO_3 #1	8	30 nA	Stopped due to outgassing, unable to get stable vacuum
WO_3 #2	60	20 nA	Irradiated successfully
WO_3 #3	65	20 nA	Irradiated successfully Removed target ladder ~3R/hour on contact

6.2.3 Release Measurements on the Material Test Stand

The materials test stand consists of a removable resistively heated tantalum boat contained in a vacuum chamber. The chamber contains a viewing port and is externally water-cooled. The sample is placed in the boat, which is heated for a predetermined time and then assessed for release of radioactive materials.

The two successfully irradiated samples were (very carefully!) removed from the sample holders. The WO_3 pellets were very delicate, thus recovered pieces were placed in molybdenum dishes for further testing. A total of four WO_3 samples were prepared from the two irradiated samples of 400-500 mg each. The temperature of the dish was determined by means of a pyrometer through the viewing window as shown in Figure 6.4. Release of the radioactive rhenium species was determined by gamma spectroscopy of the sample both before and after heating. The loss of WO_3 target material due to volatilization was also calculated. Results are shown in Figure 6.5. The pressure for a typical experiment was 1×10^{-4} torr, which is similar to the pressure in the ion source during ion beam production. Photographs of two different samples before and after heating and of the material test stand apparatus are shown below in Figures 6.2 and 6.3. Figure 6.4 is a photograph of the heated sample taken through the viewing window. Figure 6.5 displays the results of the release measurements in

graphical form. From Figure 6.5, a compromise temperature of 1100 ° C would give 20-25% release without unreasonable (<10 %) target material loss.

Figure 6.2
Two WO_3 samples: W1 (after heating) and W4 (before heating)

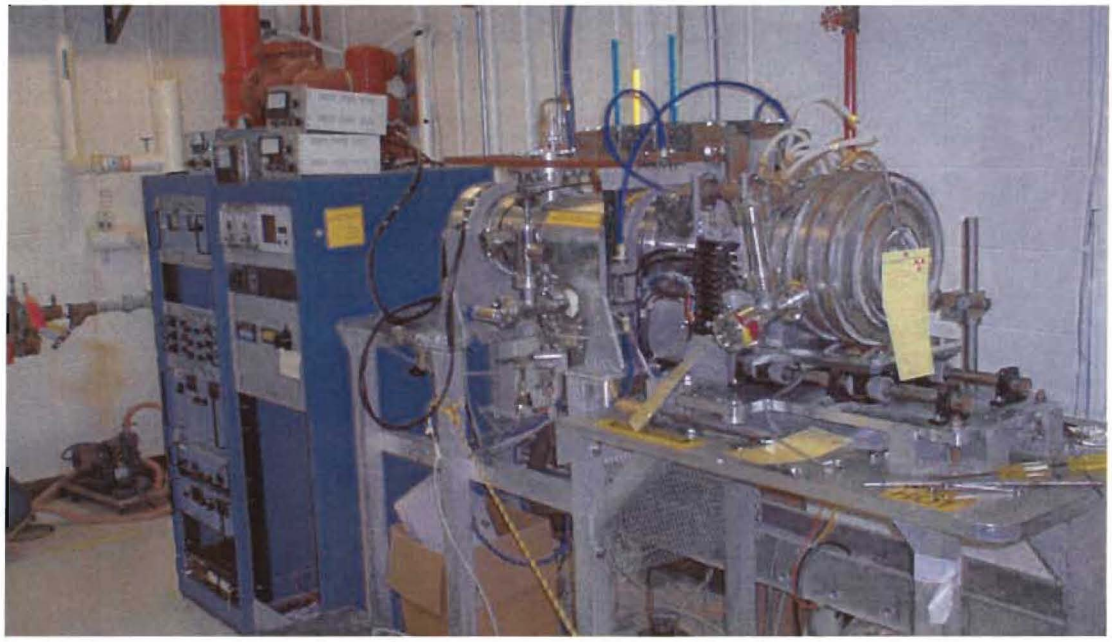

Figure 6.3
ORNL Material Test Stand

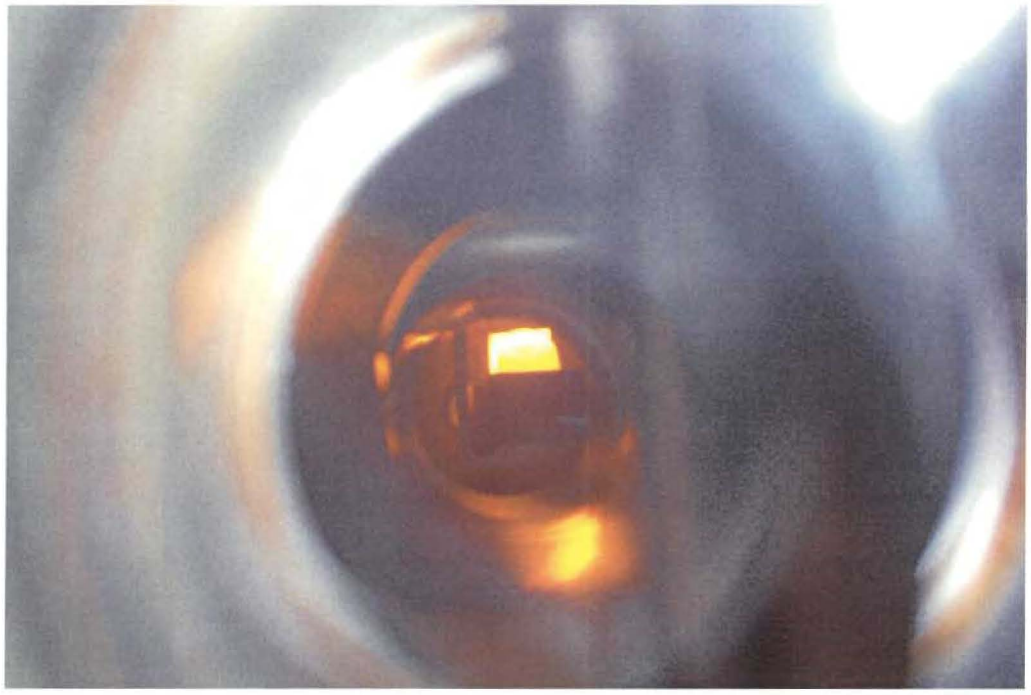

Figure 6.4
Photograph of the heated sample taken through the viewing window

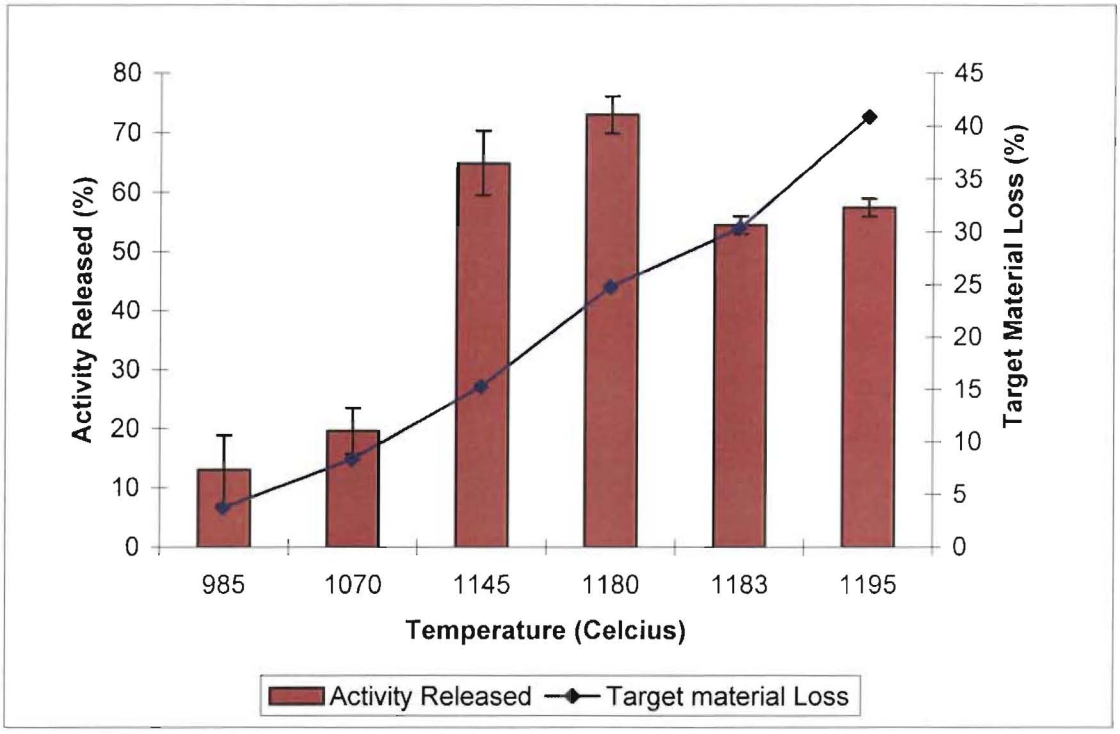

Figure 6.5
Release of rhenium isotopes from WO_3 target material for 2 hour heating times (some target loss is volatilization of albumin binder material).

6.2.4 Online Test Using the On-Line Test Facility (OLTF)

The purpose of this experiment was to determine the efficiency of the electron beam plasma source to produce positive ions of rhenium. Briefly, a tungsten oxide (Alfa Aesar, 99.998%) target was irradiated which was connected to a transfer tube. The transfer tube was heated so as to keep the rhenium oxide ions in the gas phase. Ideally, the ions would be transported into the path of an intense electron beam, producing positive ions, which could be extracted and implanted onto a moving tape system, which is monitored continuously by a high purity germanium detector. A bending magnet in between the ion source and tape collection system allowed for selection of various masses. A diagram of the online test facility at ORNL is shown in Figure 6.6.

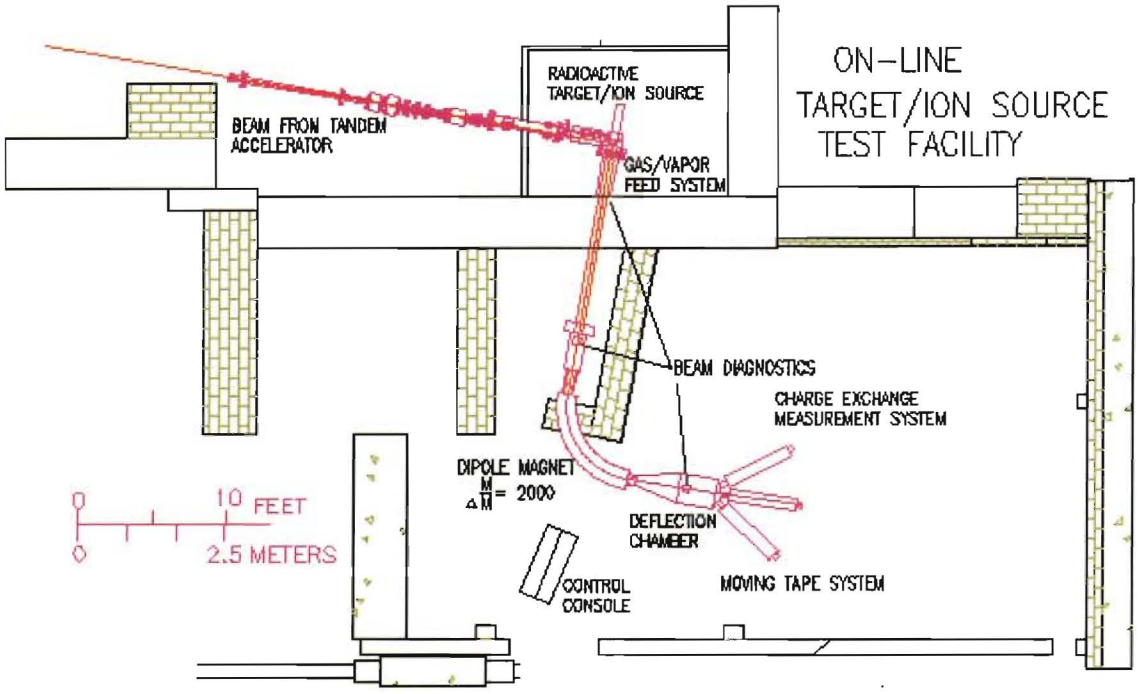

Figure 6.6
On-Line Test Facility at ORNL

The electron beam plasma source generates positive ions by means of electron bombardment. A schematic of this ion source is shown in Figure 6.7. The proton beam is perpendicular to the page and is incident on the target material reservoir. Gas phase species travel through the vapor transport tube, which is maintained at a high temperature (>1500 °C) to keep the desired species in the gas phase. The entire apparatus is constructed of tantalum. The gas phase species are ionized by electrons emitted from the hot (>2000 °C) cathode and positive ions are subsequently extracted.

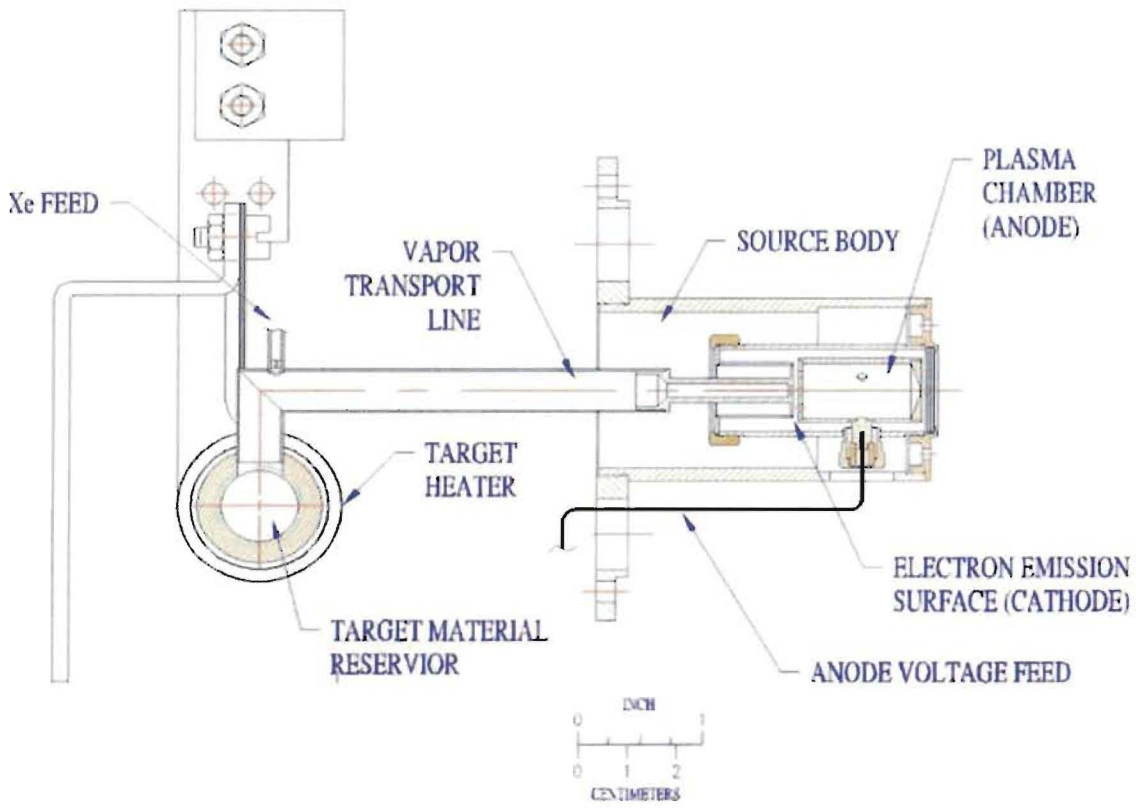

Figure 6.7
Schematic of the electron beam plasma source

The tantalum target holder was loaded with ~7 grams of natural abundance WO_3 powder. A calibrated Xenon leak was used to monitor efficiency of the ion source before and after loading with the target material. Xenon ionization efficiency was stable at about 15 %, indicating the ion source was performing normally.

The target material was irradiated for nearly 24 hours with 50 nA of 40 MeV protons. All masses of the rhenium isotopes as well as the mass of their respective oxides were systematically scanned with the bending magnet. The

heater current was increased (eventually the vacuum was compromised) and the anode voltage and current were changed. Unfortunately, there was no evidence of any radioactive rhenium isotopes at the end of the beamline as determined by gamma-ray spectroscopy. Based on the germanium detector efficiency and background radioactivity the rhenium beam intensity was <500 atoms/sec.

A necropsy was conducted on the ion source to determine the fate of the rhenium species produced. A photograph of this necropsy is shown below in Figure 6.8. Note in particular the scorch marks on target material reservoir. Although it is difficult to see in the photograph, corrosion was evident on the cathode assembly and the vapor transport tube.

Figure 6.8
Photograph of the electron beam plasma ion source necropsy

Each piece was analyzed for radioactivity using a calibrated high purity germanium detector. Figure 6.9 shows a diagram of the ion source assembly indicating normalized levels of radioactivity assayed on each piece.

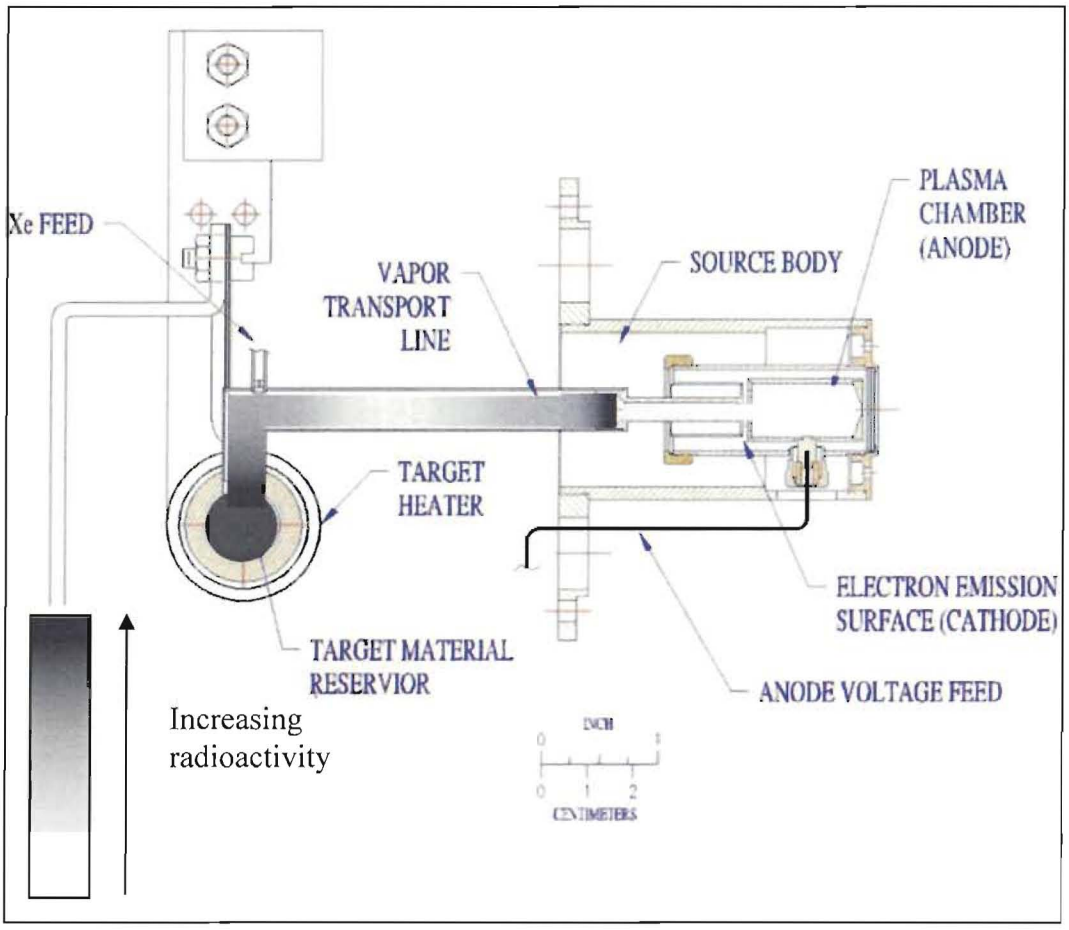

Figure 6.9
Necropsy results with radioactivity levels

Radioactivity was primarily deposited in the target chamber, first part of the transport tube, last part of the transport tube and on the rear of the cathode. Very little radioactivity was found deposited on the anode or the extractor.

6.2.5 Conclusion from ORNL Data

The rhenium in this experiment can only be present as an oxide or in metallic form and only the oxide species is volatile, thus it is suspected that in the hotter parts of the transfer tube and cathode (>2000 ° C) this oxide molecule may decompose before it has had a chance to be ionized and thus is deposited on the transfer tube. This decomposition step is illustrated in the Gibbs free energy diagram shown in Figure 6.10. This diagram (generated by HSC Chemistry [4]) displays the most thermodynamically favorable composition of molecules as a function of temperature.

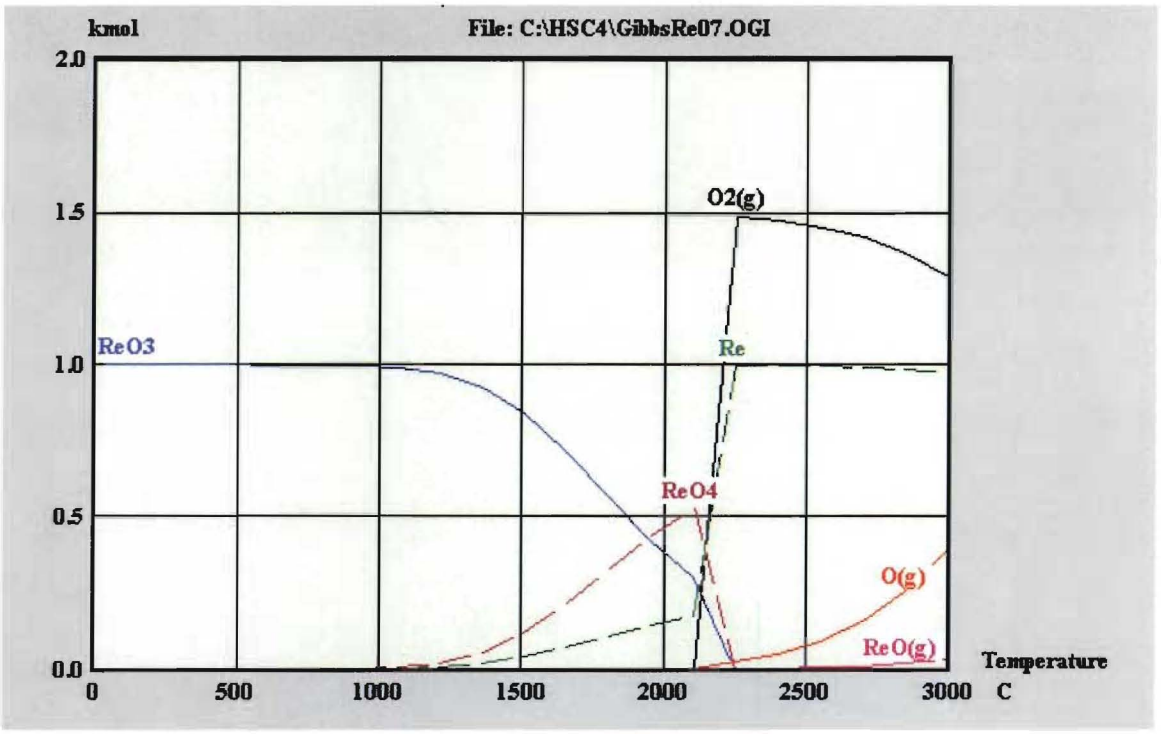

Figure 6.10
Gibbs free energy diagram illustrating the decomposition of rhenium oxide at elevated temperatures

6.3 Experiments Conducted at TRIUMF

6.3.1 Overview

To overcome the problem of decomposition of the volatile rhenium oxide species, a proof-of-principle cusp ion source was constructed, commissioned with H^- ions and finally tested with ^{188}Re. This type of ion source uses a magnetic field to contain a plasma and negative ions are produced by thermal electron capture. This type of cusp source is widely used for the production of H^- ion beams for injection into medical cyclotrons. There has also been some precedence for producing negative ions of rhenium in other disciplines [5, 6]. These facts make this type of ion source a good possible choice for producing high intensities of molecular negative ion beams of rhenium oxide.

6.3.2 Materials and Methods

The design of the ion source test stand was based around a pre-existing cusp body, which was mounted to a small vacuum box. The extractor system is a duplicate of the extraction system for the main TRIUMF 500 MeV cyclotron. A plasma is generated by electron emission from the tungsten filament at ~130 A. This plasma is maintained in a stable state by the addition of hydrogen gas, thus generating H^- ions. Thus the majority of the ions implanted into the Faraday cup (including during the rhenium experiments) are H^-. The extraction lens (Ext.

Lens, 2 kV) and faraday cup (Bias, 15 kV) are maintained at a positive voltage to extract negative ions. Documents concerning the safety and design of this device can be found in Appendix 1. An electrical schematic of the system is given in Figure 6.11 (values shown are the maximum rating of the power supplies) and photographs of the system are shown in Figures 6.12 and 6.13.

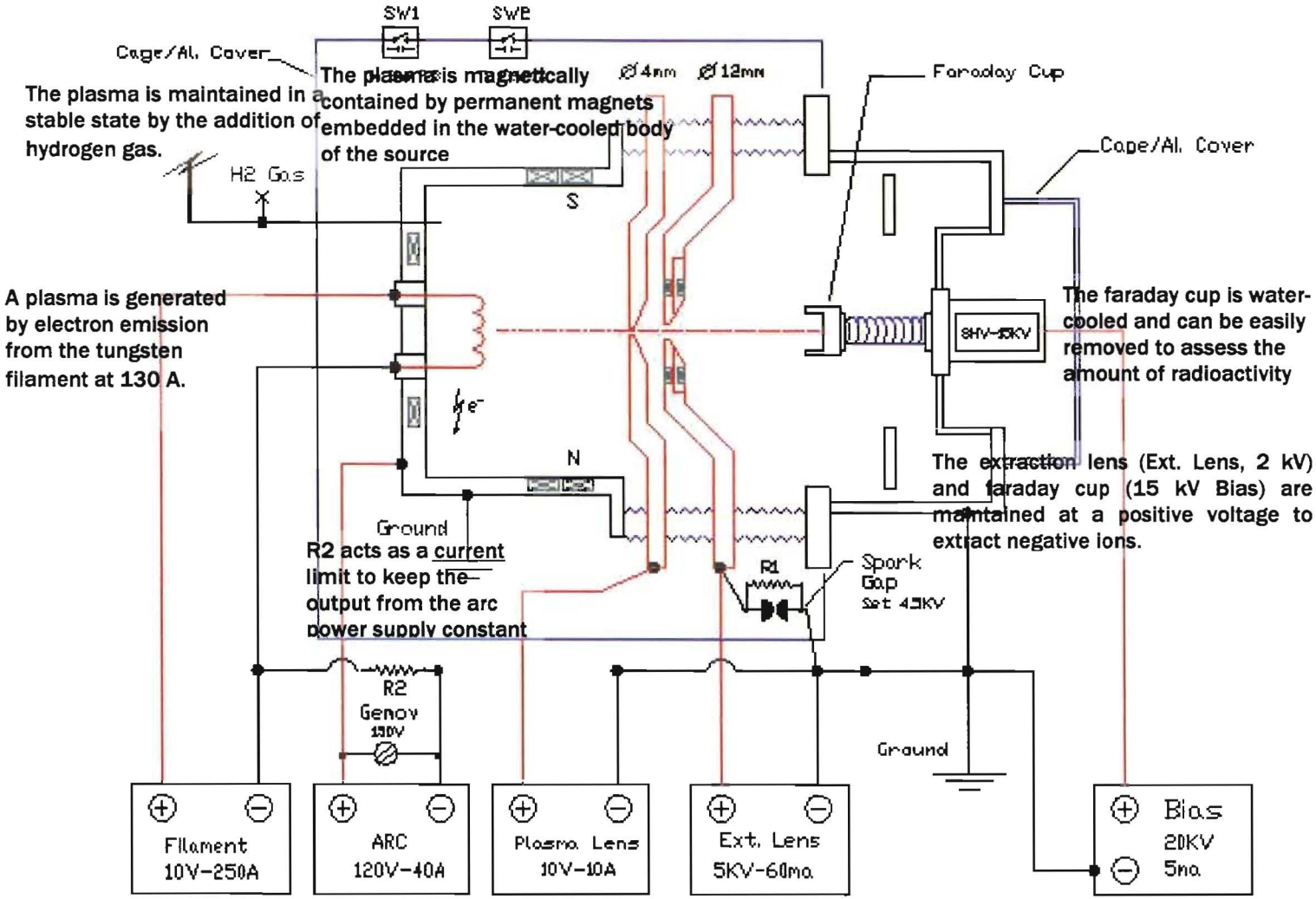

Figure 6.11
Electrical schematic of the rhenium ion sourc

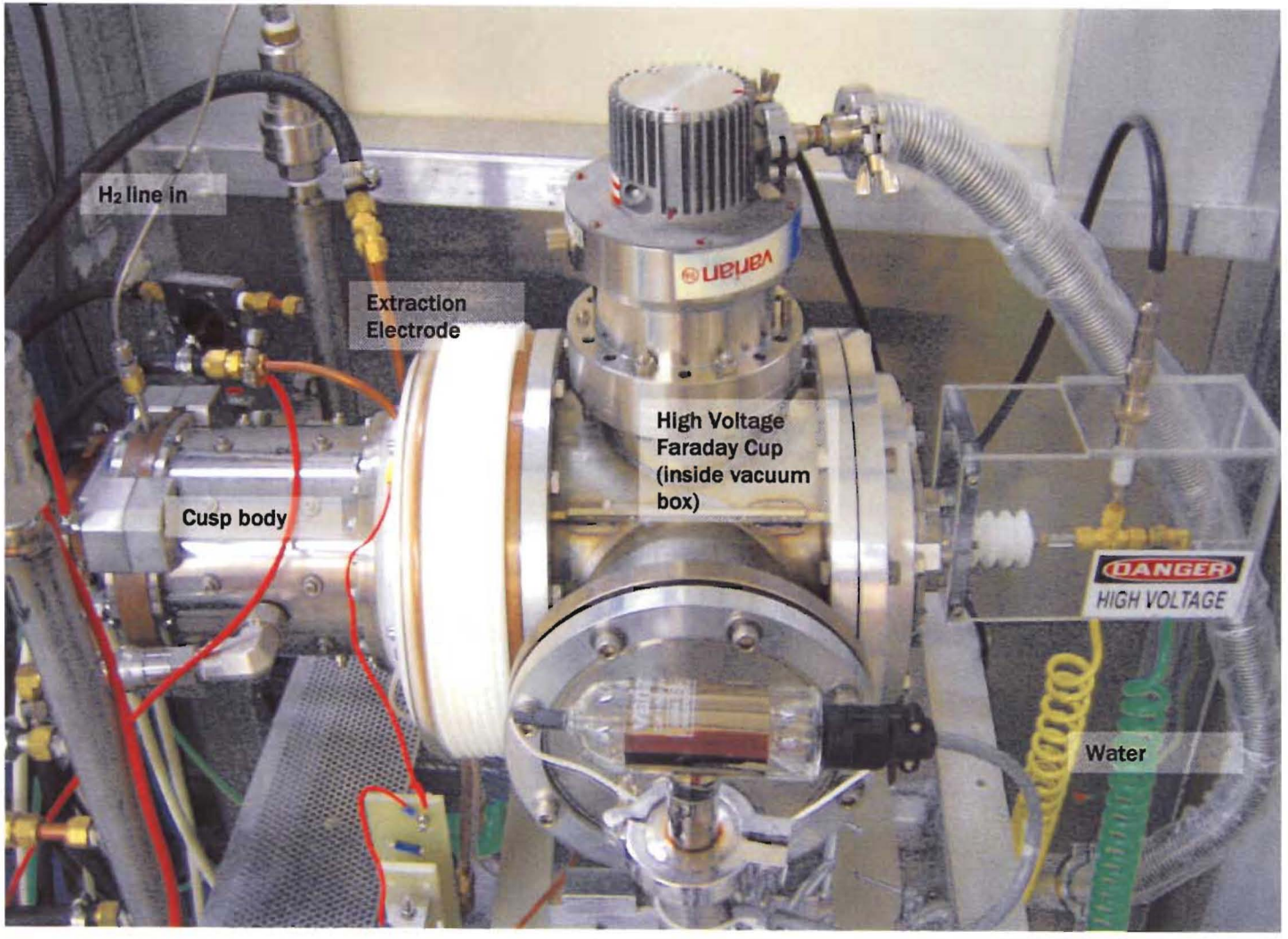

Figure 6.12
Rhenium ion source

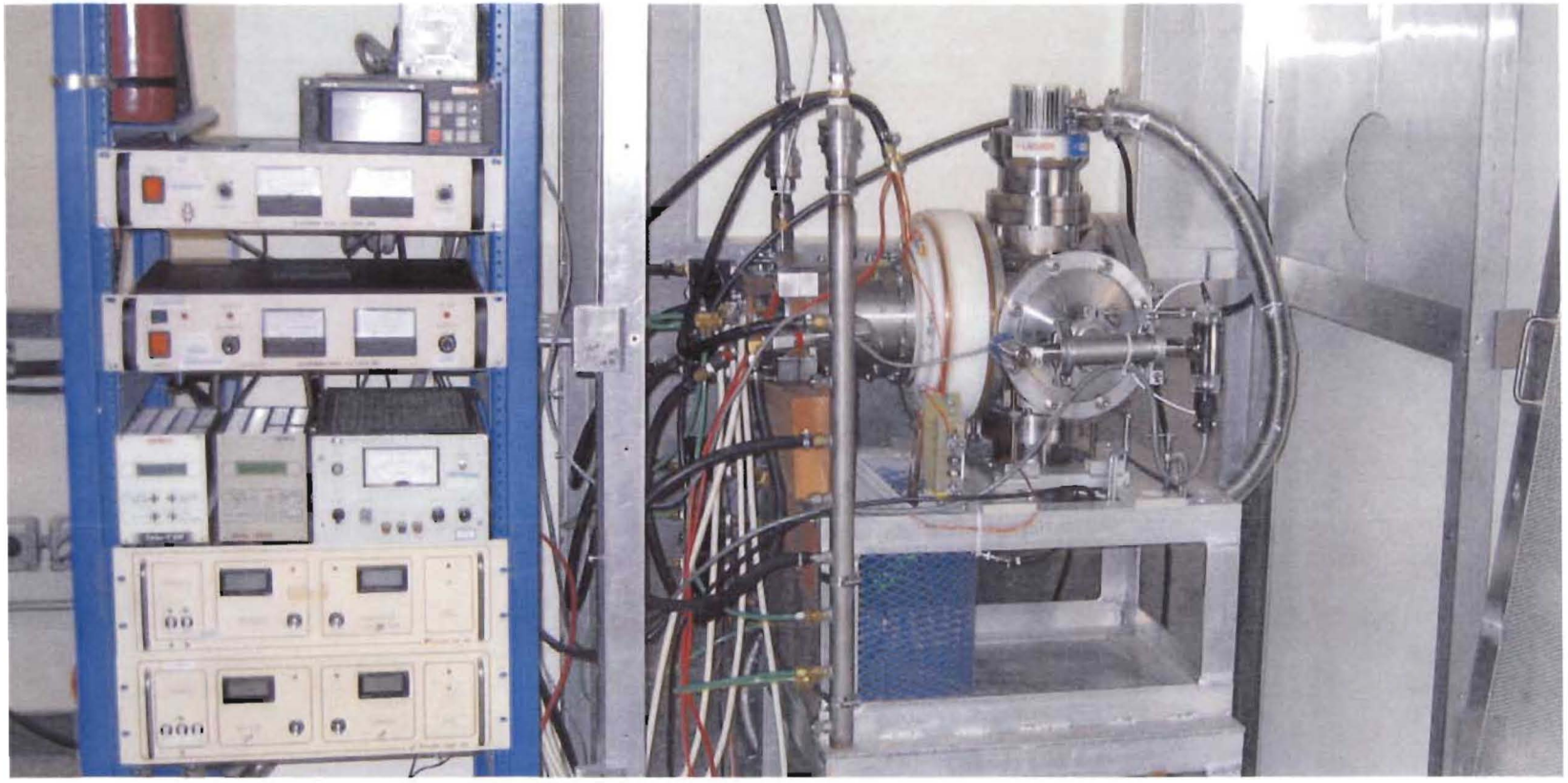

Figure 6.13
Rhenium ion source test stand and associated equipment

The final Faraday cup design consisted of a water-cooled copper disc, which was maintained at 15 kV during normal operation. The Farday cup is shown in Figure 6.14. Water is forced up through a smaller concentric tube in the center of the copper pipe and returns around the outside of the smaller tube. The high voltage is connected through the port in the bottom of the plastic covering. The copper part of the Faraday cup can be purged of water and disconnected for assessment of radioactivity.

Figure 6.14
Water-cooled Faraday cup

6.3.3. Experimental and Results

Commissioning with H^-

Typical operating parameters for the rhenium ion source are given in Table 6.2.

Table 6.2
Typical operating parameters for the rhenium ion source

Vacuum /Torr	Filament /I/V	Arc /I/V	Ex. Lens /I/V	F. Cup /I/V
5×10^{-5}	139 A/ 3.6 V	5.0 A/ 100 V	40 mA/ 2 kV	1.2 mA/ 15 kV

Currents of 1.2 mA of H^- on the Faraday cup were achieved with this configuration. A photo of the original, uncooled Faraday cup after a one-hour irradiation can be found below.

Figure 6.15
Faraday cup after one hour irradiation with 1.2 mA of H^-

As shown by the discoloration and deformation of the Faraday cup, the power of the accelerated beam was in excess of what the Faraday cup could withstand. Installation of the water-cooled faraday cup shown in Figure 6.14 alleviated this problem.

The temperature of the plasma

Several tests were conducted to determine the temperature of the plasma as function of the resistor R2 (see Figure 6.11). As the filament current is increased, the arc across the plasma increases. The resistor R2 limits the feedback between these two power supplies, thus the goal of these experiments was to determine the highest value of this resistor while maintaining a temperature high enough to keep the rhenium oxide species volatile. A graph of this effect can be found below in Figure 6.16. Based on these results, a resistor of three ohms was used for further experiments.

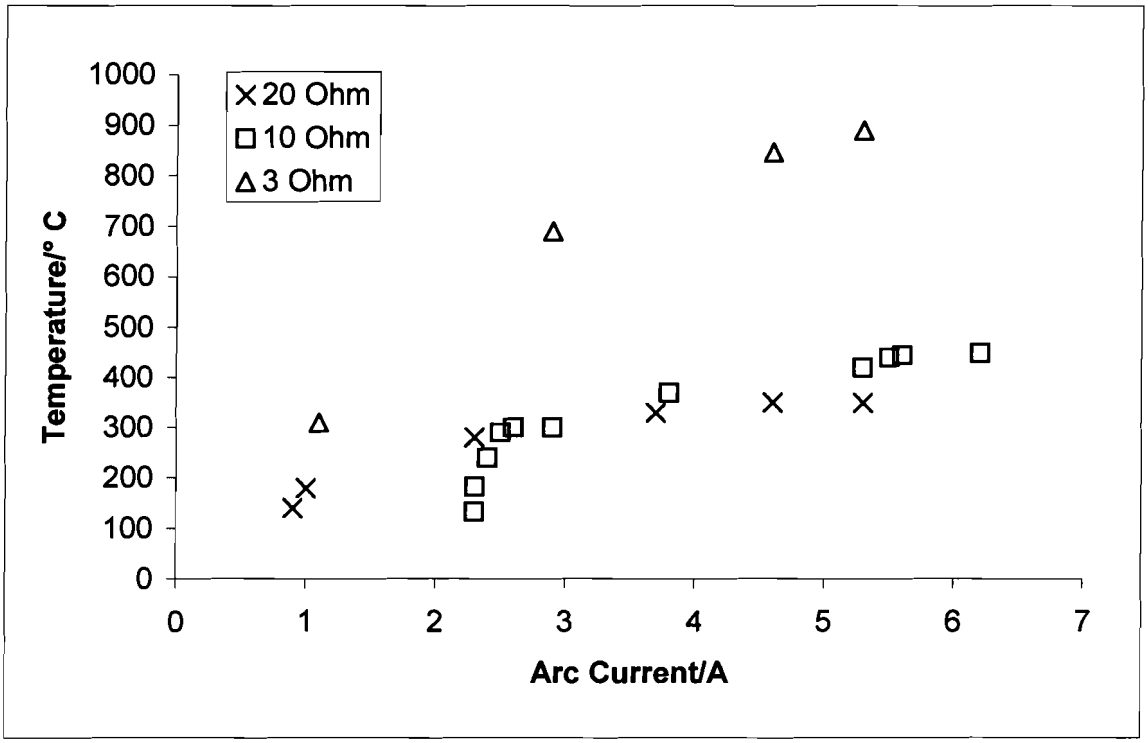

Figure 6.16
Plasma temperature change with resistance of R2

Experiments with ^{188}Re

^{188}Re was generously made available from a ^{188}W generator [7] by Prof. Urs Hafeli (UBC, Department of Pharmaceutical Sciences). The generator was eluted with saline and transported to TRIUMF in a type 1A package suitable for the transport of radioactive materials. The radioactivity ($H^{188}ReO_4$) was dried onto a quartz dish and this dish was placed in the center of the ion source on a Ta wire stand. When the ion source is in operation, the plasma heats up the dish and at temperatures >500 °C the rhenium oxide becomes volatile. The ions were extracted and implanted on the Faraday cup, which was removed for gamma spectroscopy to determine the amount of radioactivity implanted.

Initial runs using only the dried ^{188}Re saline solution resulted in little (<5 %) vaporization of the rhenium. This was greatly improved by the addition of cold (non-radioactive) rhenium oxide. Several runs were performed with the addition of cold rhenium oxide (50-200 mg). With the addition of the maximum amount (200 mg) of rhenium oxide, no arc current could be achieved. Inspection of the filament indicated that a rhenium metal deposit had formed on the filament, thus it is likely that the plasma was compromised. With the addition of 50-150 mg of cold rhenium oxide, rhenium ions were implanted in the Faraday cup. A maximum of 10^{12} atoms of rhenium per second were achieved.

6.3.4 Conclusions

Although only modest beam currents were achieved in the proof-of-principle ion source (at these levels it would take an estimated 37 days to separate 1 mg of rhenium), these results are nevertheless encouraging. It is suspected that the majority of the vaporized rhenium is condensing out on the water-cooled source body. This could be drastically reduced by a heated chamber inside the cusp body. In addition, a resistively heated quartz boat would allow for more control over the vaporization step. These modifications are currently being pursued at TRIUMF.

6.4 References

1. Bechtold, V., P. Fesenfeld, and H. Schweickert. *Industrial Applications of the Karlsruhe Compact Cyclotron.* in *11th International Conference of Cyclotrons and their Applications.* 1987.

2. Jia, W. and G.J. Ehrhardt, *Enhancing the specific activity of Re-186 using an inorganic Szilard-Chalmers process.* Radiochimica Acta, 1997. **79**(2): p. 131-136.

3. Zhang, Z.Y., et al., *Preparation of Re-186 and Re-188 with high specific activity by the Szilard-Chalmers effect.* Journal of Labelled Compounds & Radiopharmaceuticals, 2000. **43**(1): p. 55-64.

4. Outokumpu, *HSC Chemistry for Windows: Chemical Reaction and Equilibrium Software 4.0.* 1999.

5. Creaser, R.A., D.A. Papanastassiou, and G.J. Wasserburg, *Negative Thermal Ion Mass-Spectrometry of Osmium, Rhenium, and Iridium.* Geochimica Et Cosmochimica Acta, 1991. **55**(1): p. 397-401.

6. Suzuki, K., Y. Miyata, and N. Kanazawa, *Precise Re isotope ratio measurements by negative thermal ionization mass spectrometry (NTI-MS) using total evaporation technique.* International Journal of Mass Spectrometry, 2004. **235**(1): p. 97-101.

7. Knapp, F.F., Jr., *Rhenium-188--a generator-derived radioisotope for cancer therapy.* Cancer Biotherapy Radiopharmaceuticals, 1998. **13**(5): p. 337-49.

Chapter 7

Conclusions and Future Directions

7.1 Introduction

The main focus of this research project was to investigate the feasibility of ^{186}Re as an isotope for radioimmunotherapy. ^{186}Re is commonly produced via neutron capture in a reactor. This leads to a product with low specific activity, which is not optimal for site specific targeting. As such, the possibility of producing high specific activity (HSA) ^{186}Re from a charged particle reaction was investigated. High specific activity ^{186}Re was produced via the ^{186}W(p,n) reaction at TRIUMF using the TR13 cyclotron. A chemistry method for the separation of trace rhenium from tungsten targets was developed. Antibodies were labeled with HSA and LSA ^{186}Re and incubated with mouse embryonic fibroblasts to

determine specific receptor binding. Cell mortality was determined by traditional methods.

In addition, studies with an ion source and a mass separator were conducted at Oak Ridge National Lab and at TRIUMF with radioactive rhenium isotopes to determine the feasibility of producing carrier-free ^{186}Re from a neutron-irradiated target

7.2 Goals

The goals for this project were as follows:

- To measure the production cross section for ^{186}Re via the ^{186}W(p,n) reaction.
- To produce ^{186}Re in high specific activity by irradiation of enriched ^{186}W in powder form and to separate the ^{186}Re product from the target material.
- To conjugate the cyclotron-produced high specific activity ^{186}Re and reactor-produced low specific activity ^{186}Re to antibodies of biological interest.
- To determine the immunoreactivity of the labeled antibodies.
- To determine if there is differential binding of antibodies labeled with HSA ^{186}Re as compared to LSA ^{186}Re.

- To investigate a means of creating ions of Re as part of an ionization and mass separation technique to produce HSA ^{186}Re from reactor targets.

7.3 Conclusions

- Cross sections for the production of ^{181}Re, ^{182m}Re, ^{182g}Re, ^{183}Re ^{184}Re, and ^{186}Re from natural tungsten were measured using the stacked foil technique for proton energies up to 17.6 MeV. The experimental values were compared to previous literature values and to the excitation functions as calculated by the EMPIRE-II nuclear reaction code. The cumulative yield of ^{186}Re was calculated using the new cross section data and it was determined that 5.5 GBq of ^{186}Re could be produced with a 50 μA, 24 hour irradiation with 18 MeV protons. While this may not be a cost-effective route to produce this isotope in high specific activity at present, it is possible that higher power accelerator targets could be developed to withstand higher beam currents and thus make this a feasible method to produce HSA ^{186}Re.
- High specific activity ^{186}Re was produced by proton bombardment of enriched ^{186}W target material. A dry distillation technique was employed to separate the ^{186}Re from the target material with high recoveries (>70% in 6 hours). Although the yield for this reaction is low, significant quantities

for research (670 MBq) could be produced in order and separated from the target material to investigate the impact of high specific activity ^{186}Re in radioimmunotherapy.

- S-benzoylmercaptoacetylglycylglycylglycine was synthesized according to previously published procedures in high purity with an overall yield of 11.5 %. This compound was successfully coordinated to ^{186}Re in high yields. An activated ester was prepared via an EDC coupling to tetrafluorophenol. This activated ester was coupled to the 1H7 antibody with variable results. The final conjugate was purified via passage through a PD10 column. The problematic step in this process was the bioconjugation of the activated ester to the antibody. This step is very sensitive to pH and a significant portion of the antibody conjugate was found (in subsequent studies) to have lost immunoreactivity. As a result the experiment was not able to differentiate the impact of HSA as opposed to LSA ^{186}Re in subsequent *in vitro* cell studies. It is likely that a different targeting agent (for example a peptide or small molecule) and receptor system may be able to elucidate this difference.
- In an offshoot study, the role of the Insulin-like Growth Factor Receptor I (IGF-1R) in radiotherapy was studied. Cells that do (R+) and do not (R-) express the IGF-1R were exposed to external beam radiation and the free

^{186}Re in solution. The results indicate that the IGF-1R may act as a radioprotectant when *in vitro* cells are exposed to X- rays but not to higher LET radiation such as β^- particles. Experiments with even higher LET (for example α particles) may shed more light on this issue.

- Experiments were conducted at Oak Ridge National Laboratory with an electron beam plasma ion source, and a proof-of-principle cusp ion source test stand was constructed at TRIUMF. Although only modest beam currents were achieved in the proof-of-principle ion source (at these levels it would take an estimated 37 days to separate 1 mg of rhenium), these results are nevertheless encouraging.

7.4 Future Directions

The most promising aspect of this thesis is the proof-of-principle cusp ion source. Although the presented *in vitro* studies were not able to illustrate the need for high specific activity ^{186}Re, there are many other models that may show this. Small molecules or peptides may prove to be more suitable targeting agents for this isotope. The ability to purify isotopes from reactor targets would also extend beyond ^{186}Re. ^{99}Mo, which is used in generators to produce ^{99m}Tc in most nuclear medicine departments worldwide, is currently produced via fission from enriched (>95%) ^{235}U. With growing concern over the availability of weapons

grade uranium, a possible application of this ion source technique would be to separate ^{99}Mo from neutron-irradiated ^{98}Mo targets, thus providing an alternative source of this important medical isotope.

Appendix 1

Memo concerning target failure

To: Jean-Michel Poutissou,
Cc: Tom Ruth, Ken Buckley
Re: Incident Report for Powder Target on TR13
From: Suzy Lapi
Date: February 7th, 2005

Incident:

On Friday, February 4th, 2005, both foil windows on the Re production powder target failed simultaneously immediately upon irradiation. Although this target had been used previously under the same irradiation conditions without problem it is suspected that because the powder used during this irradiation was of smaller grain size that it reacted with air that was trapped in between the aluminum foil and the target powder. This caused a rapid increase in volume and hence the failure of the foil. The result of this incident is loose powder in the vacuum tank. Swipes indicated no contamination of the target selector or floor below. The target collimators were contaminated with 1400 cpm of radioactivity. A gamma spectrum indicated that this radioactivity was due to the decay of rhenium isotopes. As the target was irradiated for only a few seconds the majority of the radioactivity present is from a previous irradiation and totaled <5μCi.

Background:

This irradiation was to be part of a series of experiments to produce high specific activity ^{186}Re. Previously (January 28th, 2005) we had irradiated a powder target with 5μA of 13 MeV protons for 30 minutes. A schematic of this target (helium window not shown) is shown in figure 1.

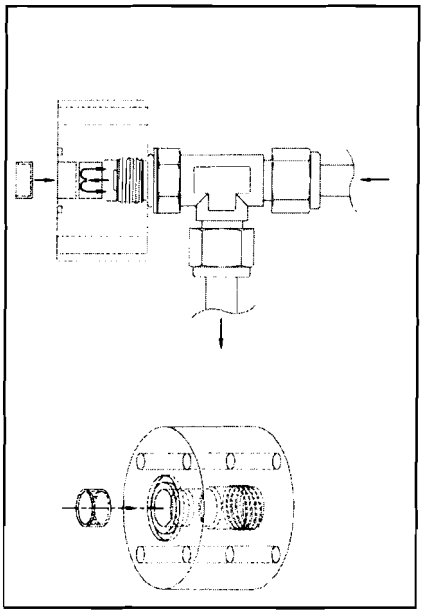

Figure 1. Powder Target Schematic.

This irradiation resulted in the production of several isotopes of rhenium with varying half-lives. Table 1 shows the approximate levels of each of these isotopes when the target was removed (February 1st, 2005).

Isotope	Half-Life	Decay Properties	Production (μCi)
^{182m}Re	64 h	EC,	10
^{182}Re	12.7 h	EC, β^+	30
^{183}Re	70 h	EC	5
^{184}Re	38 d	EC	7
^{186}Re	3.7 d	EC, β^-	15

Table 1. Production of Re isotopes via Irradiation of a Tungsten Target

The Re isotopes were extracted from the tungsten target using a dry distillation technique. The apparatus required for this extraction is shown in figure 2.

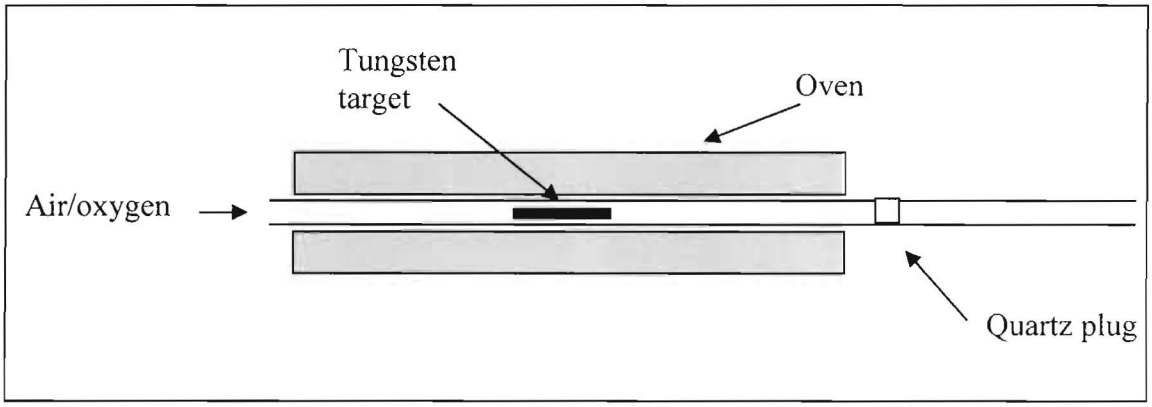

Figure 2 Dry distillation apparatus

The target was placed in the center of a quartz tube. The tube was then heated with an oven to approximately 1000°. The rhenium isotopes, which are present as $HReO_4$, are volatile at this temperature and evaporated out of the target. The $HReO_4$ then condenses out onto the cooler section of the quartz tube on a plug of quartz wool which is located outside the oven. The whole procedure took place inside a fumehood. After this procedure the Re isotopes (which are absorbed on the quartz plug) were removed. Re isotope recovery was ~70%. The target material was regenerated by heating it up to 700° under a stream of 7.5% H_2 in Argon. This process results in a finer grain size of target material that was present originally. After the reduction process the target material can be exposed to air at room temperatures without further reactions. The purpose of regenerating the target material is to simulate the regeneration of the enriched target material, which will be used to produce the pure ^{186}Re.

In the future the target will be packed under an inert atmosphere (helium) in a suitable glovebox to prevent this from happening again. We believe that this should resolve any further complications with this target.

Appendix 2

Documents Concerning the

Rhenium Ion Source Test Stand

TRIUMF
ENGINEERING DESIGN REVIEW

DR:

☐ Conceptual/Preliminary ☒ Final

Project/Experiment: LS73 **Date:** July 12th

System: Rhenium Ion Source Test Stand **REA No:**

Review Item: **Account No:**

Review Date/Time 7/12/2006 **Review Location:** Board Room

Person Responsible: Suzy Lapi

Panel: Mike McDonald Chair **Distribution:**

Tom Ruth

Ken Buckley

Keerthi Jayamanna

Peter Machule

Action Required:

Item	Description	By	Approved
	Install Grounding hook		
	Verify Water flow >10L/minute		
	A protocol will be written for SOP		
	Doors will be installed on the electronics rack		
	The cage will be padlocked when in use		
	Water flow meters will be interlocked to the filament PS		

☐ Approval to Proceed

☐ Proceed with Comments:

☐ Do Not Proceed and Resubmit By:

GRA No:	Date:

TRIUMF

RECORD OF GRADED RISK ASSESSMENT

This assessment is for:

- [x] An experiment
- [x] A new project or design
- [ ] Engineering Change Request (ECR)
- [ ] A report of a non-conformance

Experiment:
EEC or LSPEC No.: LS73
Title: Production and Evaluation of HSA 186Re
Spokesperson: Suzy Lapi

Project:
Title: Rhenium Ion Source Development
Project Leader: Suzy Lapi

ECR:
ECR No.:

Non-conformance:
Date:
Fault Report No.:
Description:

Person Responsible:

RISK ASSESSMENT[1]:

CONSEQUENCE	SEVERITY OF MAXIMUM CREDIBLE CONSEQUENCE					
	Low		Moderate		Severe	
Injury:	No lost time		No hospitalization		Hospitalization	x
On-site dose:	$H < 15$ mSv	x	15 mSv < H < 50 mSv		H > 50 mSv	
Off-site dose:	$H < 0.5$ mSv	x	0.5 mSv < H < 1 mSv		H > 1 mSv	
Radioactive release:	$A < 5\%$ of DRL	x	5% of DRL < A <DRL		A > DRL	
Accelerator down-time:	1 day < T_d <1 week	x	T_d >1 week			
Beam line down-time:	$T_d \leq 1$ month	x	T_d >1 month			
Monetary loss:	L ≤ $100,000	x	L > $100,000			

LIKELIHOOD	FREQUENCY OF OCCURENCE					
	Unlikely		Not Likely		Likely	
	$f<10^{-5}$ /year		$10^{-5}<f<10^{-1}$ /year	x	$f>10^{-1}$/year	

ASSESSMENT Based on the supplied documentation I (we) have assessed the risk as:

Low [ ] Moderate [x] Critical [ ]

(see comments on back of form)

Name: Ken Buckley **Signature:** [signature] **Date:** [illegible]

Name: Mike McDonald **Signature:** [signature] **Date:** Aug 5/05

[1] See *Graded Risk Assessment*, TSOP-03 for definition of terms